ISTANBUL TECHNICAL UNIVERSITY ★ INFORMATICS ENISTITUE

SOIL SALINITY MAPPING BY INTEGRATING REMOTE SENSING DATA WITH GROUND MEASUREMENTS; A CASE STUDY IN LOWER SEYHAN PLATE, ADANA, TURKEY

M.Sc. THESIS

Anali Azabdaftari

Department of Communication Systems

Satellite Communication and Remote Sensing program

Thesis Advisor: Prof. Dr. Filiz SUNAR
Anabilim Dalı :   Herhangi Mühendislik, Bilim
Programı :   Herhangi Program

May 2015

SOIL SALINITY MAPPING BY INTEGRATING REMOTE SENSING DATA WITH GROUND MEASUREMENTS; A CASE STUDY IN LOWER SEYHAN PLATE, ADANA, TURKEY

M.Sc. THESIS

Anali Azabdaftari
(705111018)

Department of Communication Systems

Satellite Communication and Remote Sensing program

Thesis Advisor: Prof. Dr. Filiz SUNAR
Anabilim Dalı : Herhangi Mühendislik, Bilim
Programı : Herhangi Program

May 2015

İSTANBUL TEKNİK ÜNİVERSİTESİ ★ BİLİŞİM ENSTİTÜSÜ

UZAKTAN ALGILAMA VERİLERİNİN YERSEL ÖLÇÜMLERLE ENTEGRASYONU İLE TOPRAK TUZLULUK HARİTALAMASI; AŞAĞI SEYHAN OVASI, ADANA, TÜRKİYE

YÜKSEK LİSANS TEZİ

Anali Azabdaftari
(705111018)

İletişim Sistemleri Anabilim Dalı

Uydu Haberleşmesi ve Uzaktan Algılama Programı

Tez Danışmanı: Prof. Dr. Filiz SUNAR
Anabilim Dalı :   Herhangi Mühendislik, Bilim
Programı :   Herhangi Program

Mayıs 2015

Anali-azabdaftari a **M.Sc.** student of ITU **Institute of Informatic** student ID **705111018**, successfully defended the **thesis** entitled "**SOIL SALINITY MAPPING BY INTEGRATING REMOTE SENSING DATA WITH GROUND MEASUREMENTS; A CASE STUDY IN LOWER SEYHAN PLATE, ADANA, TURKEY**", which she prepared after fulfilling the requirements specified in the associated legislations, before the jury whose signatures are below.

Thesis Advisor :   **Prof. Dr. Filiz SUNAR**   ....
                    Istanbul Technical University

Jury Members :   **Prof. Dr. Derya MAKTAV**   ....
                    Istanbul Technical University

                    Prof. Dr. Suha BERBEROGLU   ....
                    Cukurova University

Date of Submission: 4 May 2015
Date of Defense: 29 May 2015

To my dear family,

FOREWORD

I would like to take this opportunity to thank many people for their support and contribute toward the completion of this dissertation. First, I would like to express my sincere appreciation to my dear advisor, Prof. Dr. Filiz SUNAR, for her patience, motivation, enthusiasm, immense knowledge and continuous guidance and support throughout my program of study and this research work. My sincere gratitude goes to my committee members Dr. Suha BERBEROGLU, Dr. Derya MAKTAV. My sincere appreciation is to Dr. Suha BERBEROGLU for technical support and providing the field work data in Cukurova area and his support during the research period. Also my gratitude goes to Landscape Planning Department of Cukurova University.

I would like to thank my Father, Prof. Dr. Behrooz AZABDAFTARI, who that supports me not only during my MSc. thesis but also during my whole life. Also I thank my mother for her great love and encouragement. At the end, many thanks to my dear friends for their help and support.

May 2015

Anali AZABDAFTARI
(Information technology
engineer)

x

TABLE OF CONTENTS

ABBREVIATIONS

FAO   **:** Food and Agriculture Organization
DN   **:** Digital Number
TOA   **:** Top of Atmosphere
EC   **:** Electrical Conductivity
TM   **:** Thematic Mapper
ETM   **:** Enhanced Thematic Mapper
MSS   **:** Multispectral Scanner system
ASTER   **:** Advanced Spaceborne Thermal Emission and Reflection Radiometer
OLI   **:** Operational Land Imager
NIR   **:** Near Infrared
SWIR   **:** Short Wave Infrared
TIR   **:** Thermal Infrared
SLR   **:** Simple Linear Regression
MLR   **:** Multiple Linear Regression

LIST OF TABLES

LIST OF FIGURES

SOIL SALINITY MAPPING BY INTEGRATING REMOTE SENSING DATA WITH GROUND MEASUREMENTS; A CASE STUDY IN LOWER SEYHAN PLATE, ADANA, TURKEY

SUMMARY

To properly respond to the global changes, which challenge the scientific community to make available the data for a decade or continuous data in order to monitor the changes of atmosphere, ocean, and land, the remote sensing science can be helpful. Only remote sensing from space, can provide the global, repeatable, continuous observations of processes, needed to understand the Earth system as a whole. Remote sensing data can be used in several applications such as, meteorological data collection, change detection and land cover mapping, disaster monitoring and so on. One of the important applications of remote sensing is to detect and monitor the soil salinity level in agricultural areas. Saline soils are present in many areas of the world. Moderate to severe salinity, which is more or less visible in the landscape, reduces the annual yields of most crops.

In the lower Seyhan plate of Adana district in Turkey, soil salinity problem can be mentioned as one of the growing problems in the area. In this study the soil salinity detection of Seyhan plate from years, 2009 to 2010 were analyzed using remote sensing methods. Multitemporal data were acquired from LANDSAT 7-ETM$^+$ satellite in four different dates (19-April-2009, 12-October-2009, 21-March-2010, 31-October-2010). The field electrical conductivity (EC) measuremnts, collected by Landscape Planning Department of Cukurova University during the years 2009 to 2010 were used as a ground-truth data together with the Landsat images.

In the introduction part of the study, definition of remote sensing and a brief summary of the topic are given. In the second chapter, as an principles of remote sensing, the electromagnetic spectrum and radiation and electromagnetic interaction with Earth's features, spectral reflectance are explained. In the third chapter, general information about soil salinity and the role of remote sensing in soil salinity detection are provided alongside some literatures related to soil salinity detection using remote sensing. In the fourth chapter, different remote sensing satellites, which are suitable for soil salinity mapping, sensors and their characteristics, are given. In the fifth chapter, digital image is defined and main image processing steps and methods are explained.

In the application chapter, the study area and the data used including satellite data and field EC measuremnts are defined. In this study, it is aimed to evaluate the soil salinity level in the study area, using the field EC measurements and remote sensing technology; and to produce the soil salinity map of Seyhan plate of Adana district. With regard to the above objectives, the following processing steps were applied. First, the map projection of all Landsat 7 ETM$^+$ images used, were changed to European 50 in order to be compatible with the projection of field collected data. Then the radiometric correction was done in order to extract the top of atmosphere (TOA) value of each band. Different salinity and vegetation indices were applied to analyze the changes of salinity level in different soil conditions. Then in order to predict the soil salinity, the correlation between field EC measurements and remote sensing data were calculated. Correlation of EC value with DN or TOA value of each band and correlation of EC value with different indices were taken in to consideration in two

regression models, the simple linear regression (SLR) and multiple linear regression (MLR). In simple linear regression, the correlation of EC value with DN or TOA of each band of satellite in sampled location was calculated, whereas in multiple regression, the correlation of EC value with DN or TOA value of all bands was computed. In the third approach, the combination of satellite bands and different vegetation and salinity indices were used as independent variables. Since the results of simple linear regression did not yield satisfactory results, the highest correlation (78.40%) was achieved using MLR method. In this correlation the all bands of satellite image dated on 21st March, 2010 and EC value was calculated. Finally the satellite data which shows the highest correlation (21st March, 2010) was chosen for producing the soil salinity map.

In the final chapter, the results obtained in the application phase and the efficiency of remote sensing in soil salinity detection and mapping are discussed. Besides, some recommendations for the future research and the problems which encountered during analysis are outlined.

UZAKTAN ALGILAMA VERİLERİNİN YERSEL ÖLÇÜMLERLE ENTEGRASYONU İLE TOPRAK TUZLULUK HARİTALAMASI; AŞAĞI SEYHAN OVASI, ADANA, TÜRKİYE

ÖZET

Günümüzde küresel çevre değişikliklerine cevap verebilmede ve atmosfer, su ve karadaki değişiklikleri sürekli izlemede, uzaktan algılama, veri ve yöntemlerinden yararlanılmaktadır. Uzaktan algılama, tekrarlanabilir ve sürekli gözleme olanağı ile bir bütün olarak yeryüzünün incelenmesinde önemli bir yardımcı araçtır. Uzaktan algılama verisi birçok uygulama da örneğin; meteorolojik veri toplama, değişim saptama ve arazi örtüsü haritalama, afet izleme vb. kullanılabilir. Toprak tuzluluğunu tespit etmek ve tuzluluk seviyesini tarımsal alanlarda izlemek uzaktan algılamanın önemli uygulamalarından biridir. Tuzlu topraklar dünyanın pek çok alanlarında mevcuttur. Şiddetli ve orta dereceli tuzluluk seviyesi bir çok ürünün yıllık verimini azalttığından tarımda önemli bir etkendir. Yüksek toprak tuzluluğu ekosisteme önemli bir tehdit olup ve bitki büyümesini olumsuz şekilde etkileyen bir faktördür. Tuzlu topraklar aynı zamanda bitki örtüsünün yok olması nedeniyle erozyona eğilimlidir ve tuzlu alanlar genellikle çıplak alanlar olarak gözlenir. Tuzlanma kırsal alandaki tarımcılıkla uğraşan kesimde gelir azalışına yol açar ve bu durum bütün olarak bölgeye sosyal ve ekonomik alanda olumsuz etki yapar. Uzaktan algılama ile uçaktan veya uydudan alınan çok bantlı ve hiperspektral veriler kullanılarak tuzdan etkilenmiş toprağın ayırt edilmesi ve zamansal değişimlerin tespitinin yapılması mümkündür.

Türkiye'de Adana ilindeki, Seyhan ovası, toprak tuzlanması sorunu ile karşı karşıyadır. Bu çalışmada Seyhan ovasında 2009'dan 2010 yılına kadar toprak tuzlanması uzaktan algılama yöntemleri ile analiz edilmiştir. Çok zamanli veri dört değişik zamanda (19-Nisan -2009, 12-Ekim -2009, 21-Mart-2010, 31-Ekim -2010 LANDSAT 7-ETM$^+$ uydusundan elde edilmiştir. Alandaki yersel elektrik iletkenlik (EC) ölçümleri Çukurova Üniversitesi Peysaj Planlama Bölümü tarafından 2009-2010 yılları arasında yapılmış ve bu veriler yer gerçeği olarak LANDSAT görüntüleri ile beraber kullanılmıştır.

Bu çalışmanın giriş bölümünde uzaktan algılamanın tanımı ve konunun kısa bir özeti verilmektedir. İkinci bölümde, uzaktan algılamanın temeli olarak elektromanyetik spektrum ve ışınım, yeryüzü özelliklerinin elektromanyetik etkileşimi ve spektral yansıtma açıklanmaktadır. Üçüncü bölümde, toprak tuzluluğu ve topraktaki tuzlanmanın tespitinde uzaktan algılamanın rolü ile literatürde yer alan bazı örnek çalışmalara yer verilmektedir. Dördüncü bölümde, toprak tuzluluğu analizine yönelik olarak farklı uzaktan algılama uyduları, algılayıcılar ve karakteristiklikleri verilmektedir. Beşinci bölümde, dijital görüntü, temel görüntü işleme prosesleri tanımlanmış ve yöntemleri açıklanmıştır.

Dijital görüntülerin ön işlemesi, görüntülerin kalitesini artırmak ve ileri analizler için görüntülerdeki hataları düzeltmek için kullanılır. Ön işleme adımı geometrik ve radyometrik düzeltme işlemlerini kapsamaktadır. Görüntü verisinin kalitesinin değişiklik göstermesi ve bazı görüntülerin herhangi bir özel ön işleme adımını gerektirmemesi nedeni ile ön işlemede tanımlayıcı bir işleme adımıları yoktur.

Radyometrik düzeltme bu çalışmada da oldu gibi parlaklık değerlerinin güvenirliğini arttırmak ve mevcut hataları azaltmak için bir ön işleme adımı olarak kullanılmıştır. Radyometrik hataların kaynağı ve uygun radyometrik düzeltme yöntemleri, kullanılan algılayıcı ve özelliklerine bağlıdır.

Yüzey yansıtım değerini elde etmek için, ilk olarak dijital değeri spektral radyans değerine dönüştürülmüş ve sonra elde edilen değer yüzey yansıma değerine dönüştürülmüştür.

Mevcut çalışmada farklı spektral indeksler, örneğin bitki örtüsü ve toprak tuzluluğu indeksleri incelenmiştir. Normalize edilmiş fark tuzluluk indeksi (NDSI), en önemli tuzluluk indekslerinden biridir. Bu indeks sayısal bir gösterge olup, elektromanyetik bantların görünür ve yakın kızıl ötesi bantlarını kullanarak tuzluluk seviyesini tespit etmek için kullanılır. Toplamda, 16 farklı tuzluluk indeksi olarak, parlaklık indeksi (BI), ve tuzluluk indeksi (SI) ve literatürdeki bazı diğer önemli tuzluluk indeksleri incelenmiştir. Normalize edilmiş fark bitki indeksi (NDVI) bitki örtüsü indekslerinin en önemlilerinden biri olup bunun yanı sıra toprak uyumlu bitki indeksi (SAVI), geliştirilmiş bitki indeksi (EVI) ve bitki oranı indeksi (RVI) değerlendirilmiştir.

Korelasyon ve regresyon analizleri değişkenler arasındaki ilişkileri göstermektedir. Korelasyon katsayısı iki değişken arasındaki doğrusal bağlantının bir ölçümüdür. Korelasyon katsayısı değerleri daima -1 ve +1 arasındadır. Korelasyon katsayısının +1'i göstermesi, iki değişkenin pozitif lineer ilişkili olduklarını; korelasyon katsayısının -1'i göstermesi, iki değişkenin negatif lineer ilişkili olduklarını; ve korelasyon katsayısının 0 olması ise, iki değişken arasında doğrusal bir ilişki olmadığını göstermektedir.

Regresyon ile ilgili iki genel yaklaşım vardır: Basit lineer regresyon (SLR) ve çoklu lineer regresyon (MLR). Basit lineer regresyonda tek bağımlı değişken "y" ve bir tek bağımsız değişken "x" arasındaki ilişki tanımlanır. Çoklu lineer regresyon bir bağımlı değişken "y" ve iki veya daha fazla bağımsız değişken x_1, x_2, x_3, ... arasındaki ilişkiyi tanımlar. Diğer bir yaklaşım ise regresyon analizinde kullanılan ''aşamalı''(stepwise) yöntemidir. Aşamalı yöntem, analizdeki bazı değişkenleri çıkararak, regresyon katsayısını arttırmayı amaçlar. Bu çalışmada bu iki yöntem, uzaktan algılama verisi ve tuzluluk verisi arasındaki ilişkiyi incelemede kullanılmıştır.

Uygulama bölümünde çalışma alanı ve kullanılan veri olarak uydu verisi ile EC ölçümleri tanımlanmıştır. Bu çalışmada, EC ölçümleri ve uzaktan algılama teknolojisi kullanılarak Adana bölgesi, Seyhan ovasinda toprak tuzluluğu haritası oluşturularak toprak tuzluluğu derecelendirilmesi amaçlanmıştır. Yukarıda belirtilen hedeflerle ilgili olarak aşağıdaki adımlar uygulanmıştır. İlk olarak, çalışmada kullanılan Landsat 7 ETM$^+$ görüntüsünun projeksiyonu, arazi ölçümlerinin alındığı projeksiyona uyumlu olacak şekilde ED 50 sistemine çevrilmiştir. Daha sonra her bir bant değerine radyometrik düzeltme uygulanarak yukarı atmosfer değerine (TOA) dönüştürülmüştür. Farklı tuzluluk ve bitki örtüsü indeksleri değişik toprak koşullarında; tuzluluk seviye değişimini analiz etmek için uygulanmıştır. Daha sonra, toprak tuzluluğunu tahmin etmek için alan EC ölçümleri ve uzaktan algılama verisinin korelasyonu incelenmiştir. Her bir bandın DN ve TOA degerleri ile EC arasındaki korelasyon ve çeşitli indeksler ile EC değerinenin korelasyonu dikkate alınarak iki önemli regresyon modelim(Basit lineer regresyon (SLR) ve çoklu lineer regresyon (MLR)) kullanılmıştır. Basit lineer regresyon da her bant da DN veya TOA ile EC değerleri arasındaki korelasyon hesaplanırken; çoklu lineer regresyon da DN veya TOA ile EC korelasyon değerleri, uydunun tüm bantları kullanılarak hesaplanmıştır. Üçüncü yaklaşımda, uydu bantları ve değişik bitki örtüleri ve tuzluluk indeksleri

kombinasyonu bağımsız değişkenler olarak kullanılmıştır. Basit lineer regresyonu çok iyi sonuc vermemiş, en yüksek korelasyon (78.40%) MLR yöntemi kullanılarak elde edilmiştir. Bu analizde 21 Mart 2010 tarihli uydu görüntüsunun tüm bantları ile EC değerini korelasyonu hesaplanmıştır. Son olarak, elde edilen sonuçlara göre en yüksek korelasyonun eldeedildiği 21 Mart 2010 görüntüsü toprak tuzluluk haritasını üretmek için kullanılmıştır.

Son bölümde, uygulama bölümünden elde edilen sonuçlara gore uzaktan algılama tekniklerinin toprak tuzluluğu tespitinde etkinliği tartışılmıştır. Ayrıca gelecekteki araştırmalara yönelik olarak analiz esnasında karşılaşılan sorunlar ve öneriler belirtilmiştir.

1. INTRODUCTION

Soil salinity is one of the widespread environmental hazards all around the world, especially in arid and semiarid regions. According to the evaluation of United Nations Food and Agriculture Organization (FAO), 397 million hectares of the total land area of the world are covered by saline soil (Figure 1.1). Africa, Asia, Australia, Europe, Latin America, Near East and North America are the most affected areas [1].

The development of saline soils is a dynamic phenomenon, which needs to be monitored regularly in order to secure up to date knowledge of their extent, degree of severity, spatial distribution, nature and magnitude.
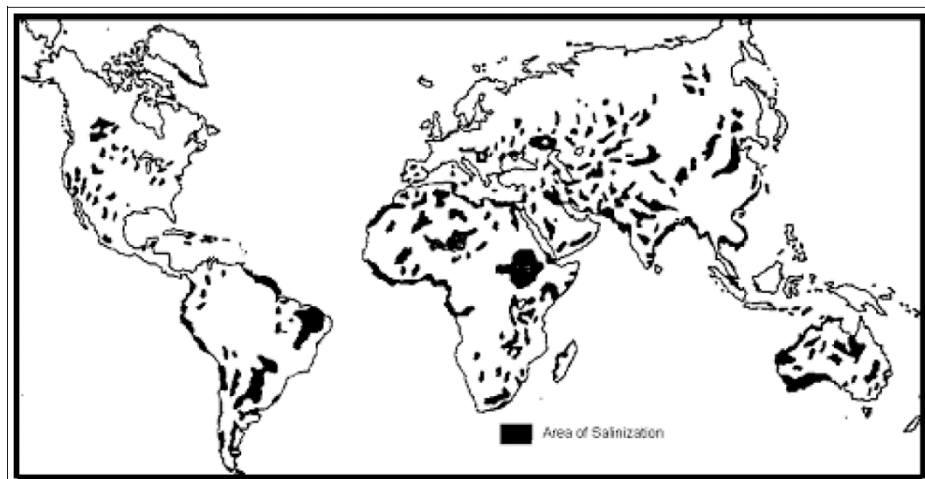
Figure 1.1 : Global distribution of salt-affected soil [2].

For monitoring dynamic processes, like salinization, remotely sensed data has great potential; it provides data by using aerial photography and infrared thermometry or multispectral data acquired from platforms such as Landsat [3].

Nowadays, there are almost no serious environmental studies, which do not use satellite images or image processing methods; however, in the 1970s and 1980s satellite images were mostly used in simple interpretations or as a map background [4].

Previously, soil salinity has been measured by collecting soil samples in the region of interest, and then the samples were analyzed in laboratory in order to determine the

amount of electric conductivity in the soil but this method was time and cost consuming. However, remote sensing data offer more efficiently and economically rapid means and techniques for monitoring and mapping soil salinity [1].There are great many satellites and sensors, which are useful in detecting and monitoring the saline soil. Multispectral data such as LANDSAT, SPOT, IKONOS, EO-1, IRS, and Terra-ASTER with the resolution can be ranged from medium to high as well as hyperspectral sensors. The sensors scan only the soil surface, while the entire soil profile is involved and should be considered. This limitation highlights the necessity of using other data and techniques, in combination with remote sensing [5].

The main objectives of this study are: (1) to understand the spectral reflectance characteristics of saline soil in Seyhan plate, (2) to explore the potential of Landsat imagery to detect and map the soil salinity over the study area, (3) to discover the correlation between field measurements and Landsat imagery, and (4) to produce the soil salinity map according to high, moderate and low saline content.

In the framework of this study, soil salinity and correlation between field measurements and Landsat imagery are being analyzed using Landsat 7 Enhanced Thematic Mapper (ETM$^+$) data (2009, 2010) in Seyhan plate of Adana District, Turkey.

Field measurements have been carried out almost simultaneously with the Landsat satellite pass in order to increase the accuracy of image analyses. Locations of the field measurements, according to latitude and longitude of samples, were specified on Landsat 7 ETM$^+$ imageries.

Atmospheric correction and Landsat data calibration were conducted in order to obtain top of atmosphere (TOA) values in sample points. Then, the correlation among electric conductivity (EC) of soil measured in sampled points and digital number value (DN) of the same point in each band was computed. Several salinity and vegetation indices were examined and were also correlated with electric conductivity of soil. Finally, the best result, which shows the highest correlation, was considered for creating the soil salinity map.

2. REMOTE SENSING

2.1 Principles of Remote Sensing

Remote sensing is the science of obtaining information about objects from a distance and not being in contact with the object of interest. Information is gathered by the processes of recording, measuring and interpreting of the imagery, derived typically from aircrafts or satellites.

Remote sensors can be either passive or active (Figure 2.1). Passive sensors record radiation that is reflected from Earth's surface, where the sun plays the role of providing an energy source and illuminates the target. Because of this, passive sensors can only be used to collect data during daylight hours; however, active sensors emit signals to the Earth's surface and record the backscattered or reflected signals.
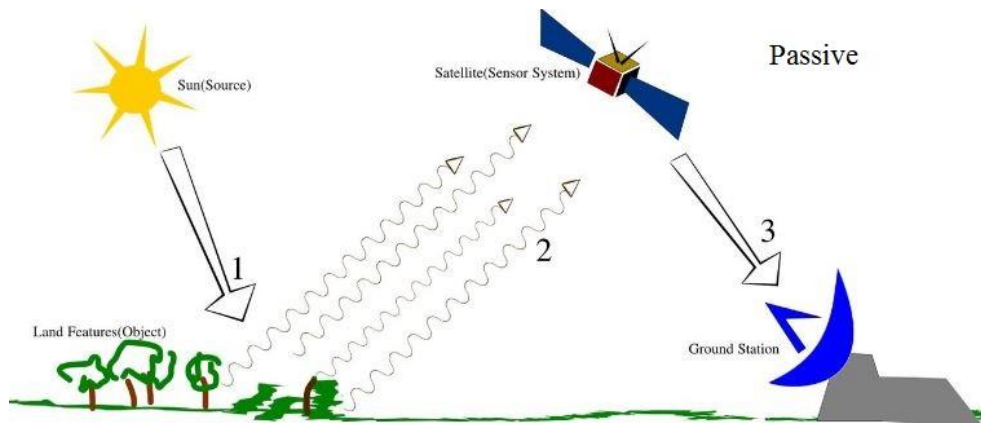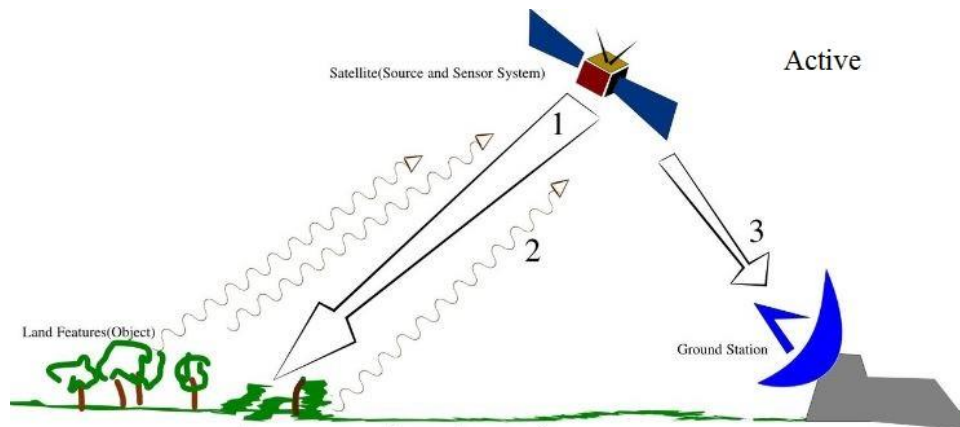
Figure 2.1 : Passive and active sensors[6].

The radiation from the sun or satellite system incident upon the Earth's surface causes three different interactions with objects: It can be absorbed, transmitted or reflected. The reflected energy is the most useful one in remote sensing applications. Reflection occurs when a ray of light is redirected as it strikes a non-transparent surface. Transmission of radiation occurs when radiation passes through a substance without significant attenuation. Absorption occurs when all the electromagnetic radiation is absorbed by objects on the Earth's surface and converted into the other form of energy or reradiated at a larger wavelength.

2.2 Electromagnetic Spectrum and Radiation

Electromagnetic wave's energy transports the energy through space in the form of periodic disturbances of electric and magnetic fields (Figure 2.2). All electromagnetic waves travel through space at the same speed, c=2.99792458 x 10^8 m/s, commonly known as the speed of light. An electromagnetic wave is characterized by a frequency and wavelength. These two quantities are related to the speed of light by the equation:

Speed of light = frequency x wavelength
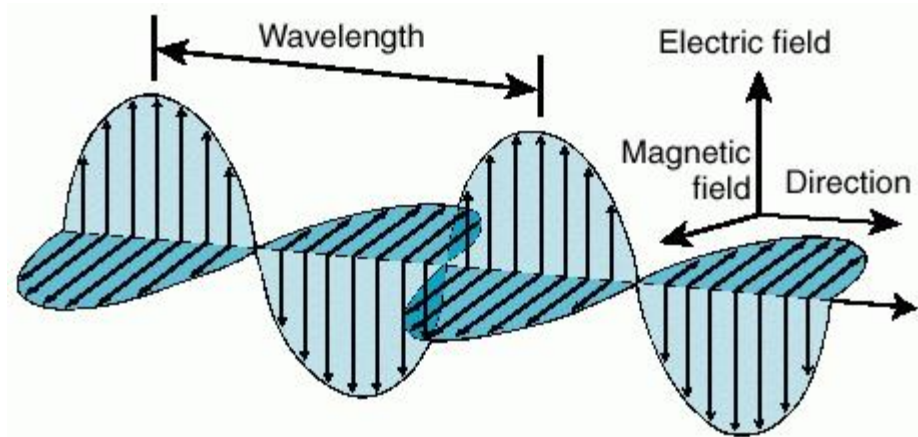
Figure 2.2 : Electromagnetic waves [7].

Light is a particular type of electromagnetic radiation that can be seen and sensed by the human eye, but this energy exists at a wide range of wavelengths. The micron is the basic unit for measuring the wavelength of electromagnetic waves. The spectrum of waves is divided into sections based on wavelength (Figure 2.3). The shortest waves are gamma rays, which have wavelengths of 10e-6 microns or less. The longest waves are radio waves, which have wavelengths of many kilometers. The range of visible region consists of the narrow portion of the spectrum, from 0.4 microns (blue) to 0.7 microns (red).
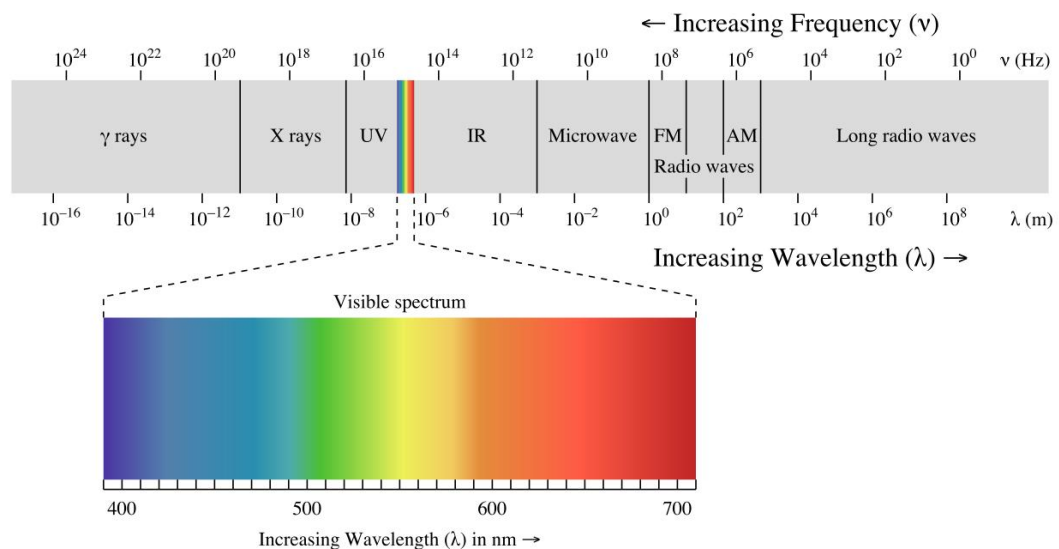
Figure 2.3 : Electromagnetic spectrum [8].

Electromagnetic radiation is reflected or absorbed mainly by several gases in the Earth's atmosphere, among the most important ones are water, carbon dioxide and ozone. Some radiation, such as visible light, largely passes (transmitted) through the

atmosphere. These regions of the spectrum with wavelengths that can pass through atmosphere are referred to as "atmospheric window ". Some microwaves can even pass through clouds, which make them the best wavelength for transmitting satellite communication signals.

Electromagnetic radiation could be redirected due to the presence of particles and gasses in the atmosphere; in this case, three different scattering mechanisms can occur:

Rayleigh scattering: It happens when the wavelength of the radiation is smaller than the particles in atmosphere such as dust and oxygen molecules.

Mie scattering: It happens when the particles in the atmosphere are almost the same size as the wavelength of radiation. Smoke, dust and water vapor are the common cause of Mie scattering.

Nonselective scattering: It happens when particles are larger than the wavelength of radiation; in this case, all wavelengths scatter almost equally. Water droplets and large dust particles can cause this type of scattering.

2.3 Electromagnetic Interaction with Earth's Features Spectral Reflectance

Objects having different surface features reflect or absorb the sun's radiation in different ways. The reflectance properties of an object depend on the particular material, its physical and chemical state (e.g. moisture) and the surface roughness as well as the geometric circumstances (e.g. incidence angle of the sunlight). The most important surface features are color, structure and surface texture.

The amount of energy reflected from the surfaces is usually expressed as a percentage of the amount of energy striking the objects. Reflectance is 100% if all of the light striking and object bounces off and is detected by the sensor. If none of the light returns from the surface, reflectance is said to be 0%. In most cases, the reflectance value of each object for each area of the electromagnetic spectrum is somewhere between these two extremes.

Across any range of wavelengths, the percent reflectance values for landscape features such as water, sand, roads, forests, etc. can be plotted and compared. Such plots are called "spectral response curves" or "spectral signatures". Differences among spectral signatures are used to help classify remotely sensed images into classes of landscape

features since the spectral signatures of like features have similar shapes. The figure below shows differences in the spectral response curves for main features (Figure 2.4).

Spectral information, recorded by a sensor can be extracted from the spectral signatures. Hyperspectral sensors have much more detailed signatures than multispectral sensors, and thus provide the ability to detect more subtle differences in aquatic and terrestrial features.
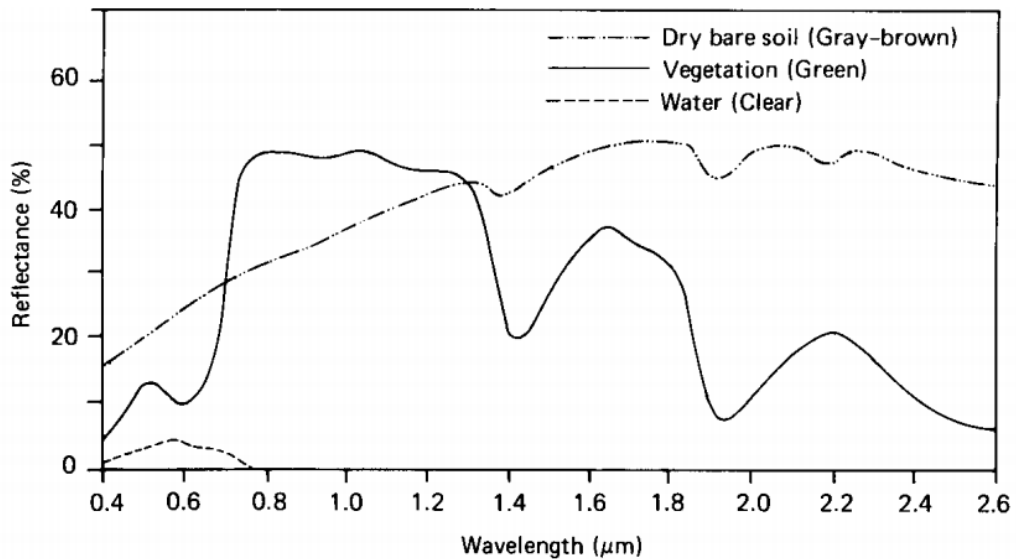
Figure 2.4 : Spectral signature of the main features [9].

2.3.1 Soil reflectance

The Earth's surface is covered mostly by the soil, which plays an important role in distinguishing the land's spectral reflectance. Soil reflectance is a function of material properties such as soil texture (percent of sand, silt and clay), soil moisture (dry, moist, saturated), organic matter content, iron oxide content, and surface roughness [10].

Soil moisture: Among all the factors affecting soil spectral reflectance, soil moisture is the most important one because of its dynamic nature and large impact on soil reflectance (Figure 2.5). Soil reflectance decreases when the moisture content increases because most of the incoming radiation is absorbed by the water in particular wavelengths.
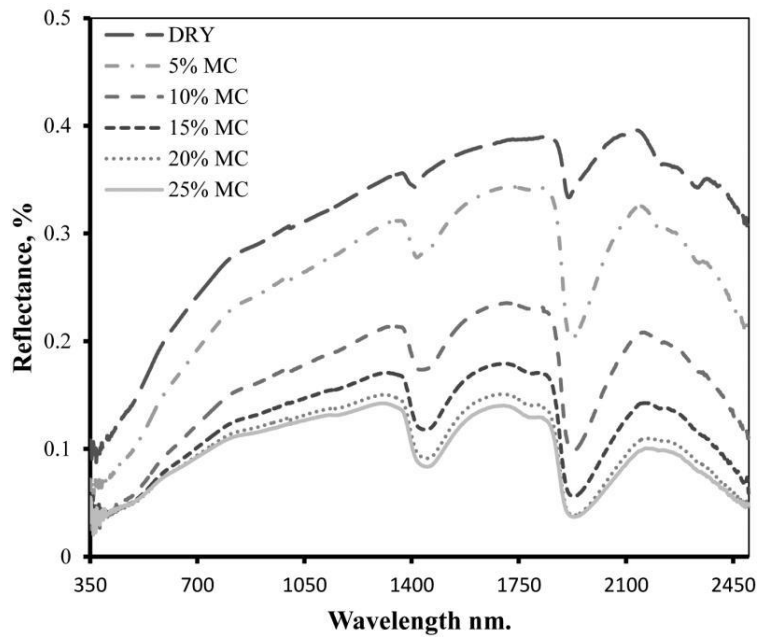
Figure 2.5 : Spectral reflectance characteristics of soil according to different moisture content [11].

Soil texture: Soil texture refers to the relative proportion of particles like sand, silt, clay in various sizes. Clay is the finer particle having less than 0.002 mm size, sand is a coarser particle having a diameter from 0.02 to 2 mm, and silt is the intermediate particle of diameter from 0.02 to 0.002 mm. Decreasing in particles size of the soil will result in increasing of reflectance. The relationship between soil texture and spectral reflectance is given in Figure 2.6.
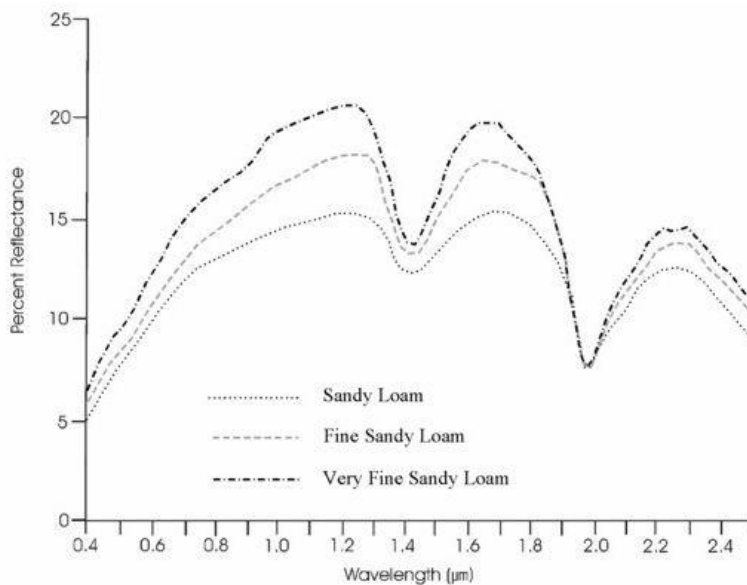
Figure 2.6 : Spectral reflectance characteristics of soil according to soil texture [12].

8

Organic matter content: Organic matter is one of the soil properties that has a significant role in soil reflectance (Figure 2.7). Organic matter controls the physical and chemical properties of soil; therefore, it is very important in agricultural aspect. Besides, the organic matter content is closely related to the color of soil, i.e, darker soils contain higher organic matter and lighter (gray and light brown) color soils contain less organic matter [13].
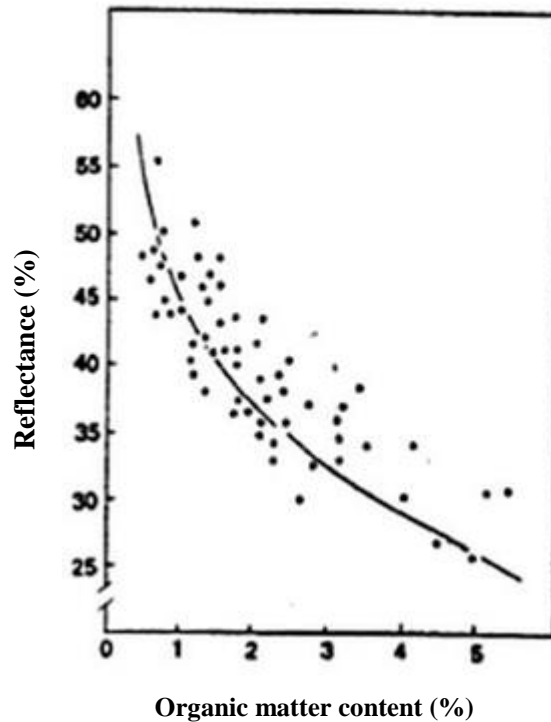
Figure 2.7 : Spectral reflectance characteristics of soil according to organic matter [13].

Iron oxide content: Increase in the iron oxide in soil can cause decrease in spectral reflectance of soil. Reddish color in some of the soil types is due to presence of high iron oxide in soil. The relationship between iron oxide and soil spectral reflectance is shown in the Figure 2.8.

9
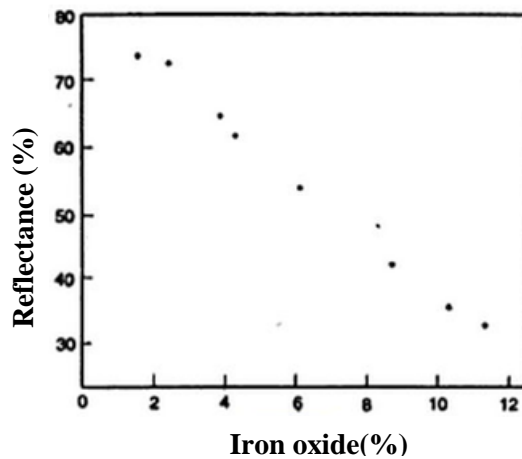
Figure 2.8 : Spectral reflectance characteristics of soil according to iron oxide [13].

Saline soil: Spectral reflectance of salt-affected soil can have very different curve according to the degree of salinization. By increasing the amount of electric conductivity, which is the indicator of saline soil, crusted saline soil spectral reflectance increases (Figure 2.9).
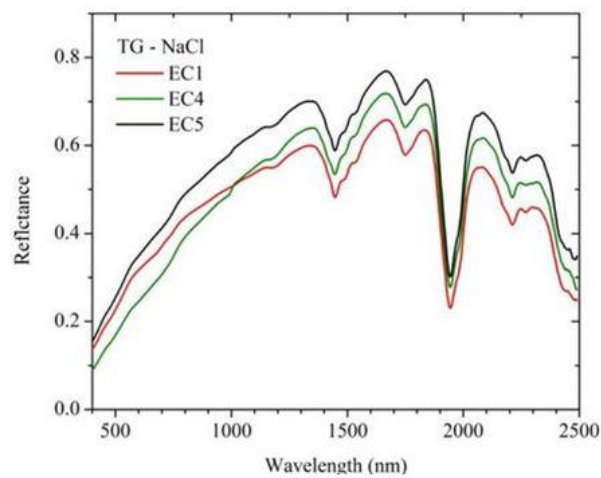
Figure 2.9 : Spectral reflectance variation with electrical conductivity (EC) [14].

3. SOIL SCIENCE AND REMOTE SENSING

3.1 Soil Definition and Properties

Alongside the air and water, soil is one the main three natural resources without which there would be no life. Soil is a major component of the Earth's ecosystem, which can support plant life as a mixture of minerals, gases, liquids, organic matter and numerous organisms; the proportion of each of these is important in determining the soil type.

Soil is a natural body that can perform four important functions (Figure 3.1): (i) it is a medium for plant growth, (ii) it is a means of water storage, supply and purification, (iii) it is a modifier of atmosphere, and (iv) it is a habitat for organisms that take part in decomposition and creation of a habitat for other organisms [15].

Soil, as formally defined in the Soil Science Society of America Glossary of Soil Science Terms, is:

1. The mineral or organic material on the surface of the Earth that serves as a natural medium for the growth of land plants.
2. The mineral or organic matter on the surface of the Earth that affects the genetic and environmental factors of climate (including water and temperature effects) and macro and micro-organisms.
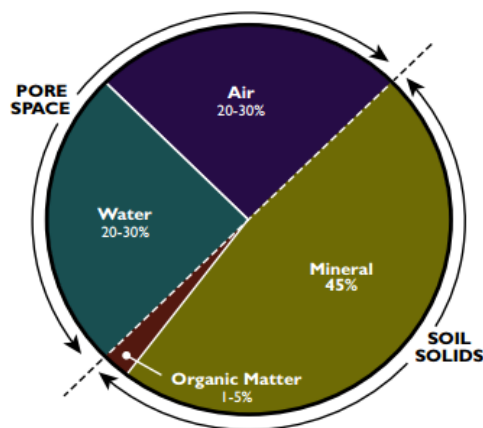
Figure 3.1 : Four components of soil.

The soil and its properties result from the interaction of chemical, physical and biological activities. The soil type is influenced by environmental factors including the parent material from which it is derived, vegetation, climate, topography and availability of water which can affect the suitability for agricultural practices and other purposes [16]. The movement and retention of water, air, and solutes in the soil, which subsequently affect plant growth and organism's activity are influenced by the texture, structure, and absorbency. Most soil chemical properties affect nutrient availability in the soil, and biological properties in soil contribute to soil aggregation, structure and absorbency as well as soil organic matter's (SOM) decomposition and mineralization [15].

The soil profile is an important tool in nutrient management. As the soil weathers and/or organic matter decomposes, the profile of the soil changes. For instance, a highly weathered, infertile soil usually contains a light-colored layer in the subsurface soil from which nutrients have washed away. On the other hand, a highly fertile soil often has a deep surface layer that contains high amounts of organic matter. A soil horizon makes up a distinct layer of soil. The horizon runs roughly parallel to the soil surface and has different properties and characteristics than the adjacent layers above and below. The soil profile is a vertical section of the soil that displays all of its horizons. The soil profile extends from the soil surface to the parent rock material. The regolith includes all of the weathered material within the profile. The regolith has two components: the solum and the saprolite. The solum includes the upper horizons with the most weathered portion of the profile. The saprolite is the least weathered portion that lies directly above the solid, consolidated bedrock but beneath the regolith.

Master Horizons: There are 5 master horizons in the soil profile. Not all soil profiles contain all 5 horizons; therefore, soil profiles differ from one location to another. The 5 master horizons are represented by the letters: O, A, E, B, and C (Figure 3.2).

O: The O horizon is a surface horizon that is composed of organic material at various stages of decomposition and can have various stages of decomposed organic matter: highly decomposed (sapric), moderately decomposed (hemic), and minimally decomposed (fibric). In a fibric O layer, plant matter is recognizable (e.g., it is possible

to identify a leaf). Sapric material is broken down into much finer matter and is unrecognizable as a plant part. Hemic is in between sapric and fibric, with some barely recognizable plant material present.

A: The A horizon is a mineral horizon which largely consists of sand, silt and clay and with appreciable amounts of organic matter. Due to the accumulation of organic matter, this layer is generally dark in color and biologically active. This horizon is usually the surface layer of many soils in grasslands and agricultural lands and are typically more coarse (less clay) compared to underlying horizons (with the exception of the E horizon).

B: The B horizon lies underneath the A horizon and is commonly called the subsoil. It is a site of deposition of certain minerals that have leached from the layer(s) above. Together, the A and B horizons form the zone in which most of the mineral and organic matter has been added, removed, transferred, or translocate through the soil-forming processes.

C: The C horizon is a subsurface horizon. It is the least weathered horizon. The C horizon is below the zones of greatest biological activity and it has not been sufficiently altered by soil genesis to qualify as a B horizon.

R: Below the C horizon in some soils is an R horizon, which is known as bedrock, such as limestone, shale, or sandstone. In a few soils the C horizon is missing, and the R horizon is directly beneath the B horizon [17].
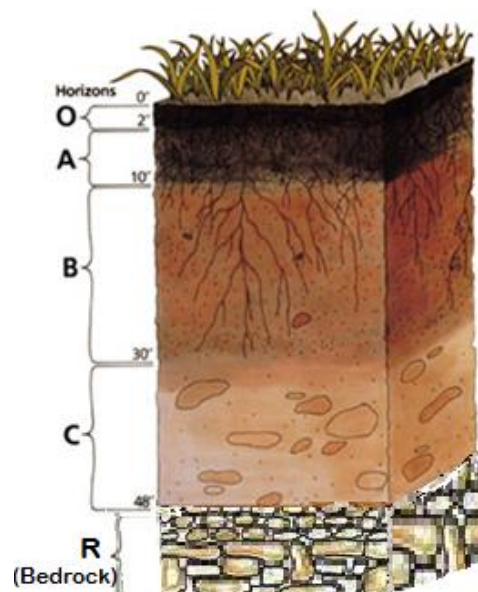
Figure 3.2 : Soil profile .

3.2 Soil Salinity

Salinity is the presence of salt in the land surface, in soil or rocks or dissolved in water, in rivers or groundwater. Salinity can develop naturally, but where human intervention has disturbed natural ecosystems and changed the hydrology of the landscape, the movement of salts into rivers and onto land has been accelerated. This is the beginning of dramatically effect on the natural environment, which reduces the viability of the agricultural sector and damages private and public infrastructure.

Soil salinity refers to the accumulation of soluble salts in the soil and is determined by measuring the electrical conductivity of a solution extracted from a water saturated soil paste[18]. According to the US Salinity Staff Laboratory, soils with conductivity of the saturation extract (EC) > 4, decisive-mens per meter (ds/m) at 25°C, Exchangeable Sodium Percentage (ESP) < 15, and pH (soil reaction) < 8.5 are referred to saline soils [1].

There are several types of salinity:

Dry land salinity is salinity that occurs in non-irrigated area. It usually occurs where deep rooted perennial vegetation is replaced by crops and pastures that use less water because they have shallow root systems and shorter growth cycles (Figure 3.3). As saline groundwater comes close (within two meters) to the soil surface, salt enters the plant root zone. Even where the groundwater does not bring much salt with it, the 'water-logging' of the root zone alone can damage or kill vegetation. Dry land salinity may also be brought about by the exposure of naturally saline soils such as hyper saline clays. Sodic soils (soils that have a high concentration of sodium ions in comparison to other ions like calcium and magnesium) can also bring about salinity.

The impact of water-logging and salinization will vary depending on soil type, climate and land use. Impacts can hardly be noticed by the untrained eye, namely reduced plant power, or a change in the vegetation mix in a particular area. More dramatic effects include the death of native plants and crops that are not salt-tolerant, which causes total bare patches of Earth, known as salt scalds. These areas act as the focal point for erosion to develop and spread, and for washing salt loads into rivers through run-off [19].

Figure 3.3 : Dry land salinity**.**

Irrigation salinity occurs when there is a localized rise in the level of groundwater which is caused by the application of large volumes of irrigation water. Rising water tables can bring salts into the plant root zone, which affects both plant growth and soil structure (Figure 3.4). Inefficient irrigation and drainage systems are a major factor of excess leakage, which increases the risk of salinity and waterlogging in irrigation areas. Poor water distribution on paddocks results in some areas being under-irrigated, causing salts to accumulate (where water tables are high) and other areas being over-irrigated and waterlogged. Irrigation salinity is made worse when water used to irrigate is derived from salty rivers or groundwater [20].

Figure 3.4 : Irrigation salinity.

Urban salinity is the result of a combination of dry land and irrigation salinity processes. Urban development and problems like over watering parks and gardens,

leaking pipes, drains and tanks, and blocking or changing natural drainage paths can cause the groundwater to rise (Figure 3.5).

Figure 3.5 : Urban salinity.

Industrial salinity results from industrial processes that concentrate salt in industrial waste water. Industrial wastewater can have high levels of salt in it due to industrial processes that concentrate salt in water. For example, in coal-fired power stations, water used for cooling is partly evaporated, which concentrates the salt in the water discharged from the coolers (Figure 3.6).

Figure 3.6 : Industrial salinity.

River salinity is caused by saline discharges from areas affected dry land, irrigation and urban salinity flowing into creeks and rivers (Figure 3.7).

Figure 3.7 : River salinity.

In general soil salinization is caused by number of factors: 1) weathering of rocks, and primary minerals, which formed *in situ* or transported by water or wind 2) groundwater movement through the soil 3) excessive irrigation that slowly start to cause the water table to rise to the level that up flux starts to draw moisture towards the upper layer of soil surface (Figure 3.8). From this moisture, water will either evaporate and salts in that water will accumulate close to the soil surface, or plants will use water then salts accumulate in the root zone.

(a)   (b)   (c)
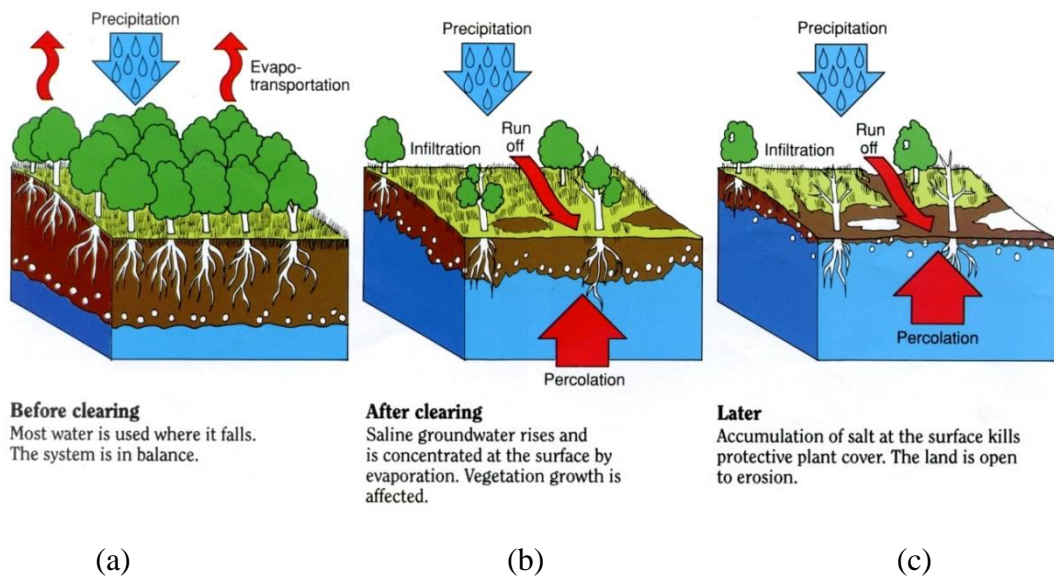
Figure 3.8 : Soil salinity process

Soil salinity symptoms can be divided in two categories as direct and indirect indicators. Direct indicators are salt features that are visible at the surface as a white

salt crust on the land; on the other hand, there are some other indirect indicators like presence of halophytic plants and the crop performance in saline soil.

Soil salinity adversely affects plant growth, crop production, soil and water quality, and it eventually results in soil erosion and land degradation. Soil salinity impact is not limited only to the environment but also has severe consequences for agriculture, society and economy. Therefore, for greater development and implementation of sufficient soil reclamation programs and preventing any further salinization to support agricultural lands and natural ecosystems, information on the spatial extent, nature and distribution of soil salinity is becoming very essential. Thus, timely detection of soil salinity, monitoring and assessment of its severity level and extent become very important in its beginning at local and regional scales [1].

3.3 Satellite Data in Soil Salinity Analysis

In recent years, methods for studying soil salinization have improved greatly. In past, soil salinity was just measured by soil sampling in situ and analyzing the amount of solute concentration and electrical conductivity in order to distinguish the saline soil from non-saline soil. Since 1960s when black-and-white and color aerial photographs were used to delineate salt-affected soils, remote sensing data and techniques started to make great progress and nowadays in almost every environmental studies remote sensing plays a significant role. Although remote sensing has been progressively employed for investigating soil sanity monitoring and mapping, the effectiveness of using ancillary data such as field data and topography beside the satellite data has been proved by Farifteh *et al*, 2005; Eldeiry, 2006 [3, 5].

Time saving, wide coverage, speed and long term monitoring are the advantages of using satellite remote sensing technology. Remote sensing uses the electromagnetic reflected energy from objects on surface to obtain information; therefore, for salinity identification soil and salt's spectral reflectance are very important which scientists call it as a direct indicator for soil salinity detection.

Multispectral and Hyperspectral satellite sensors are suitable for mapping and monitoring soil salinity. SPOT, IKONOS, ASTER can be categorized as multispectral sensors while EO-1 Hyperian and Hymap fall in Hyperspectral sensors category. In 1993, Goossens *et al* studied the multispectral sensors usefulness for soil salinity research. Accuracy of Landsat TM, MSS, and SPOT XS imagery have been examined

and compared for soil salinity mapping [21]. Their results indicate that Landsat TM was best for soil salinity mapping; however, Ahmed and Andrianasolo, (1997) have found that SPOT XS data provide more detailed and more exact information rather than Landsat TM [22].

Landsat TM imagery was used by Elnaggar and Noller in 2009 to map soil salinity in central Malheur County. They research's results have shown that there is significant relationship between EC values and reflectance in Landsat bands 1, 2, 3 and 4 as well as the Brightness (BI) and Wetness (WI) indices. They have found that Landsat TM imagery is effective in distinguishing the bare soil from saline soil, which has a high spectral reflectance in comparison with bare soil, due to a high salt content on the surface [23].

There is a study which shows the usefulness of Landsat TM and MSS in soil salinity mapping based upon the remotely sensed data in the Ardakan area located in the central Iranian Deserts [24]. They used Landsat MSS and TM data obtained on two different dates (September 14, 1975 and September 11, 2004) for multitemporal analysis. Field work was done in order to choose representative training sites and Maximum Likelihood Supervised classification was choosen as a classification method in both imageries but with different training classes and different band combinations. Due to miss-calssification of the TM thermal band excluded image, second classification was done based on the thermal band in band combination which showed higher accuracy about 90% and revealed the role of TM thermal band in improving image classification results. The overall correlation between the two classification images is found as 60.97%, meaning that in the 29 year period, about 39% of the total area suffer from changes. They also concluded that because of the presence of other soil properties like desert crust and salt type according to spectral reflectance, the precise estimation of salt-affected lands from satellite remote sensing is rather difficult. Therefore, for soil salinity detection and mapping, extra field work besides the hyperspectral remotely sensed data is needed to have a better result.

There is a wide usage of vegetation indices in the studies related to soil salinity occurred through a period of time in various regions. NDVI is one of the most used vegetation index which shows the best results for studies concerning salinization in agricultural areas and stressed-out vegetation canopies. In 2013, Alexander Platonov *et al* sutdied the soil salinity using multi-temporal satellite images in the agricultural

fields of syrdarya province of Uzbekistan. They considered two main approaches; analysis of reflectance from bare soil and analysis of vegetation stress by soil salinity. According to their study, all measured soil salinity parameters have low correlation coefficients with NDVI_Max (maximum multi-annual) so they tried to aggregate the values from both sources and then used an average value as an input for the analysis. They found that the result of correlation was slightly improved [25].

The evaluation of the role of different indices on soil salinity by analyzing several band ratios was the main purpose of the study of Al-Falaky *et al*. They developed forty band ratios from the 6 TM original bands to select the bands required for the particular need. The regression model of dependent soil variable (EC) and independent deduced band variables was introduced to SPSS system, and the best independent variables were decided. As a result of the correlations, inverse spectral bands (visible and middle infrared bands) 1/TM1,1/TM2 and 1/TM7 showed the best correlation with the soil EC land data, and finally a soil salinity map based on the this correlation was prepared [26].

4. REMOTE SENSING SATELLITES

In general, any object that can orbit around the any other object is called a satellite. As an example, the moon is a satellite because it orbits around the Earth, but there are many artificial and man-made satellites, which are launched into space and can orbit the Earth for different purposes. Some satellites are used for taking images from other planets or the Earth's surface and some other satellites are used in communication. There are so many satellites with different characteristics from different countries. Among all the satellites, Landsat Thematic Mapper (TM), Landsat Multispectral Scanner System (MSS), Landsat Enhanced Thematic Mapper Plus (ETM+), Advanced

Spaceborne Thermal Emission and Reflection Radiometer (Terra-ASTER) are more suitable for mapping and monitoring soil salinity as multispectral satellite sensor with mid-resolution. Because of the presence of short wave infrared and long wave infrared among the bands of both satellites that are more advantageous in soil and vegetation based studies, Landsat and Aster can be categorized as a most preferred satellites for salinity detection.

4.1 Landsat System

Landsat satellites were first launched in 1972 with Landsat 1. For 40 years, the Landsat satellites have provided scientists with continuous data and variety of characteristics that has contributed to human knowledge of the water cycle, climate, ecosystems, and the changing Earth and more.

4.1.1 Characteristics of Landsat

In the last half century deliberating of environmental change over the time was possible for scientist using Landsat satellite. The continuous global record, medium spatial resolution and the opening of the Landsat archives to the public in 2008 has made this dataset one of the most prevalent in Earth system studies.

Overall there are 6 Landsat satellites from beginning up to now, Landsat 1-3, Landsat 4-5, Landsat 7 and Landsat 8. Each of Landsat satellites has their own characteristics and these are given in the next section.

4.1.1.1 Sensors and specifications

MSS (Multi Spectral Scanner), TM (Thematic Mapper), ETM (Enhanced Thematic Mapper), ETM$^+$ and OLI (Operational Land Imager) sensors can be named as Landsat satellite system's sensors.

The Landsat Multispectral Scanner (MSS) sensor was onboard Landsat 1 through 5, and acquired images of the Earth nearly continuously from July 1972 and collected data until January 2013 when the mission of Landsat 5 was expired. MSS data was acquired with a 6-bit system and has 80-meter spatial resolution while TM and ETM$^+$ acquire data in an 8-bit system.

TM sensor has spatial resolution of 30 meter with 6 bands in NIR and SWIR portion of spectrum while the Thermal band has 120 meter resolution. Specific technical information of Landsat 5 TM is given in the Table 4.1 and Table 4.2.

Table 4.1 : Technical information of Landsat 5 TM.

Properties	Description
Operator	U.S. Geological Survey (USGS)
Launch date	1 March 1984
Altitude	705 km (438 mi)
Life time	5 years
Orbit	Sun-synchronous, circular Near-polar
Slope of orbit	98.2
Quantization	8 bit (256 levels)
Swath width	185 km (115 mi)
Repeat cycle	16 days
Sensors	MSS (Multi Spectral Scanner) TM (Thematic Mapper)

Table 4.2 : Imaging characteristics of Landsat 5 TM.

Band	Spectral Resolution (m)	Wavelength (µm)	Description
1	30	(0.45-0.52)	Blue
2	30	(0.52-0.60)	Green
3	30	(0.63-0.69)	Red
4	30	(0.76-0.90)	Near Infrared
5	30	(1.55-1.75)	Short wave Infrared
6	120	(10.4-12.5)	Thermal Infrared
7	30	(2.08-2.35)	Short wave Infrared

Enhanced Thematic Mapper Plus (ETM[+]) sensor has been mounted on the Landsat 7, it has 7 bands with 30 meter resolution and one extra panchromatic band with 15 meter resolution while the resolution of Thermal band has been improved to 60 meter. Specific technical information of Landsat 7 ETM[+] is given in the Table 4.3 and Table 4.4.

Table 4.3 : Technical information of Landsat 7 ETM[+].

Properties	Description
Operator	U.S. Geological Survey (USGS)
Launch date	15 April 1999
Altitude	705 km (438 mi)
Life time	5-6 years
Orbit	Sun-synchronous Near-polar
Slope of orbit	98.2
Quantization	8 bit (256 levels)
Swath width	185 km (115 mi)
Repeat cycle	16 days
Sensors	ETM[+] (Enhanced Thematic Mapper)

Table 4.4 : Imaging characteristics of Landsat 7 ETM[+].

Band	Spectral Resolution (m)	Wavelength (μm)	Description
1	30	(0.45-0.52)	Blue
2	30	(0.52-0.60)	Green
3	30	(0.63-0.69)	Red
4	30	(0.76-0.90)	Near Infrared
5	30	(1.55-1.77)	Short wave Infrared
6	60	(10.4-12.5)	Thermal Infrared
7	30	(2.08-2.35)	Short wave Infrared
8	15	(0.52-0.90)	Panchromatic

OLI and TIR are two sensors of Landsat 8 Earth-observation satellite as a last part of the Landsat Data Continuity Mission. The technical information of Landsat 8 is given in Table 4.5 and Table 4.6.

Table 4.5 : Technical information of Landsat 8.

Properties	Description
Operator	U.S. Geological Survey (USGS)
Launch date	11 February 2013
Altitude	705 km (438 mi)
Life time	5-6 years
Orbit	Sun-synchronous
	Near-polar
Slope of orbit	98.2
Quantization	8 bit (256 levels)
Swath width	185 km (115 mi)
Repeat cycle	16 days
Sensors	OLI (Operational Land Imager)
	TIRS(Thermal Infrared Sensor)

Table 4.6 : Imaging characteristics of Landsat 8**.**

Band	Resolution (m)	Wavelength (μm)	Description
1	30	(0.43-0.45)	Costal aerosol
2	30	(0.45-0.51)	Blue
3	30	(0.53-0.59)	Green
4	30	(0.64-0.67)	Red
5	30	(0.85-0.88)	Near Infrared
6	60	(1.57-1.65)	Short wave Infrared
7	30	(2.11-2.29)	Short wave Infrared
8	15	(0.50-0.68)	Panchromatic
9	30	(1.36-1.38)	Cirrus

10	100(30)	(10.60-11.19)	Thermal Infrared
11	100(30)	(11.50-12.51)	Thermal Infrared

4.2 Aster System

The advanced spaceborne Thermal Emission and Reflection Radiometer (ASTER) is an imaging instrument on the Earth Observing system (EOS) Terra, which was launched in 1999. Aster is a cooperative effort between NASA, Japan's Ministry of Economy, Trade and Industry (METI), and Japan's Earth Remote sensing Data Analysis Center (ERSDAC). ASTER data is used to create detailed maps of land surface temperature, reflectance, and elevation. ASTER captures high spatial resolution data in 14 bands, from the visible to the thermal infrared wavelengths, and provides stereo viewing capability for digital elevation model creation. The technical information of ASTER is given in Table 4.7 and Table 4.8.

Table 4.7 : Technical information of ASTER.

Operator	NASA and EOS
Launch date	18 December 1999
Altitude	705 km (438 mi)
Life time	6 years
Orbit	Sun-synchronous Polar to polar
Quantization	8 bit (256 levels)
Swath width	60 km (37.28-mi)

Repeat cycle		16 days	
Sensor		ASTER	

Table 4.8 : Imaging characteristics of ASTER.

Band	Spectral Resolution (m)	Wavelength (µm)	Description
1	15	0.52-0.600	Visible green/yellow
2	15	0.630-0.690	Visible red
3N	15	0.760-0.860	Near infrared
3B	15	0.760-0.860	Near infrared
4	30	1.600-1.700	Short-wave infrared
5	30	2.145-2.185	Short-wave infrared
6	30	2.185-2.225	Short-wave infrared
7	30	2.235-2.225	Short-wave infrared
8	30	2.295-2.365	Short-wave infrared
9	30	2.360-2.430	Short-wave infrared
10	90	8.125-8.475	Thermal infrared
11	90	8.475-8.825	Thermal infrared
12	90	8.925-9.275	Thermal infrared
13	90	10.250-10.950	Thermal infrared
14	90	10.950-11.650	Thermal infrared

5. DIGITAL IMAGE PROCESSING

5.1 Digital Image

Objects in the real scene can be represented by a two-dimensional image. The images can be divided in two categories, analog and digital. Aerial photographs are examples

of analog images while satellite images acquired using electronic sensors are examples of digital images. A digital image is consisting of two-dimensional arrays of pixels, which are the picture elements and represent a square area on Earth's surface that is a measure of sensor's ability to resolve the objects of different sizes (Figure 5.1). Each pixel has brightness value, which is also called as intensity value in the digital image. Intensity value usually is a single number that represents the brightness of the pixel such as the solar radiance in a given wavelength band reflected from the ground, emitted infrared radiation or backscattered radar intensity. The most common pixel format is the byte images, where this number is stored as an 8-bit integer giving a range of possible values from 0 to 255. Typically, zero is taken to be black and 255 is taken to be white. Values in between, make up the different shades of gray.
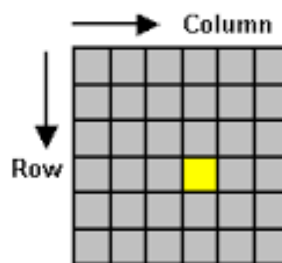
Figure 5.1 : Digital image.

5.2 Image Statistics

For analyzing the digital remote sensing data, image statistics are important. In general, bivariate and multivariate statistics of the multispectral remotely sensed data are considered. This normally involves computing the maximum and minimum values of each band, mean, standard deviation, variance, covariance matrix, correlation matrix, and frequencies of brightness values for each band. Such statistics provides valuable information necessary for processing and analyzing remotely sensed data.

5.2.1 Histogram

The histogram is popular graphical tool. İt is used to summerize discrete or continuous data that are measured on an interval sacale. It is often used to illustrate the major features of the distribution of the data in an appropriate form. In remote sensing, the image histogram describes the statistical distribution of image pixels in terms of the number of pixels at each DN (Figure 5.2). It is calculated simply by counting the

number of pixels in the scene at each brightness value. Image histogram also can be defined, as is a graphical representation of the tonal distribution in a digital image. It plots the number of pixels for each tonal value. Image histogram contains no information about the spatial distribution of pixels and just specifies the number of pixels at each DN; however, spatial information can be extracted from the histogram. Histogram is also a useful tool for image enhancement. Stretching, as a common contrast enhancement technique, is used to expand the range of DNs at one or both ends of plot [27].
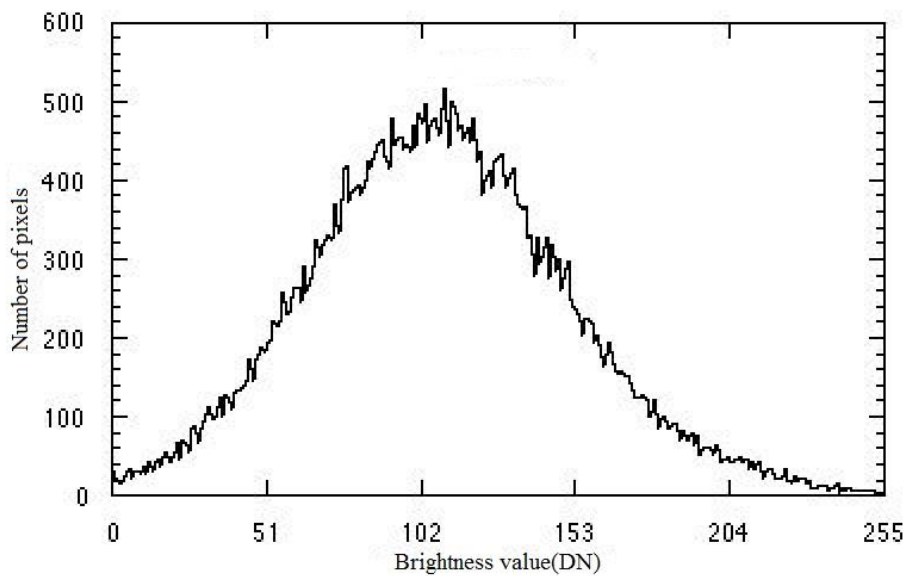
Figure 5.2 : Approximately normal distributed histogram.

5.2.2 Statistical parameters

Mean (µ): The mean is equal to the sum of every possible value divided by the number of values (Figure 5.3). There are two ways for calculating mean of DN: in the first approach, the sum of the DNs of all pixels in the image is divided by the total number of pixels; while, the second approach weights the DN by corresponding histogram value and then sums the weighted DNs [27].

BV= Brightness value

μ_B= mean of blue band

28
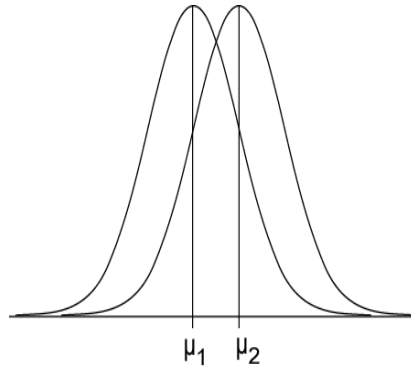
Figure 5.3 : Mean value.

Variance (σ^2): is the average squared deviation of all possible observations from the sample mean. The variance of a band of imagery, σ^2, is computed using the following equation:

$$Var_B = \frac{\sum_{i=1}^{n}(BV_{iB} - \mu_B)^2}{n - 1} \qquad \textbf{(5.1)}$$

Standard Deviation (σ): is the positive square root of the variance, which is used to quantify the amount of variation of a set of data values (Figure 5.4). A standard deviation close to 0 indicates that the data points tend to be very close to the mean of the set, while a high standard deviation indicates that the data points are spread out over a wider range of values. Image standard deviation can be used as a measure of image contrast [27].

$$S_B = b = \sqrt{Var_B} \qquad \textbf{(5.2)}$$
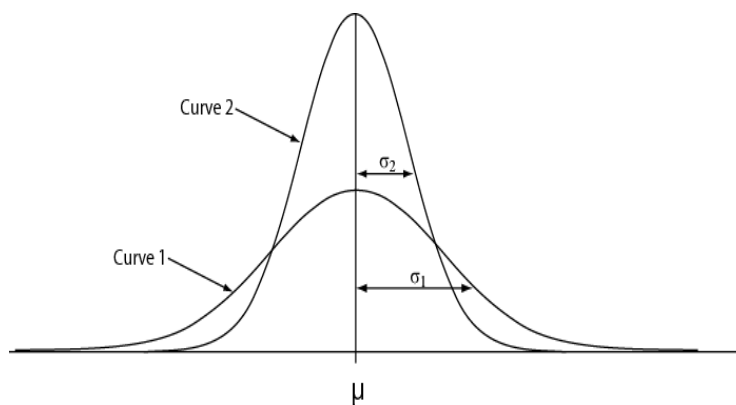
Figure 5.4 : Standard deviation.

Covariance: is a measure of how much two random variables change together. If the variables tend to show similar behavior, the covariance is positive and when the

29

variables tend to show opposite behavior, the covariance is negative. The sign of the covariance therefore shows the tendency in the linear relationship between the variables.

$$COV_{BG} = \frac{SP_{BG}}{n-1} \tag{5.3}$$

$$SP_{BG} = \sum_{i=1}^{n}(BV_{iB} \times BV_{iG}) - \frac{\sum_{i=1}^{n}BV_{iB}\sum_{i=1}^{n}BV_{iG}}{n} \tag{5.4}$$

SP= corrected sum of product

5.2.3 Correlation

The correlation is one of the most common and most useful statistics. A correlation is a single number that describes the degree of relationship between two variables. The correlation between two bands (for example, Blue and Green bands) of remotely sensed data, r_{BG}, is the ratio of their covariance (cov_{BG}) to the product of their standard deviations $S_B S_G$.

$$r_{BG} = \frac{cov_{BG}}{s_B \, s_G} \tag{5.5}$$

Correlation coefficient "r" measures the degree to which B and G bands go together always between −1 and 1.

r ≡ Pearson's product-moment correlation coefficient

$r \approx 0 \Rightarrow$ no correlation

$r > 0 \Rightarrow$ positive correlation

$r < 0 \Rightarrow$ negative correlation

The closer r is to 1 or −1, the stronger the correlation. In order to measure the direction and strength of the linear relationship between two quantitative variables, scatter plots are used for implying straight-line association. Strong linear relationship happens, when the points lie close to a straight line and weak if they are widely scattered (Figure 5.5).

| Perfect positive correlation | Strong positive correlation | Moderate positive correlation |
| Perfect negative correlation | Strong negative correlation | Moderate negative correlation |
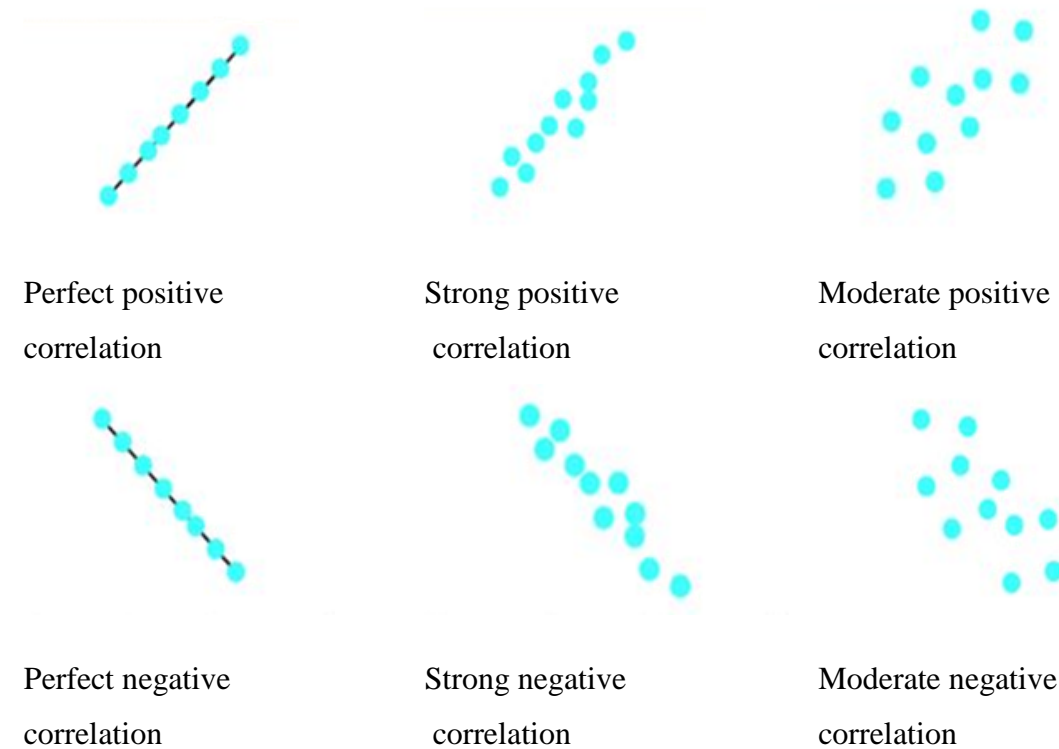
Figure 5.5 : Correlational direction and strength.

Regression Model: Regression is a statistical technique for assessing the relationship between dependent and one or more independent variable. The relationship between two variables is characterized by how they vary together. In regression, one variable is considered independent (=predictor) variable (*X*) and the other the dependent (=outcome) variable *Y*; however, in correlation, the two variables are treated as equals.

Simple Linear Regression: Simple linear regression is typically used to model the relationship between two variables X and Y so that given a specific value of X, that is, $X = x$, it is possible to predict the value of Y [28].

There are some basic assumptions in calculation of simple regression such as;

Linearity: The relationship between Y and X is linear (straight-line relationship).

Residuals: Residuals are independent and normally distributed.

Homoscedasticity: The variance of the residuals is equal for all X

Error measurement: There is no measurement error on X (impractical assumption): < 10% is assumed to be an adequate measurement error.

In simple linear regression, different values of x will produce different values of y according to the following equation:

$$y = \beta_0 + \beta_1 x \qquad \textbf{(5.6)}$$

31

The slope β_1 is the mean increase in Y for increase in X or vice versa and intercept β_0 is the starting point when X= 0. Both Y and X vary according to normal distributions when normal distributions all have the same standard deviation. Regression line describes how the mean response changes with x. If there are several observations with the same X value, the response of Y to a given X is a random variable that can take different values. Regression equation and line represent the simple linear equation and describe the shape of the relationship between the variables in 2-dimensional space (Figure 5.6).
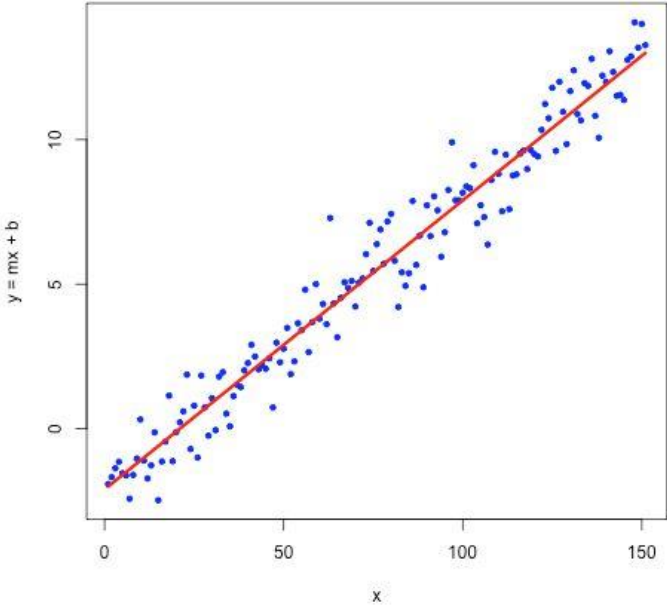
Figure 5.6 : Simple linear regression.

Multiple Linear Regression: An extension of simple linear regression is multiple regression. This regression method predicts the value of one variable (Y) based on the value of two or more other variables (X_1, X_2, …., X_k) (Figure 5.7).
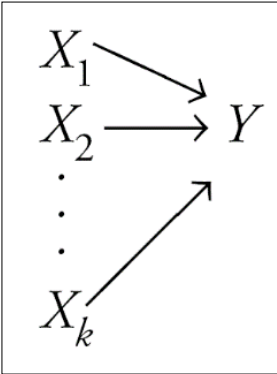
Figure 5.7 : Multiple regression.

$$y_{pred} = A + B_1X_1 + B_1B_2 + \ldots + B_nX_n \tag{5.7}$$

Ypred = dependent variable or the variable to be predicted.

X = the independent or predictor variables

A = "raw score equations" include a constant or Y

B= weights or partial regression coefficients.

Multiple linear regression produces a model that identifies the best-weighted combination of independent variables to predict the dependent variable. MLR estimates the relative importance of several hypothesized predictors and assesses the contribution of the combined variables to change the dependent variable.

There are some basic assumptions in calculation of multiple regressions such as;

Independence: The data of any particular subject are independent of the data of all other subjects.

Normality: In the population, the data on the dependent variable are normally distributed for each of the possible combinations of the level of the X variables.

Homoscedasticity: In the population, the variances of the dependent variable for each of the possible combinations of the levels of the X variables are equal. **Linearity**: In the population, the relation between the dependent variable and the independent variable is linear when all the other independent variables are held constant.

Multiple regressions simultaneously consider the influence of multiple explanatory variables on a response variable Y. The purpose is to look at the independent effect of each variable while "adjusting out" the influence of potential confounders. A multiple regression model with two explanatory variables fits a regression plane in *3-dimensional* space (Figure 5.8).
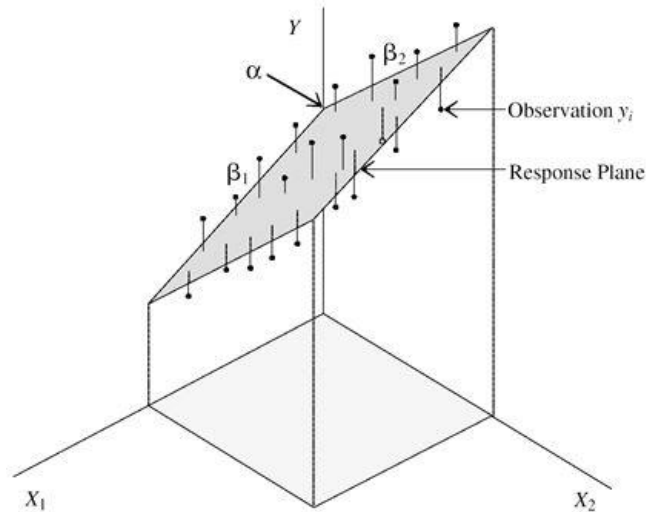
Figure 5.8 : Regression plane in 3-d space.

α : Intercept α predicts where the regression plane crosses the Y axis, S

β_1 : The slope for variable X_1 (β_1) predicts the change in Y per unit X_1 holding X_2 constant

β_2 : The slope for variable X_2 (β_2) predicts the change in Y per unit X_2 holding X_1 constant

In order to know differences of simple linear regression and multiple linear regression, Table 5.1 is provided:

Table 5.1 : Comparison of simple linear regression and multiple linear regression.

Simple linear regression	Multiple linear regression

One dependent variable Y predicted from one independent variable X	One dependent variable Y predicted from a set of independent variables $(X_1, X_2 ....X_k)$
One regression coefficient	One regression coefficient for each independent variable
R^2: proportion of variation in dependent variable Y predictable from X	R^2: proportion of variation in dependent variable Y predictable by set of independent variables (X's)

Stepwise Regression: Stepwise method is a semi-automated process of building a model by successively adding or removing predictors in a stepwise manner until there is no justifiable reason to enter or remove more. Stepwise regression requires two significance levels: one for adding variables and one for removing variables. The cutoff probability for adding variables (p-value) should be less than the cutoff probability for removing variables so that the procedure does not get into an infinite loop.

Nonlinear Regression: In order to mathematically describe the nonlinear relationship between a response variable and one or more predictor variables, it is suggested to use nonlinear regression. Specifically, when it is not possible to adequately model the relationship with linear parameters it is better to use nonlinear regression instead of ordinary least squares regression. The data are fitted by a method of successive approximations. Exponential functions, logarithmic functions, power functions, Gaussian functions are the examples of nonlinear functions. In order to assess the nonlinear regression, the response variables should follow the special trend of one of the functions. Since the field measurements data of our study was not suitable for any trend nonlinear regression, it was not used in the analysis.

5.3 Image Resolution

Remote sensing systems have four resolutions in the spatial, spectral, temporal and radiometric measurement domains.

Spatial Resolution: The spatial resolution (also known as ground resolution) is the ground area imaged for the instantaneous field of view (IFOV) of the sensing device.

Spatial resolution may also be described as the ground surface area that forms one pixel in the satellite image. The IFOV or ground resolution of the Landsat Thematic Mapper (TM) sensor, for example, is 30 m. The ground resolution of weather satellite sensors is often larger than square kilometers. There are satellites that collect data at less than one-meter ground resolution but these are classified military satellites or very expensive commercial systems (Figure 5.9).

Figure 5.9 : Same imagery with different spatial resolution, a) 2.4 m, b) 30 m.

Spectral Resolution: The spectral resolution of a sensor system is the number and width of spectral bands in the sensing device. The simplest form of spectral resolution is a sensor with one band only, which senses visible light. An image from this sensor would be similar in appearance to a black and white photograph from an aircraft. A sensor with three spectral bands in the visible region of the EM spectrum would collect similar information to that of the human vision system. The Landsat TM sensor has seven spectral bands located in the visible and near to mid-infrared parts of the spectrum and Landsat ETM[+] sensor has one panchromatic band in addition to the same seven bands of TM sensor.

Multispectral and hyperspectral images consist of several bands of data. For visual display, each band of the image may be displayed one band at a time as a grey scale image, or in combination of three bands at a time as a color composite image. Interpretation of a multispectral color composite image will require the knowledge of the spectral reflectance signature of the targets in the scene (Figure 5.10).
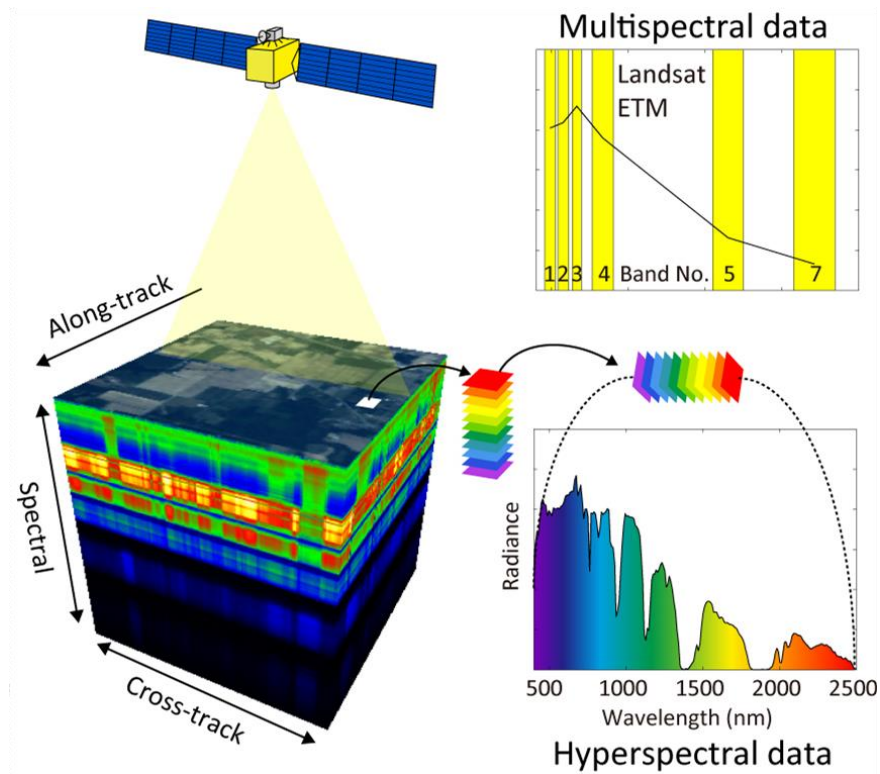
Figure 5.10 : Comparison of multispectral and hyperspectral sensors.

Radiometric Resolution: Radiometric resolution refers to the smallest change in intensity level that can be detected by the sensing system. Radiometric resolution is limited by the number of discrete quantization levels used to digitize the continuous intensity value. Higher radiometric resolution allows a sensor to provide a more detailed measurement within a specific portion of the electromagnetic spectrum (Figure 5.11).

4 bit quantization   3 bit quantization   2 bit quantization   1 bit quantization
      (16 level)   (8 level)   (4 level)   (2 level)
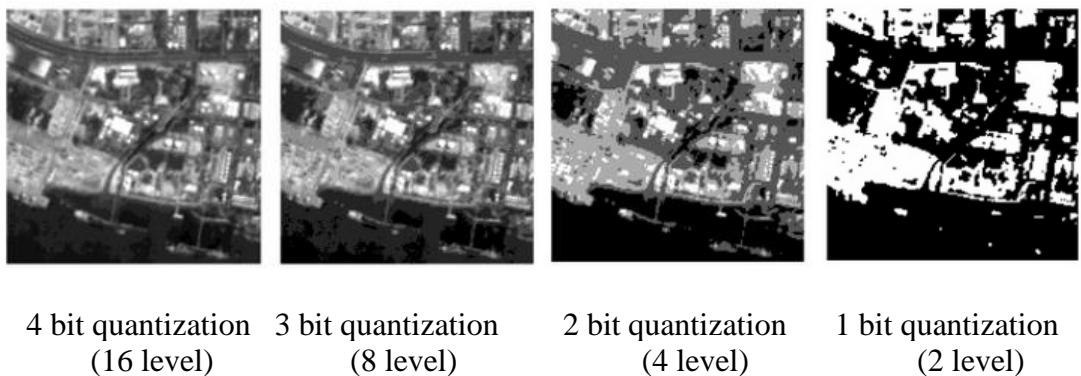
Figure 5.11 : Different levels of quantization.

Temporal Resolution: Temporal resolution refers to how often a remote sensing platform collects images of an area. Geo-stationary satellites can provide continuous data, while the more common orbiting satellites can only provide data each time they pass over an area (Figure5.12). Landsat 7 makes over 14 orbits per day, in its sun-synchronous orbit. During the full 16 days of a repeat cycle, coverage of the areas between those shown is achieved.

Images of an area, taken at different times (monthly, yearly or per decade) can be used for multitemporal analysis. Seasonal changes of vegetation, the expansion of cities over decades and documentation of forest clearance in the tropical rainforests are the examples of multitemporal analysis (Figure 5.13).
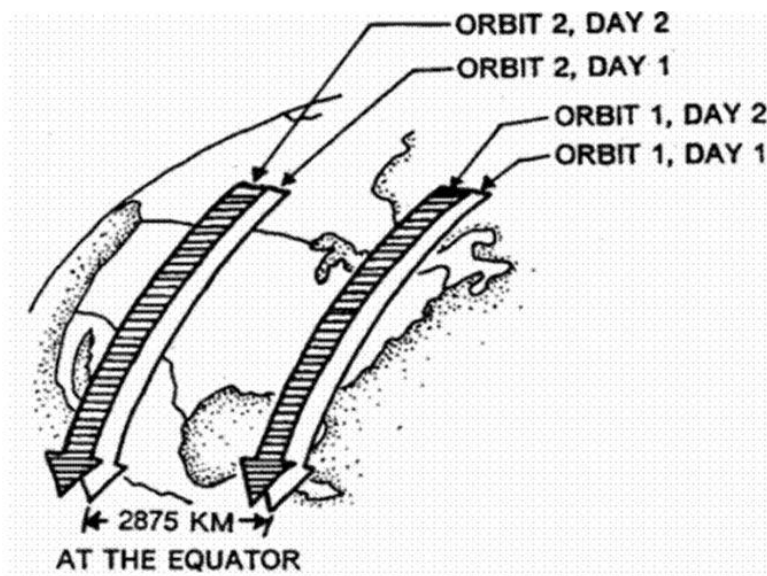
Figure 5.12 : Temporal resolution.
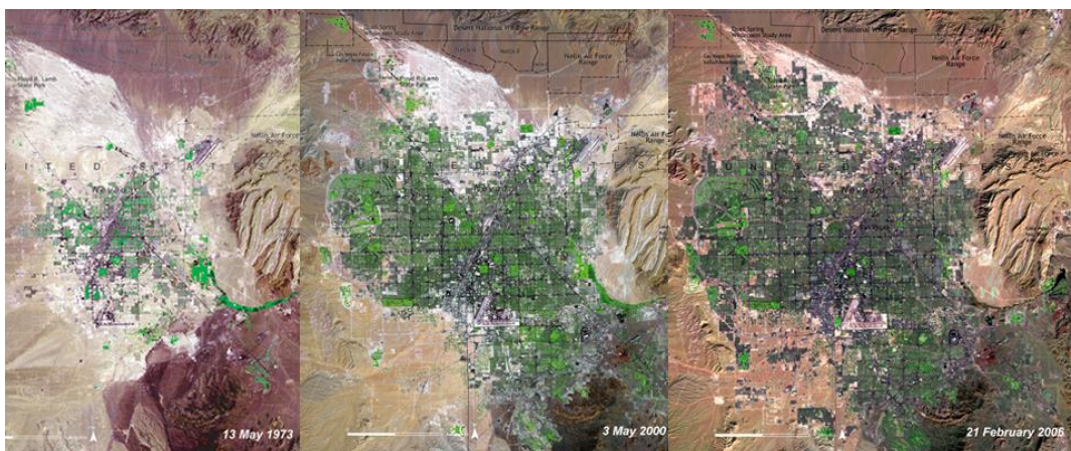
Figure 5.13 : Landsat images of Las Vegas over time in 1973, 2000 and 2006.

5.4 Preprocessing

Preprocessing of the satellite images is essential to enhance the visual appearance of images and to ease the handling of datasets. Image preprocessing involves the processing phases such as atmospheric correction or normalization, image registration, geometric correction and masking prior to further processing steps like classification and change detection.

Atmospheric Correction: The objective of atmospheric correction is to retrieve the surface reflectance (that characterizes the surface properties) from remotely sensed imagery by removing the atmospheric effects. Radiometric corrections should be done on the raw digital image data to correct for brightness values of the object on the ground, that have been distorted because of sensor calibration or sensor malfunction problems. The distortion of images is caused by the scattering of reflected electromagnetic light energy due to a constantly changing atmosphere. This is one source of sensor calibration error.

Atmospheric correction algorithms basically consists of two major steps: first, conversion of the Digital Number (DN) to Spectral Radiance (L_λ) and second, conversion of this spectral radiance to surface reflectance. In first step, the spectral radiance (L_λ) is calculated using the following equation :

$$L_\lambda = Gain \times DN + Bias \qquad (5.8)$$

where;

L_λ is the cell value as radiance,

DN is the cell value digital number,

Gain is the gain value for a specific band, and

Bias is the bias value for a specific band.

The second step involves the calculation of the top of atmosphere (TOA) reflectance for each band, which corrects for illumination variations (sun angle and Earth-sun distance) within and between scenes.

$$\rho\lambda = \frac{\pi \, d^2 L_\lambda}{ESUN_\lambda \cos \theta} \qquad (5.9)$$

where;

ρ_λ is reflectance as a function of bandwidth,

d is the Earth-sun distance correction,

L_λ is radiance as a function of bandwidth,

$ESUN_\lambda$ is exoatmospheric irradiance, and

θ_s is solar zenith angle.

Regarding sensor (ETM+), one of the most important and widely used application of atmospheric correction is unstripping of Landsat 7 satellite.

The scan-line corrector (SLC) of the Landsat 7 (ETM+) sensor failed permanently in 2003, and approximately 22% of the data in a Landsat 7 scene missed. Acquiring imagery without a functional SLC became a major obstacle for Landsat ETM+ data applications. Landsat 7 products have data gaps, but are still useful and maintain the same radiometric and geometric corrections as data collected prior to the SLC failure [29].

In order to fill the gaps of Landsat 7 data, it is logical to make use of the information of the neighboring pixels to restore spectral reflectance of missing pixels. This method can be used by correction algorithms found in popular remote sening softwares like ERDAS, ARCGIS and ENVI. Here is the example of destripped Landsat 7 imagery of the study area (Seyhan plate in Adana district) corrected by ERDAS software (Figure 5.14).

(a)   (b)
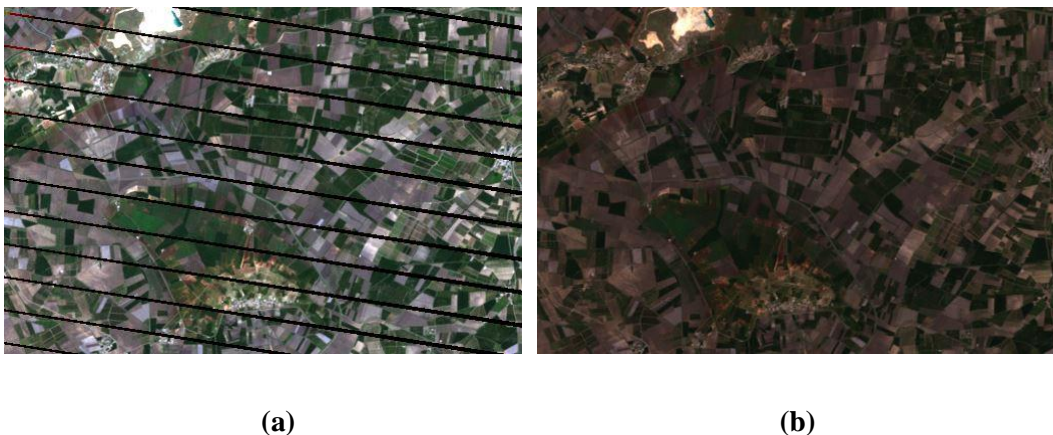
Figure 5.14 : Scan line correction of the Landsat 7 image: a) Stripped image, b) Destripped image.

Geometric correction: Digital images collected from satellite sensors often contain systematic and unsystematic geometric errors. Some of these errors can be corrected by using ephemeris of the platform, known internal sensor distortion characteristics. Other errors can only be corrected by matching image coordinates of physical features, recorded by the image to the geographic coordinates of the same features, collected from a map or Global Positioning System (GPS). Conversion of the data to real world coordinates are carried out by analyzing well distributed Ground Control Points (GCP). Resampling is used to determine the digital values in order to place them in the new pixel locations of the corrected output image while using three different methods.

Nearest neighbor: Nearest neighbor resampling uses the digital value from the pixel in the original image which is nearest to the new pixel location in the corrected image. This is the simplest method and does not alter the original values, but may result in some pixel values being duplicated while others are lost. This method also tends to result in a disjointed or blocky image appearance (Figure 5.15 a).

Bi-linear interpolation: Bilinear interpolation resampling takes a weighted average of four pixels in the original image nearest to the new pixel location. The averaging process alters the original pixel values and creates entirely new digital values in the output image (Figure 5.15 b).

Cubic convolution: is a method used to determine the gray levels in an image through a weighted average of the 16 closest pixels to the input coordinates. The resulting value is then assigned to the output coordinates. This method generally is considered better than bilinear interpolation, and it does not have the disjointed appearance of nearest neighbor interpolation. Cubic convolution requires about 10 times the computation time required by the nearest neighbor method (Figure 5.15 c).

(a)   (b)   (c)
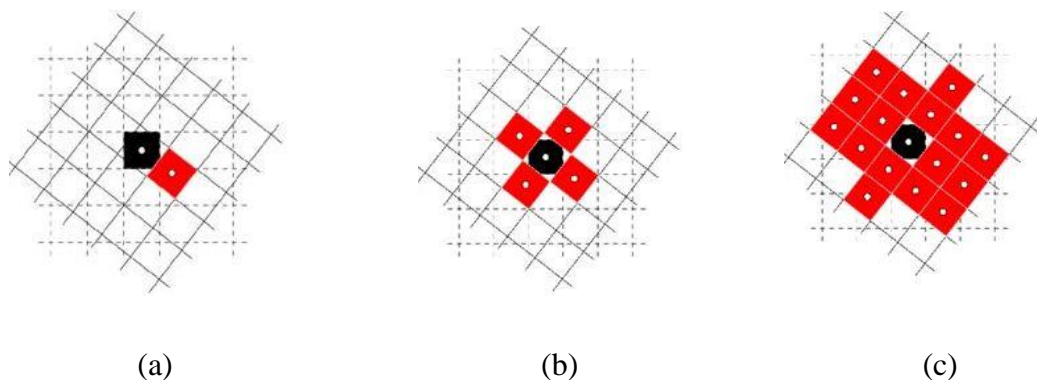
Figure 5.15 : Resampling methods. a) Nearest neighbor, b) Bi-linear interpolation, c) Cubic convolution.

5.5 Spectral Indices

Spectral indices are the combinations of spectral bands at two or more wavelengths that indicate relative abundance of features of interest. There are various types of indices with different arithmetic formula used for different cases according to the characteristics of features and purpose of study.

The indices were progressed in four different stages. The first indices are those developed from simple band ratios and used for inferring the spectral properties of vegetation through its growing period. The second stage is referred to the development of indices designed to reduce the impacts of the background such as soil response. The third indices are developed to compensate for the effects of atmospheric distortion. The fourth and final stage of development procedure refers to the new spectral indices development different from vegetation health. Indices that are used for burned area assessment and fire severity are in the last developed group of indices. By applying the spectral indices to remotely sensed data, the sensitivity of certain surface properties is maximized. Furthermore, the indices are capable of normalizing or reducing effects due to sun angle, viewing angle, the atmosphere, topography, instrument noise, etc. to make consistent spatial and temporal comparisons possible [30].

5.5.1 Soil salinity indices

A wide range of band combination and indices are developed for vegetation strength, crop assessment and land use change in many studies. However, there is not enough information about the band combinations/indices meant for saline soil and salt-affected lands in the literature. In general, the soil indices as arithmetic relations of bands are resulted from the spectral characteristics of soil [31].

Fukuhara introduced a soil index (SI) to eliminate the effect of vegetation canopy reflectance in a partially vegetated terrain. Similarly, various spectral salinity indices were derived from the values of all or part of the image spectral bands for salt mineral detection and mapping [32].

Khan, *et al* in 2001, proposed band combinations to discriminate salt-affected areas. Bands used in the salinity indices were selected after examining the spectral reflectance pattern of salt-affected soils. They found that salt-affected soil reflect more incident light energy in visible spectrum (0.45–0.68 mm) than those of other land cover

features [33]. Metternichit and Zinck (1997) also found that salt-affected lands had high spectral reflectance in the visible portion, particularly in the blue and red range [34].

Normalize Differential Salinity Index (NDSI) was proposed as one of the most used salinity indices by using the band red (R) and near infrared (NIR) portion of spectrum. It is computed by dividing the difference between Near-infrared reflectance and Red visible reflectance to their sum, as indicator of soil salinity [33].

$$NDSI = (R - NIR)/(R + NIR)$$

<div align="right">(5.10)</div>

Beside the NDSI, there are different indices used for distinguishing saline soil or evaluating salt-affected soils. The common salinity indices used in literature are summerized in Table 5.2.

Table 5.2 : Common salinity indices used in literature.

Salinity indices	Equation[*]	Reference
Normalized Differential Salinity Index	$NDSI = \dfrac{(R - NIR)}{(R + NIR)}$	[33]
Brightness Index	$BI = \sqrt{R^2 + NIR^2}$	[33]
Salinity index 1	$SI = \sqrt{B \times R}$	[33]
Salinity index 2	$SI = \sqrt{G \times R}$	[35]
Salinity index 3	$SI = \sqrt{G^2 + R^2 + NIR^2}$	[35]
Salinity index 4	$SI = \sqrt{G^2 + R^2}$	[35]
Salinity index 5	$SI = \dfrac{B_5}{B_6}$	[36]
Salinity index 6	$SI = \dfrac{B_4 - B_5}{B_4 + B_5}$	[36]
Salinity index 7	$SI = \dfrac{B_5 - B_6}{B_5 + B_6}$	[36]
Salinity index 8	$SI = B_5 - B_6$	[36]
Salinity index 9	$SI = \dfrac{(B_5 \times B_6 - B_6 \times B_6)}{B_5}$	[36]
Salinity index 10	$SI = \dfrac{B}{R}$	[37]
Salinity index 11	$SI = \dfrac{(B - R)}{(B + R)}$	[37]
Salinity index 12	$SI = \dfrac{G \times R}{B}$	[37]
Salinity index 13	$SI = \dfrac{B \times R}{G}$	[37]
Salinity index 14	$SI = \dfrac{R \times NIR}{G}$	[37]

Abbriviation used in equations:

B= Blue; G= Green; R= Red;

NIR= Near infrared;

B_5= Short wave infrared; B_6= Short wave infrared

Among the indices given in Table 5.2, the most popular two indices which are relatively good in distinguishing saline soil are the first two indexes.

$$BI = \sqrt{R^2 + NIR^2} \qquad \textbf{(5.11)}$$

$$SI = \sqrt{B \times R} \qquad \textbf{(5.12)}$$

Where B and R stand for the spectral reflectance measurements acquired in the visible (Blue) and (Red) regions, respectively.

There are also other indices calculated by using hyperspectral satellite data. Three different salinity indices developed by Bannari *et al* (2008) to detect the light and moderate soil salinity effects using EO-1 ALI data are given below [36].

$$SI - 1 = ALI9 - ALI10 \qquad \textbf{(5.13)}$$

$$SI - 2 = (ALI6 - ALI9)/(ALI6 + ALI9) \qquad \textbf{(5.14)}$$

$$SI - 3 = (ALI9 - ALI10)/(ALI9 + ALI10) \qquad \textbf{(5.15)}$$

These indices can also be used in other satellites such as Landsat TM due to spatial resolution similarity between two satellites.

Table 5.3 shows the spectral bands of the EO-1 ALI sensor and their respective wavelengths in comparison with spectral bands of Landsat ETM$^+$. The pixel size of ALI is very similar to Landsat7 ETM$^+$, except for the higher-resolution (10 m) in the panchromatic (Band 1) for ALI, and is 30 m in all other bands, 2 to 10 [38].

Table 5.3 : Comparison between the ALI and ETM+ bands and spectral ranges.

EO-1 ALI			Landsat ETM [+]		
Band	Wavelength(μm)	Alternate designation	Band	Wavelength(μm)	Description
1	0.048-0.69	(PAN)	8	0.52-.90	panchromatic
2	0.433-0.453	(MS-1')	Not available		VNIR(blue)
3	0.45-0.515	(MS-1)	1	0.45-0.52	VNIR(blue)
4	0.525-0.605	(MS-2)	2	0.53-0.61	VNIR(green)
5	0.63-0.69	(MS-3)	3	0.63-0.69	VNIR(red)
6	0.775-0.805	(MS-4)	4	0.78-0.90	VNIR
7	0.845-0.89	(MS-4')	Not available		VNIR
8	1.2-1.3	(MS-5')	Not available		SWIR
9	1.55-1.75	(MS-5)	5	1.55-1.75	SWIR
10	2.08-2.35	(MS-7)	7	2.09-2.35	SWIR
	Not available		6	10.40-12.50	TIR

5.5.2 Vegetation indices

Vegetation indices can be used in soil salinity studies besides the salinity indices because halophytic plants grow naturally in saline soils, and can be adapted to high soil salinity. Therefore, vegetation has been used as an indirect indicator to predict and map soil salinity. Many studies prove the effectiveness of NDVI index in soil salinity detection. Pérez González *et al* and Bannari *et al* have agreed that NDVI has a significant role in salinity examination, but some scientists have not the same viewpoint. Pérez González [39] found that NDVI was very proper in detecting halophytic plant and relating it to saline soils by correlating the NDVI of halophytic vegetation with EC of soil; however, in 2008 Metternicht *et al* argued that detecting soil salinity using the NDVI was challenging because the presence of vegetation could cause spectral confusion with the reflectance properties of salt [34].

Vegetation indices reflect the physical characteristics of vegetation including leaf area, biomass, photosynthetic activity, productivity and percent cover and minimize the consequences of internal factors such as canopy geometry and soil properties and

external factors such as the noises caused by sun angle and atmosphere on the spectral data [40].

To define an index that is sensor–independent, the ratio must be specified in terms of geophysical parameter, such as reflectance. One of the earliest indices used in remote sensing applications was "Ratio Vegetation Index (RVI)".

$$RVI = \frac{NIR}{R}$$

(5.16)

where;

NIR = Near infrared

R= Visible (Red) portion of electromagnetic spectrum.

The Normalized Difference Vegetation Index (NDVI) is the most often used vegetation index and because of the ratio properties of it, it is an operational vegetation index, which make the NDVI to reduce most of the noise caused by changing sun angles, topography, clouds or shadow, and atmospheric conditions. It defined as the ratio of the difference between near-infrared reflectance and red visible reflectance to their sum, is an indicator of vegetation productivity.

$$NDVI = (NIR - VIS)/(NIR + VIS)$$

(5.17)

Where, *VIS* and *NIR* stand for the spectral reflectance measurements acquired in the visible (red) and near-infrared regions, respectively. Calculations of NDVI for a given pixel always result in a number that ranges from minus one (-1) to plus one (+1); however, no green leaves give a value close to zero. A zero means no vegetation and close to +1 (0.8 - 0.9) indicates the highest possible density of green leaves. It is used extensively to monitor vegetation on continetal and global scales, but appears to be a poor indicator of vegetation biomass if the ground cover is low, as in arid and semi arid regions [41].

Similar to the normalized difference vegetation index, red and near-infrared canopies reflectance or radinaces are utilized for producing the new index named Soil Adjusted Vegetation Index (SAVI), which is a superior vegetation index for low cover environment.

$$SAVI = \frac{NIR - VIS}{NIR + VIS + L} \times (1 + L) \qquad \textbf{(5.18)}$$

Where, "L" is a constat that is empirically determined to minimize the vegetation index sensitivity to soil backgroynd reflectance variation. If L is zero, SAVI is the same as NDVI. For intermediate vegetation cover ranges, L is typically around 0.5. the factor (1+L) ensures that the ranges of SAVI is same as NDVI, namely [-1,+1] [42].

Backgrund soil is mostly effective in vegetation indices in the case of intermediate levels of vegetation on area. In highly vegetated areas, there are not significant soil signals coming out of vegetation canopy while there is not enough vegetation for separating the canopy scattered and soil reflected signals on lowly vegetated region [31]. SAVI incorporates canopy background correction, for example, a correction for the underlying soil background.

Atmosphere is one of the other external factors that are not related to vegetation itself and can influence vegetation index behavior. Assossiaton of an empirical term for atmosphere correction leads to Enhanced Vegetation Index (EVI) [27].

$$EVI = G \times \frac{NIR - RED}{L + NIR + C_1 VIS - C_2 BLUE} \qquad \textbf{(5.19)}$$

C1, C2 are the coefficients of the aerosol resistance term, which uses the blue band to correct for aerosol influences in the red band.

5.6 Image Classification

Image classification is the process to produce thematic maps from imagery. The themes can range from different categories such as soil, vegetation and water in general or in more detailed description type of soils, vegetation and water depths. The most important factor in creating thematic map from remotely sensed imagery is that the categories selected for the map should be distinguishable in the image [27].

Electromagnetic radiation reflected by similar objects on the Earth's surface can have similar spectral properties. The goal of classification is to identify homogeneous groups of pixels with similar spectral signature, and based on their spectral information represented by the digital numbers, classify them in different groups or classes and by this process make it possible to model the Earth's surface. Different methods have

been developed to classify digital images by spectral properties of the objects present in the image.

5.6.1 Density slicing

One of the most common and simple image processing routine for information extraction is density slicing. Density slicing is the process in which the pixel values are sliced into different ranges and for each range, a single value or color is assigned in the output image. It is also known as level slicing and works best on single band images. It is especially useful when a given surface features has a unique and generally, narrow set of DN values (Figure 5.16).

A=255-200 DN
B=199-170 DN
C=169-140 DN
D=139-120 DN
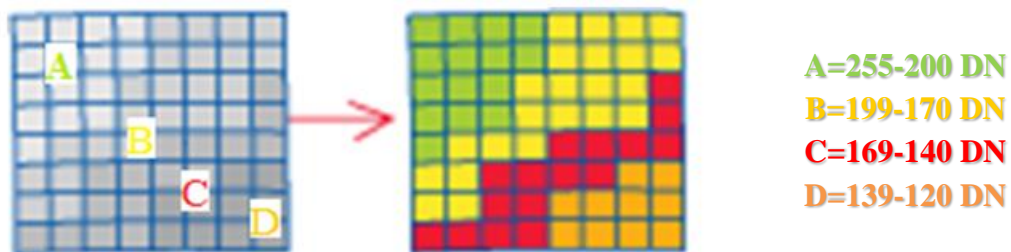
Figure 5.16 : Density slicing.

5.6.2 Supervised classification

In supervised classification, the spectral features of some areas of known land cover types are extracted from the image based on the experience and prior knowledge of the region or using thematic map. These samples of land cover types are known as the "training areas". Every pixel in the whole image is then classified as belonging to one of the classes depending on how close its spectral features are to the spectral features of the training areas. A few pixels in a scene do not match and remain unclassified, because these may belong to a class not recognized or defined.

5.6.3 Unsupervised classification

This method is more computer-automated, and the computer uses techniques to determine the pixels with similar data values and groups them into classes. The user must have knowledge of the area being classified when the groupings of pixels with common characteristics, produced by the computer, have to be related to actual features on the ground (such as wetlands, developed areas, coniferous forests, etc.).

5.7 Accuracy Assessment

Accuracy indicates that how well the classified images identifies the land cover type on the ground. The accuracy of a classification is usually assessed by comparing the classification with some reference data that is believed to accurately reflect the true land cover. Sources of reference data include among other things ground truth, higher resolution satellite images, and maps derived from aerial photo interpretation.

Accuracy assessment should not be based on the training pixels. The problem with using training pixels is that they are usually not randomly selected, and that the classification is not independent of the training pixels. Using training pixels usually results in an overly optimistic accuracy assessment. The results of an accuracy assessment are usually summarized in a confusion matrix.

6. APPLICATION

The effectiveness of remote sensing data in detection of saline soils and its impact on agricultural farming area was examined by using Landsat 7 ETM $^+$ with 30 meters resolution and field collected data in Seyhan plate, Adana.

6.1 Study Area

Cukurova is a district in south central of Turkey covering the provinces of Adana and Mersin. Adana lies in the heart of Cukurova and is located at the Northeastern edge of the Mediterranean Sea where it serves as the gateway to the Cukurova plain (Figure 6.1).

Cukurova is located in the coordinates of 37°02′52″ North latitudes and 35°17′54″ East longitudes. The total area of the Çukurova is about 38,000 km², Turkey's biggest delta plain with a large stretch of flat and fertile land, which is among the most agriculturally productive areas of the world. The climate (relatively mild and humid in the winter months) and the alluvial soil make the area highly suitable for agriculture. Akarsu irrigation basin and Seyhan plate are located in Cukurova plain.

The delta is very flat, with the majority of the area being less than 20m above the sea level. The slope of the delta ranges between 0.1 to 1 %. The soil in the delta is alluvial which is developed from deposites of three main rivers.

Since 1980s, DSI started monitoring of the shallow water table level (monthly) and salinity (once a year in July), very intensively over the entire irrigated area. As reported by salinity of the shallow water table has been consistently decreasing over the years. Before the implementation of the project, the major driving force for bringing salt to the soil surface was the dry summer climate. The soil water flux was reversed to a downward direction after implementation of irrigation. Irrigation water supplied from the Seyhan reservoir has very low sodium content and the increase in its use, also contributed to the decline in salinity. This general trend of decrease of salinity agrees

with observations made in the downstream area where a salinity level of previously rain-fed land decreased with initiation of irrigation [43].
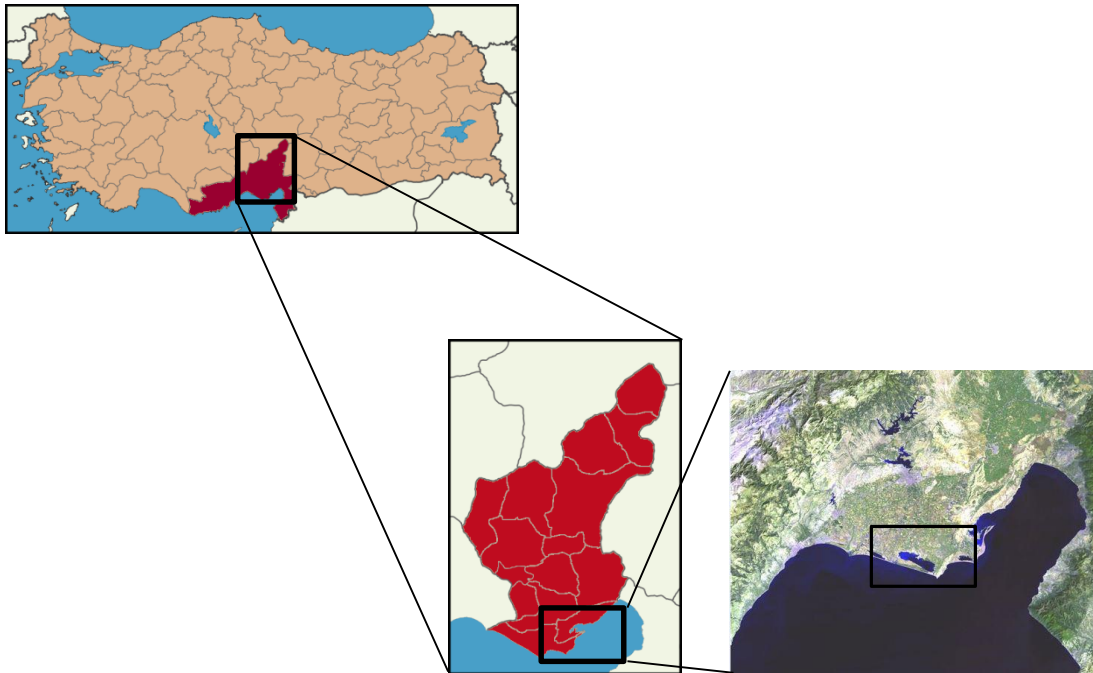
Figure 6.1 : Map and satellite image of the study area.

6.2 Data Used

For soil salinity mapping with remote sensing two types of data are required. The first and most important one is remotely sensed data like multispectral and hyperspectral satellite images acquired simultaneously with ground observations and the second one is ground-based salinity measurements.

6.2.1 Satellite data

In this study, the Landsat 7 ETM$^+$ satellite images with 30-meter resolution were used. Data is downloaded from the US Geologic survey's Earth Explorer database (http://earthexplorer.usgs.gov) for four different dates according to field measurements dates. The images were georectified to a Universal Transverse Mercator (UTM) coordinate system, using World Geodetic System (WGS) 1984 datum, assigned to north UTM zone 36 and Path 175 Row 34, 35. In order to overcome the problem of matching the time and seasonal differences of field work with remotely sensed data, the most compatible and close dates were selected. The dates of satellite images used are given in the Table 6.1.

Table 6.1 : The dates of Landsat 7 data used and field measurements.

Date of field measurements	Date of satellite pass
02-05-2009	19-04-2009
04-10-2009	12-10-2009
04-10-2010	31-10-2010
24-03-2010	21-03-2010

Data set consists of four Landsat images belonging to years 2009 and 2010 winter and summer cropping seasons, hence it is possible to evaluate the soil salinity conditions in both seasonal and annual periods. Since the study area is covering two frames of Landsat satellite (175/ 34 and 175/ 35), both frames of scene are downloaded and are mosaicked using ENVI software (5.0) to create a whole scene of the study area (Figure 6.2).

(a)   (b)

(c)
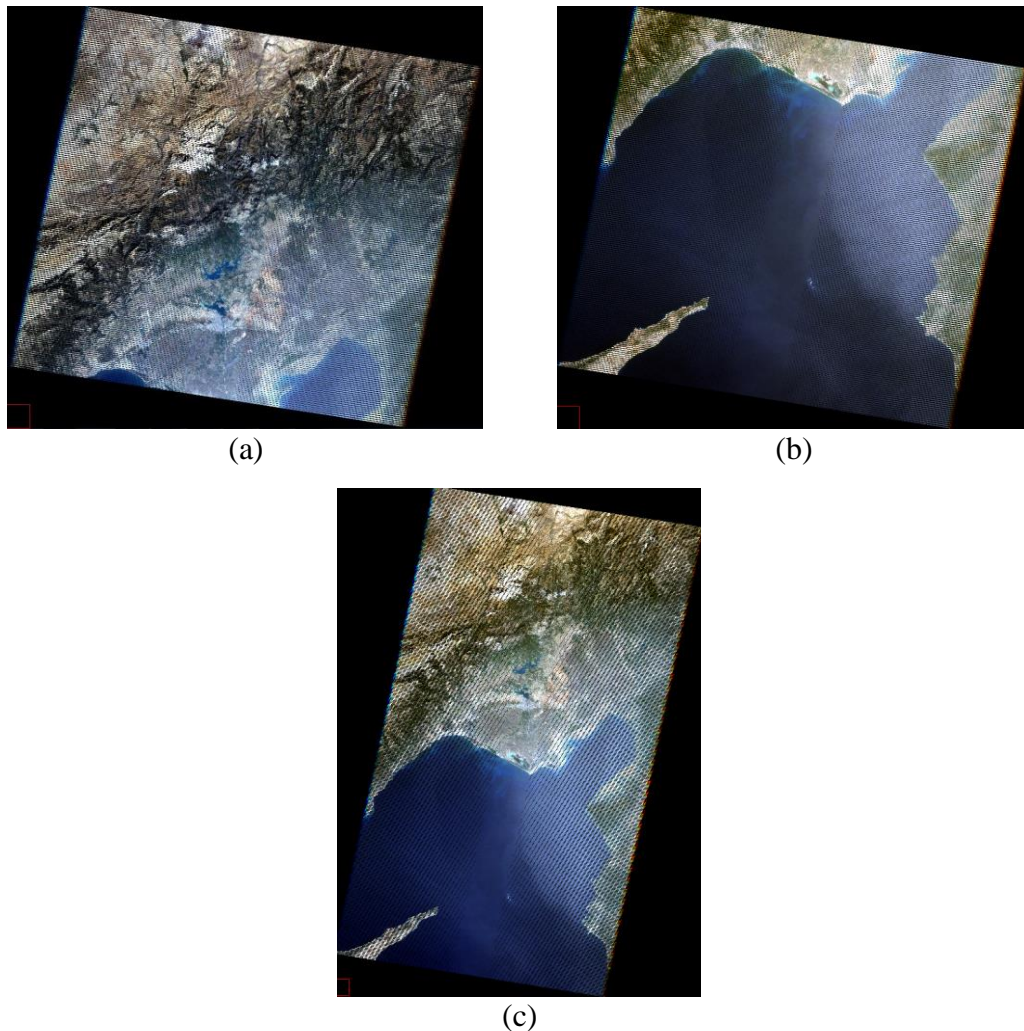
Figure 6.2 : Landsat 7- 12/10/2009 data (a) Frame 175/ 34 (b) Frame 175/ 35 (c) Mosaic image.

All Landsat 7 ETM+ data images were projected to the UTM Zone 36 with a geodetic system of WGS 84; however, the field data was collected in ED 50. Hence, satellite images are projected from WGS 84 to ED 50 in order to be compatible with filed observations.

6.2.2 Ground truth measurements

Fieldwork performed by Cukurova University, Remote sensing and GIS group in May 2009, October 2009, October 2010 and March 2010, are used in the analysis. Field measurements was done with TUBITAK project which name was "Analysis and Optimization of Irrigation Efficiencies in Order to Reduce Salinization Impacts in Intensively Used Agricultural Landscapes of the Semiarid Mediterranean Turkey (*MedSalin*)" in 2012, Adana.

Because of different weather conditions like rain and hot weather that affect the soil humidity and dynamic nature of plants, the most appropriate days were selected for fieldwork. In these dates, different numbers of soil samples and soil electrical conductivity were collected by using the EM-38 device. 688, 269,153, 27 samples were collected in dates of 12-Oct-2009, 31-Oct-2010, 19-Apr-2009, 21-Mar-2010, respectively (Figure 6.3).

Figure 6.3 : A field photo showing EC measurements by EM-38 device.

The EM-38 provides rapid survey with best sidelong resolution in depths of 0.75 to 1.5 meters in both vertical and horizonat directions [44]. The EM38 equipment has two modes for soil electrical conductivity measurements using electromagnetic induction: horizontal (average for 0–75 cm) and vertical (average for 0–150 cm soil horizon). Values of EM38 readings (mS m -1) were divided by 100 to convert to ECa

in units of dS m -1 , according to the EM38 manual [25]. The readings in different depths were callibrated by the calibration equation. After that, callibration outcome as a final result of EC value was obtained. As a next step, salinity point locations in the field were positioned on their corresponding to Landsat images for four different dates.This process was conducted in the same way as specifying the Ground Control Points (GCP) as done in the registration process. Figure 6.4 shows the distribution of 153 sample points on the Landsat image of 19th April 2009. The data collected in these surveys were used in salinity mapping in Seyhan plate of Adana.

Figure 6.4 : Distribution of field samples on the 19-Apr-2009 Landsat imagery.

6.3 Preprocessing

Before applying the indices and soil salinity analysis, some corrections should be applied to multitemporal Landsat images. In order to remove or reduce the influence of the atmoshpere, atmospheric correction is required. According to the purpose of study, it is useful to know the reflectance value, which largely removes variations between images due to sensor differences, the Earth-sun distance and solar zenith angle (caused by different scene dates, overpass time and latitude differences). Especially, this correction should be done in the studies, which are related to establishment of a relationship between ground measurements and spectral reflectance values [45].

Reflectance calibration is applied by deriving the reflectance value from the DN and calculating the top of atmosphere reflectance or TOA reflectance, which is the reflectance measured by a space-based sensor flying higher than the Earth's

atmosphere and includes contributions from clouds and atmospheric aerosols and gases. The correction was applied on a pixel-by-pixel basis for each scene and the output reflectance values scaled to an 8-bit data range. Some of the parameters for the conversion are available in the image header files, while the exoatmospheric irradiance values for Landsat 7 from NASA's (National Aeronautics and Space Administration) [46].

Reflectance values are extracted by using the reflectance calibration process provided by ENVI program for all images and their metadata provided in file with MTL extension. The resulted images are used as source images for the further analysis.

6.4 Spectral Indices

6.4.1 Soil salinity indices

Various spectral salinity indices developed in numerous studies related to salt detection and soil salinity mapping, are summarized in Table 5.2, in section 5.5.1. In this study, all different salinity indices, given in Table 5.2, are examined for all the Landsat images from years 2009 to 2010 and the result of most used four salinity indices (NDSI,SI 09, SI 14) are given in the Figure 6.5, Figure 6.7, Figure 6.9 and Figure 6.11. The Landsat image dated 31-October-2010 is not a mosaic image and it consists of only one frame (175, 35) covering the lower part of the study area. The frame (175, 34) that covers the upper part of the study area was not used in this study because of non-availability in the USGS archive.

Figure 6.5 : NDSI images of Seyhan plate (a)19th April,2009, (b) 12th   October, 2009, (c) 21st March, 2010, (d) 31st October, 2010.

As observable from NDSI images, saline areas with higher NDSI values are shown by brighter colors while the surfaces with low salinity are shown by darker colors. In this study, three main classes (Citrus, Wheat, and bare soil) were taken into consideration and nine different sites as a "Region of Interenst (ROI)" were selected in the study area for a better interpretation of the index images produced. The training sites were picked out from satellite images as representing these three classes. These nine sites (Citrus 1, Citrus 2, Citrus 3, Wheat 1, Wheat 2, Wheat 3, Bare soil 1, Bare soil 2, Bare soil 3) were chosen according to crop thematic map produced by Landscape Planning Department of the Cukurova University.

Table 6.2 shows the average NDSI value of three ROI's, selected for each class in four different satellite data obtained through 2009 to 2010.

Table 6.2 : Average NDSI values in three different ROI's.

Date	19-Apr-2009	12-Oct-2009	21-Mar-2010	31-Oct-2010
Citrus	-0.25	-0.10	-0.22	-0.23
Wheat	-0.27	0.04	-0.31	0.03
Bare soil	-0.15	0.04	-0.06	0.06

Figure 6.6 demonstrate the changes in the average NDSI values of three different classes from 2009 to 2010. Overall, Bare soil class has higher salinity among two other classes. As can be seen from the graph, Wheat shows more fluctuation in comparison with Bare soil and Citrus. Low amount of NDSI value is observed in the 19th April and it reaches to the highest amount in 12th October, 2009 and same progress occurs in the year 2010. The high amount of NDSI value in fall season (October) and low amount of it in the spring season (April-March) can be related to the presence of Wheat in farmland during March to April, which hinders the satellite sensor to sense the amount of soil salinity in spring season.
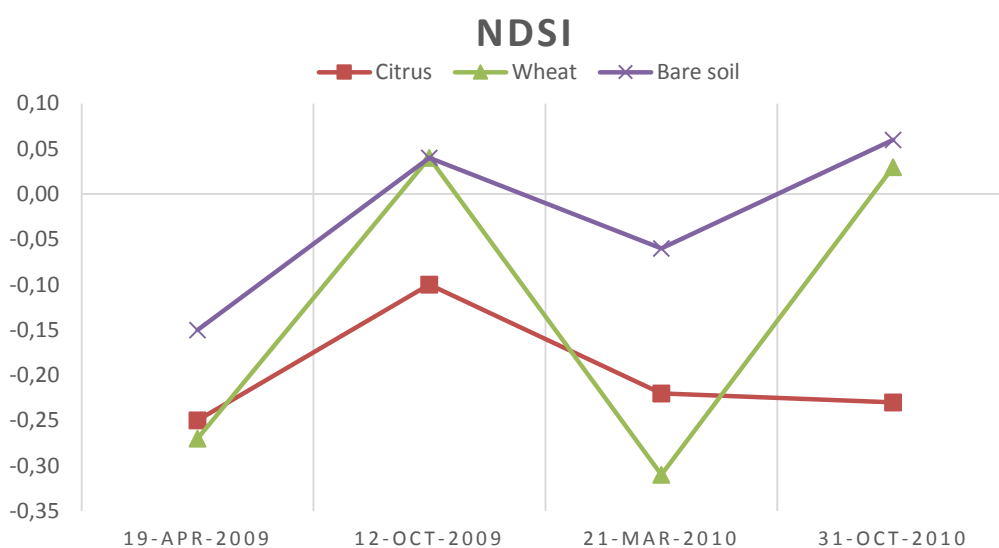
Figure 6.6 : Changes in the average NDSI values in the selected ROI's.

With regard to the Figure 6.7, high amount of salinity index (SI) value are represented with lighter colors like bright gray colors, where the low SI values are shown with dark colors.

Figure 6.7 : SI images of Seyhan plate (a)19th April,2009, (b) 12th October, 2009, (c) 21st March, 2010, (d) 31st October, 2010.

The average SI values of three classes and line graph of SI values, which shows the change trend of the selected three classes, are given in the Table 6.3 and Figure 6.8 respectively.

Table 6.3 : Average SI values in three different ROI's.

Date	19-Apr-2009	12-Oct-2009	21-Mar-2010	31-Oct-2010
Citrus	52.28	52.59	45.51	36.59
Wheat	48.90	60.85	42.39	41.63
Bare soil	55.61	59.16	54.56	43.75

With regards to the Figure 6.8, it can be noticed that all three clases almost shows the same trend of change in the period of 19th April, 2009 to 31st October, 2010. Among all, again Wheat shows more peaks in this period and reaches the highest amount in 12th October, 2009 and the lowest one in 21st March, 2010, because of the presence of crops on the field in this season.

SI
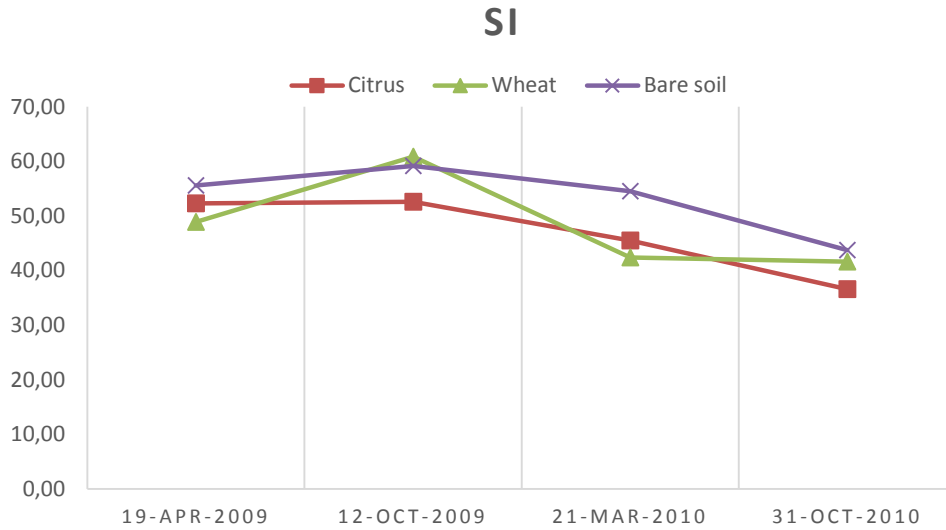
Figure 6.8 : Changes in the average SI values in the selected ROI's.

Regarding to SI 09 index results given in Figure 6.9, the high value of SI 09 which reperesent the high monunt salinity are shown in light colors and low SI 09 values are seen in darker colors and non saline areas are shown by black colors.

(a)   (b)

(c)   (d)

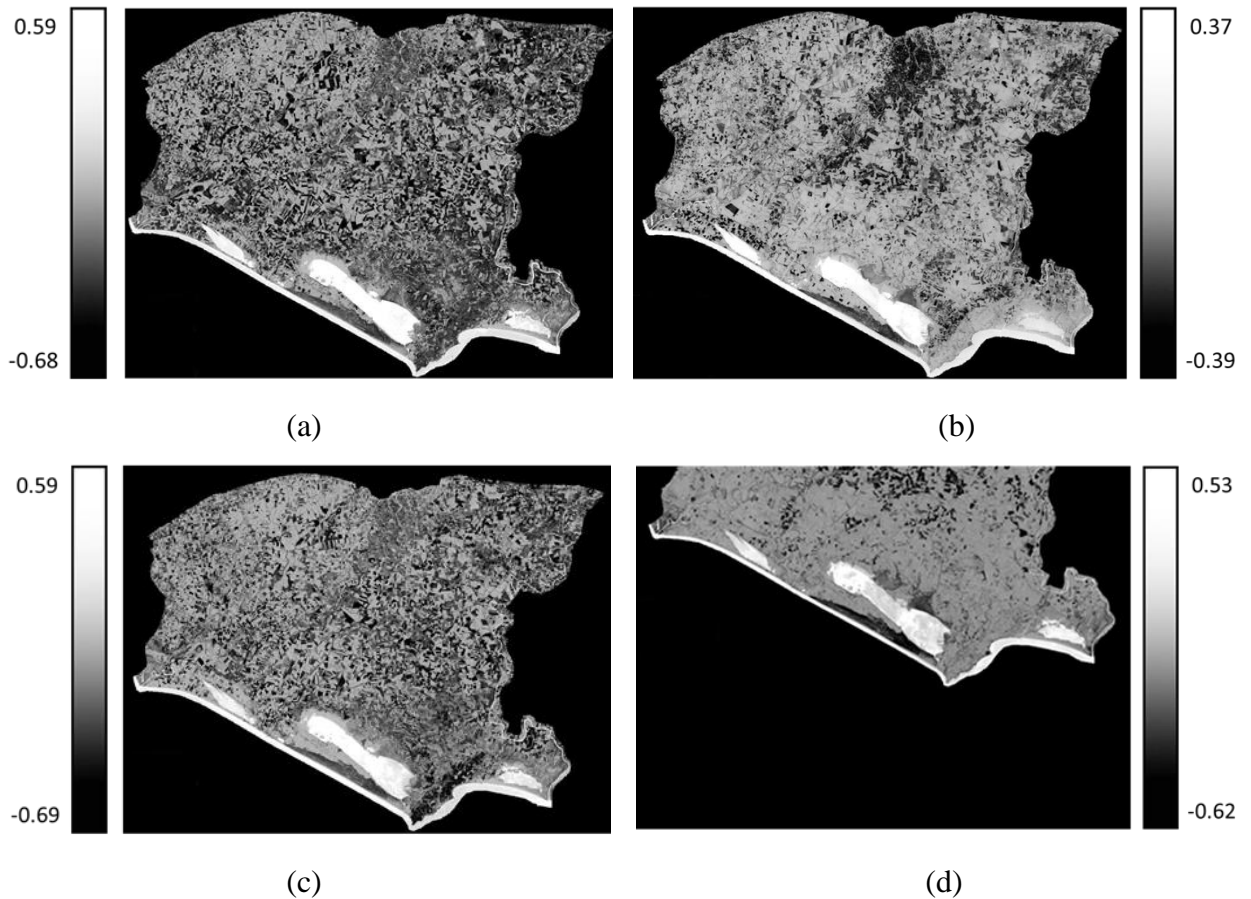**Figure 6.9 :** SI 09 images of Seyhan plate (a)19th April,2009, (b) 12th October, 2009, (c) 21st March, 2010, (d) 31st October, 2010.

The SI 09 average values given in Table 6.4 and the change trend of SI 09 given in Figure 6.10 show that among the three classes Bare soil class track the steady pattern during 19th April, 2009 to 21st March, 2010 and then gradually decreses untill it reaches to the lowest SI 09 value in 31st October, 2010. The other two classes, Citrus and Wheat, approximately follow the similar trend.

Table 6.4 : Average SI 09 values in three different ROI's.

Date	19-Apr-2009	12-Oct-2009	21-Mar-2010	31-Oct-2010
Citrus	79.71	59.86	64.98	49.42
Wheat	70.14	56.71	65.98	37.76
Bare soil	71.09	55.78	63.71	39.95
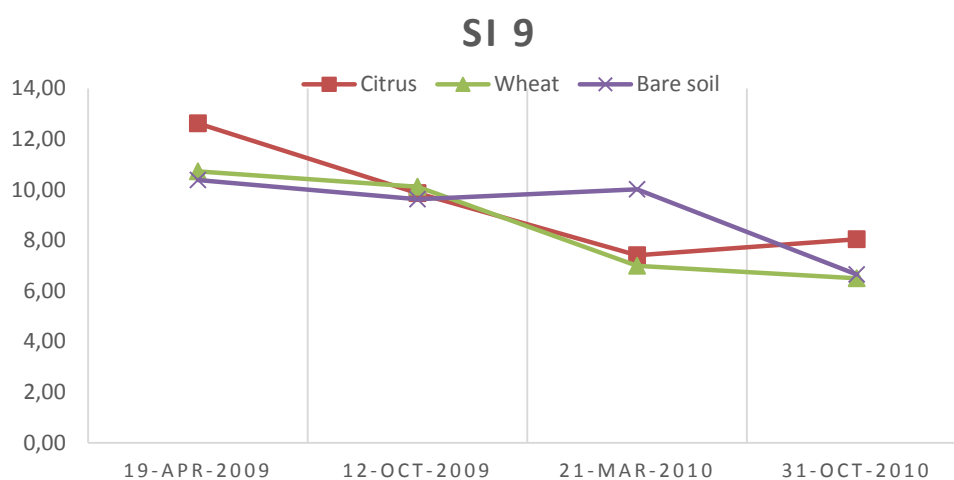
Figure 6.10 : Changes in the average SI 09 values in the selected ROI's.

As obvious from Figure 6.11, areas with more salinity are illustrated by light colors while the low saline parts are shown by dark colors and non saline part are seen as black.

Figure 6.11 : SI 14 images of Seyhan plate (a)19th April,2009, (b) 12th October, 2009, (c) 21st March, 2010, (d) 31st October, 2010.

Table 6.5 provides the average values of SI 14 in three different ROI's during the 19th April, 2009 to 31st October, 2010 period of time while, the Figure 6.12 gives the information of change trend of all classes according to amount of salt in the soil.

Table 6.5 : Average SI 14 values in three different ROI's.

Date	19-Apr-2009	12-Oct-2009	21-Mar-2010	31-Oct-2010
Citrus	79.71	59.86	64.98	49.42
Wheat	70.14	56.71	65.98	37.76
Bare soil	71.09	55.78	63.71	39.95

From the Figure 6.12 it is clear that all three classes follow the similar trend of changes with all decreasing during April to October and then gradually increasing until 21th March, 2010 and then decreasing again. However, the SI 14 value of Citrus remained higher that other classes over this period.

SI 14

Legend: Citrus, Wheat, Bare soil
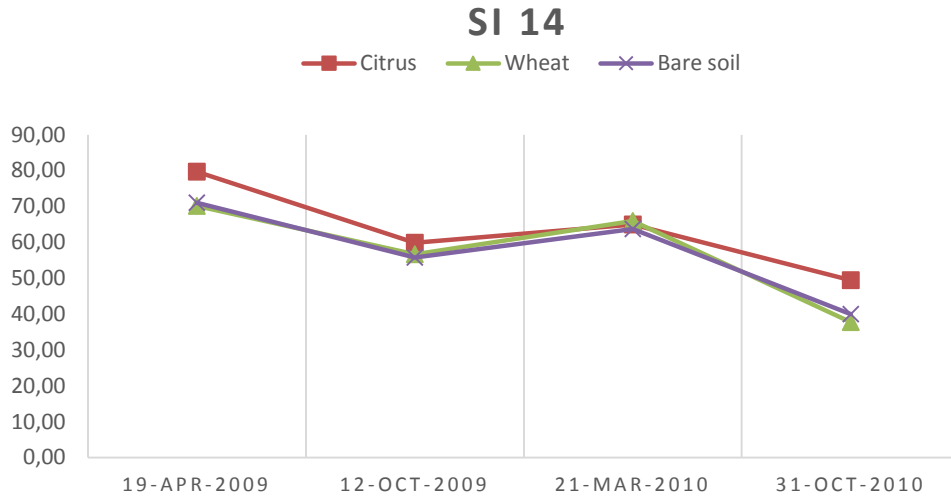
Figure 6.12 : Changes in the average SI 14 valuesin the selected ROI's.

6.4.2 Vegetation indices

Regarding to vegetation indices, the output images of NDVI and EVI indices, which are the most popular ones, are given in the Figure 6.13 and 6.15 respectively.
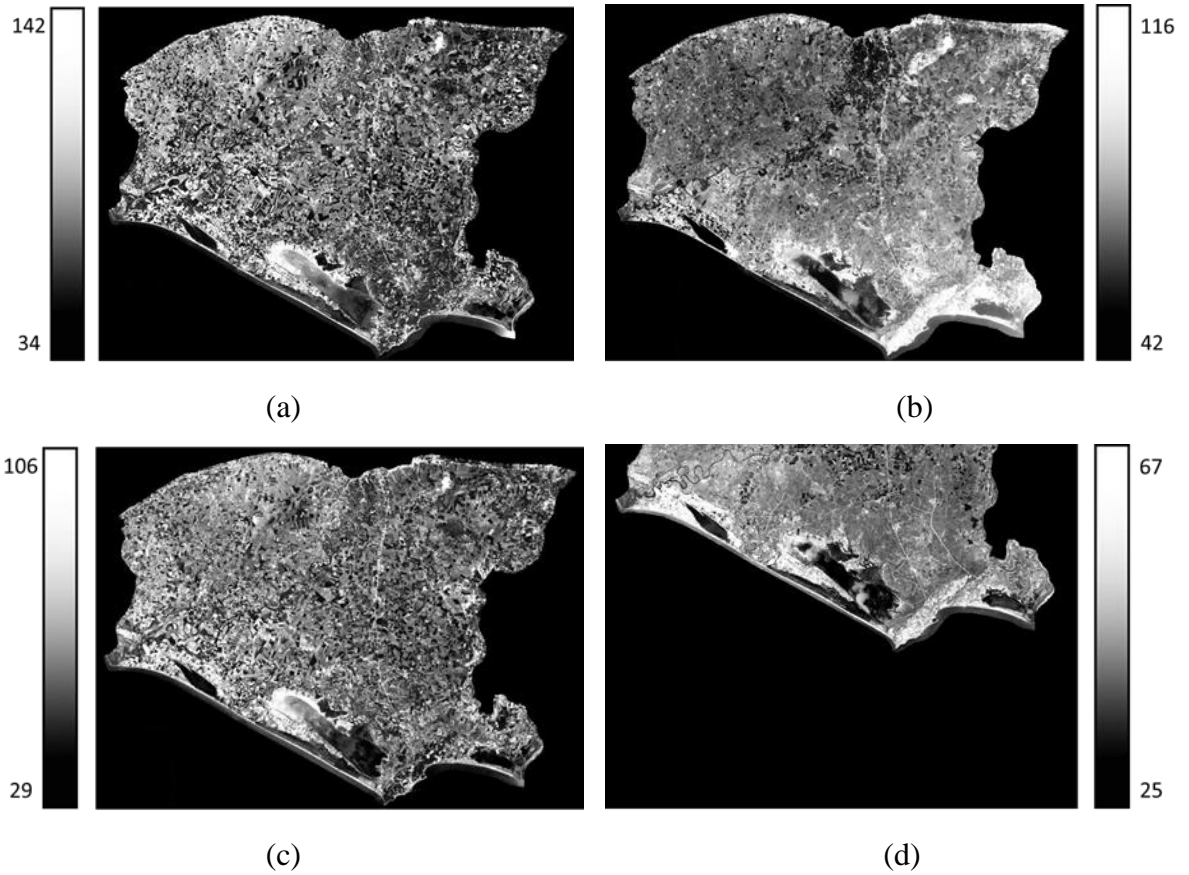

(a)

(b)

(c)

(d)
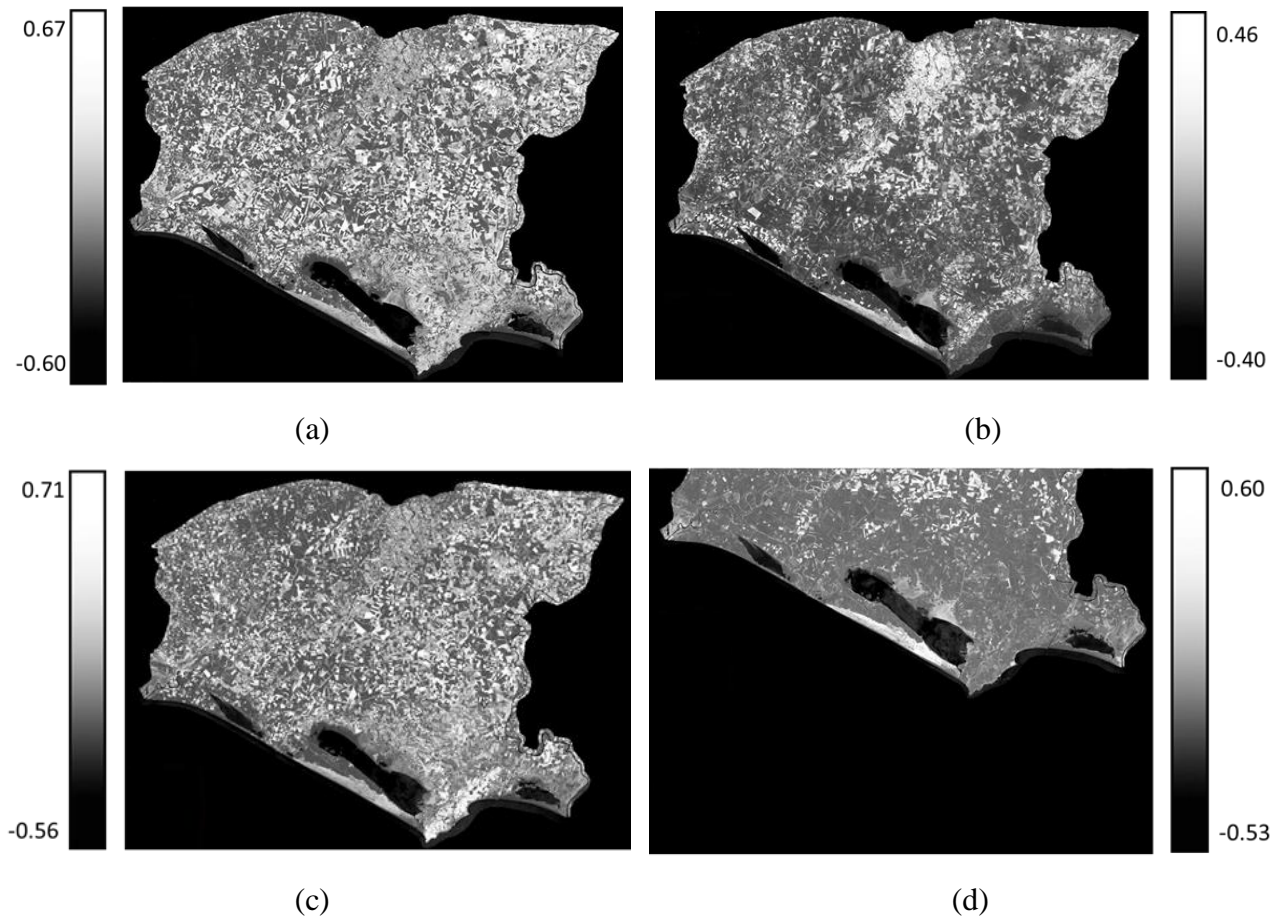
Figure 6.13 : NDVI images of Seyhan plate (a) 19th April, 2009, (b) 12th October, 2009, (c) 21st March, 2010, (d) 31st October, 2010.

In series of NDVI images of years 2009 to 2010, the changes of vegetation cover, by presenc of soil salinity in the area is represented. As shown in the Figure 6.13, the high values of NDVI are shown in white color, which, represent a higher consistency of the vegetation. Pixels get darker by the decrease in NDVI value. The ones close to -1 (dark color) represent the field with lack of vegetation, having bare soil or rock surface. In the NDVI image of the12th October 2009, it is seen that the area is covered with low vegetation that is shown by dark color and in the NDVI image of the 21st March, 2010 the vegetation are visible in the area by bright white color in the images.

Table 6.6 shows the average NDVI value of each three similar sites in four different dates through 2009 to 2010. These representative areas make it possible to estimate the overall trend of NDVI value in whole study area.

Table 6.6 : Average NDVI values in three different ROI's.

Date	19-Apr-2009	12-Oct-2009	21-Mar-2010	31-Oct-2010
Citrus	0.25	0.10	0.22	0.23
Wheat	0.27	-0.04	0.31	-0.03
Bare soil	0.15	-0.04	0.06	-0.06

As shown in Figure 6.14, the highest NDVI values during the peak growing season were obtained in the spring seasons (April-March). Overall, NDVI variations among the different salinity level sites were exactly opposite to the NDSI value, and amount of these indices are equal in absolute values, which means that, the more the soil is saline, the more halypathic vegetation such as Wheat can grow.
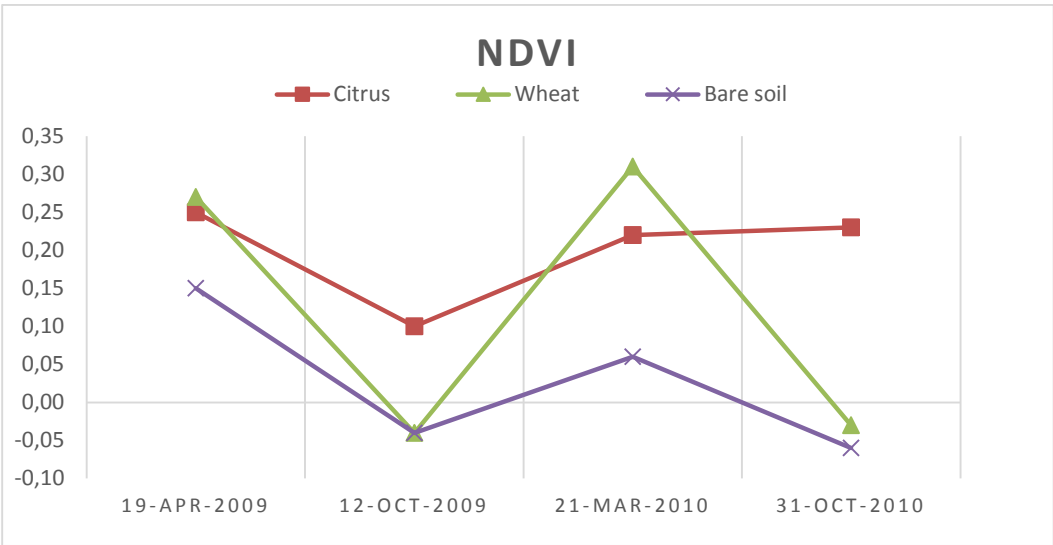
Figure 6.14 : Changes in the average NDVI valuesin the selected ROI's.

The Figure 6.15 refers to the changes of SAVI in four different satellite data sets, obtained from 2009 to 2010. Same as NDVI, highly vegetated areas are shown by light colors and areas with no vegetation are represented with dark colors.

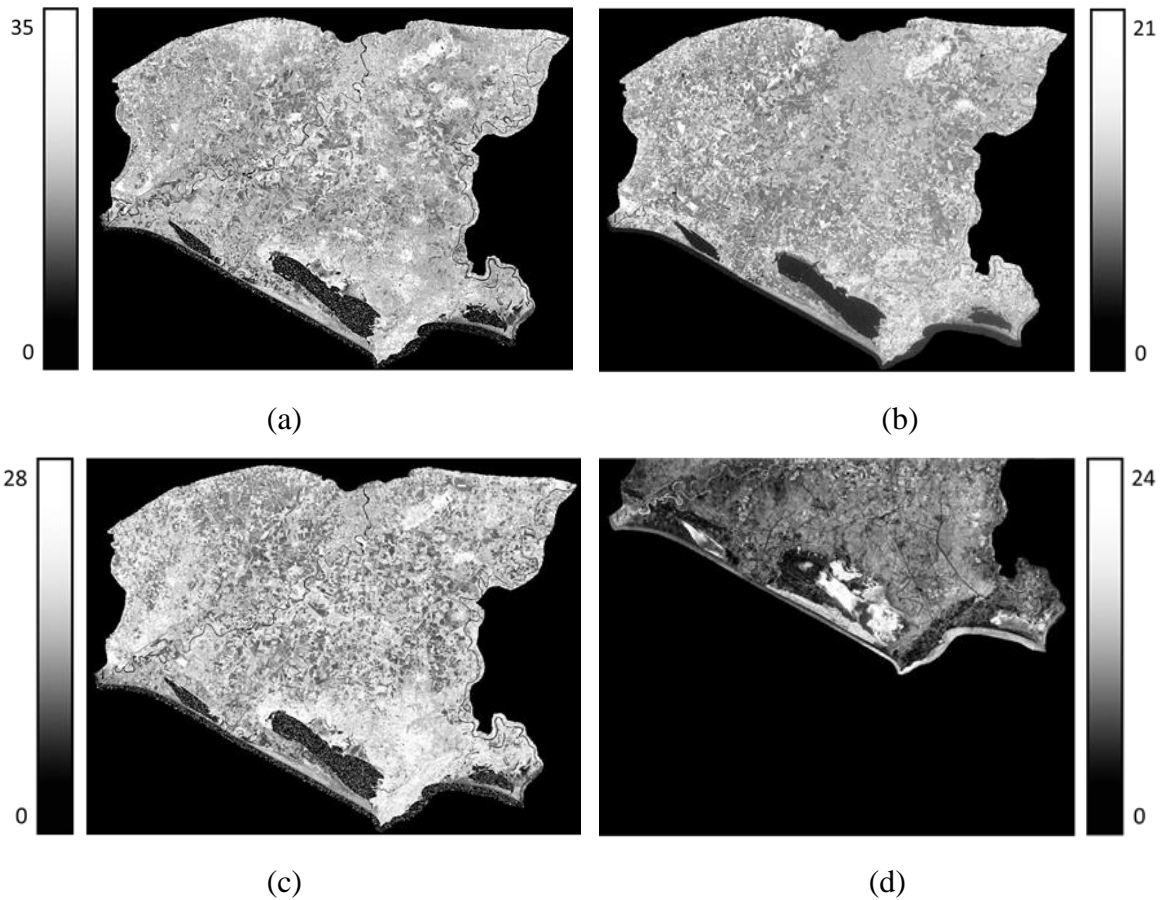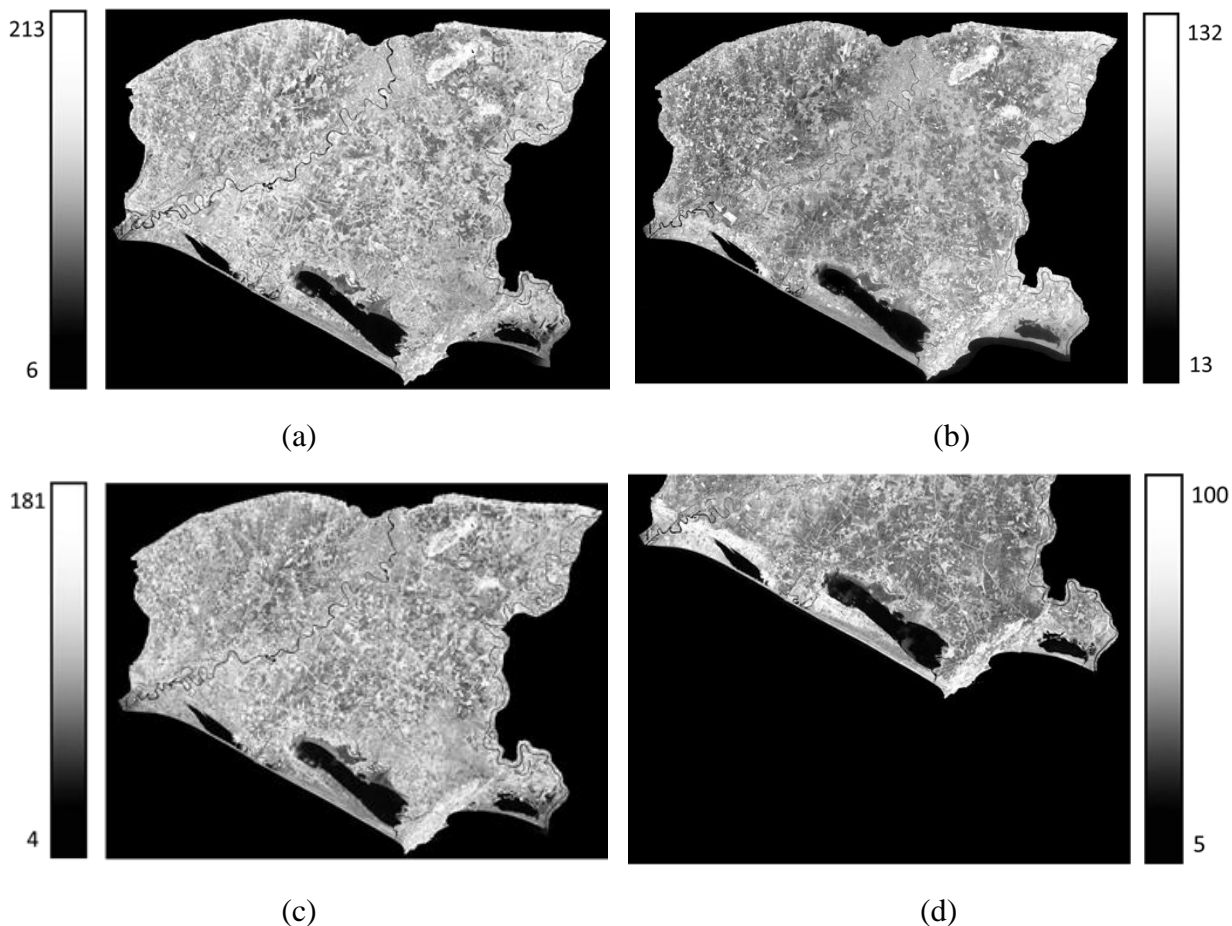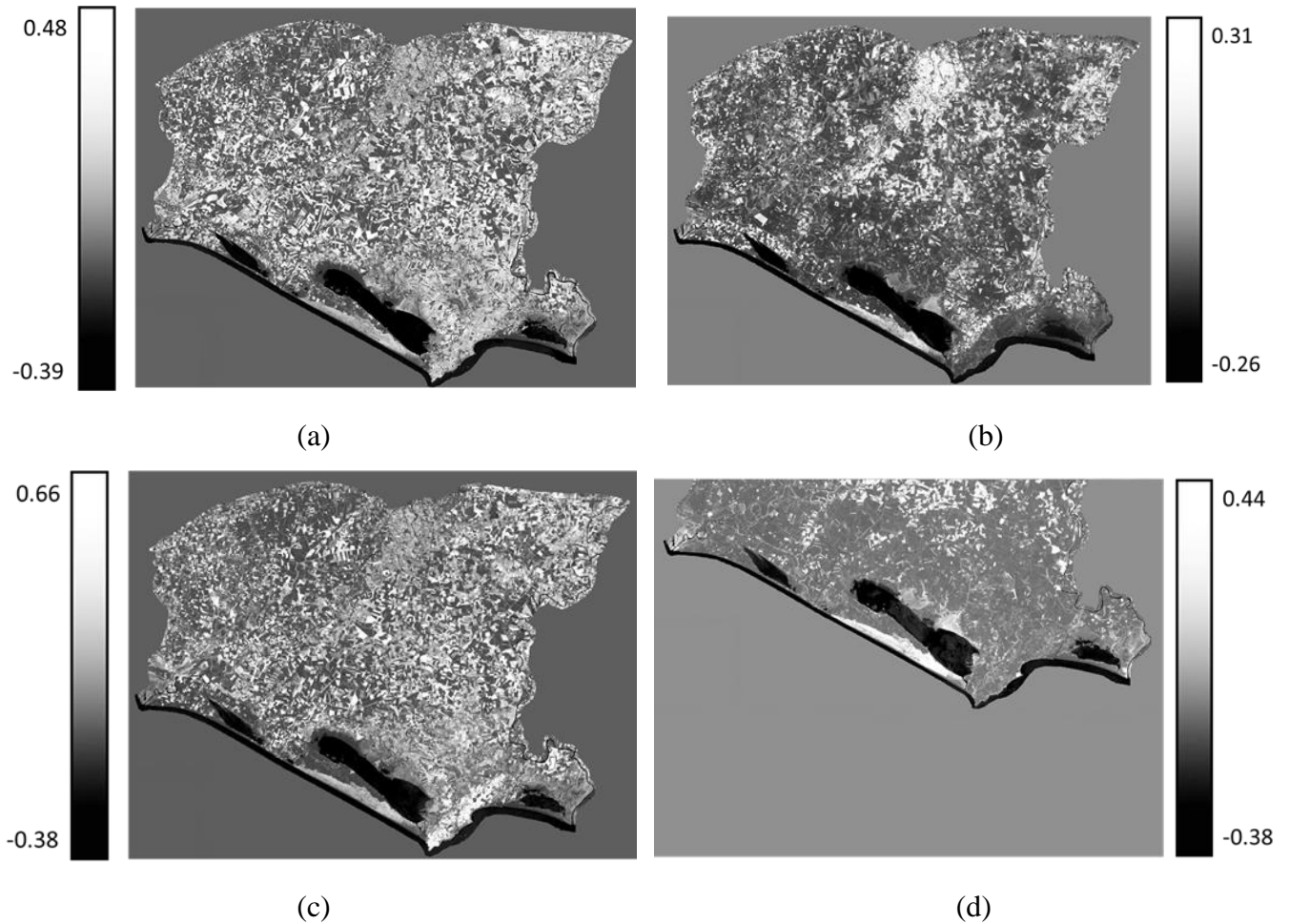**Figure 6.15 :** SAVI images of Seyhan plate (a)19th April,2009, (b) 12th October, 2009, (c) 21st March, 2010, (d) 31st October, 2010.

The average SAVI values are given in Table 6.7 and change trend of SAVI in Figure 6.16, illustrates that, all classes follow the same pattern as NDVI results. It can be seen that the SAVI value reaches to the highest amount on 21st March, 2010 in comparison to the Citrus and Bare soil during the 2009 to 2010.

Table 6.7 : Average SAVI values in three different ROI's.

Date	19-Apr-2009	12-Oct-2009	21-Mar-2010	31-Oct-2010
Citrus	0.16	0.07	0.14	0.15
Wheat	0.17	-0.02	0.21	-0.02
Bare soil	0.10	-0.04	0.04	-0.04
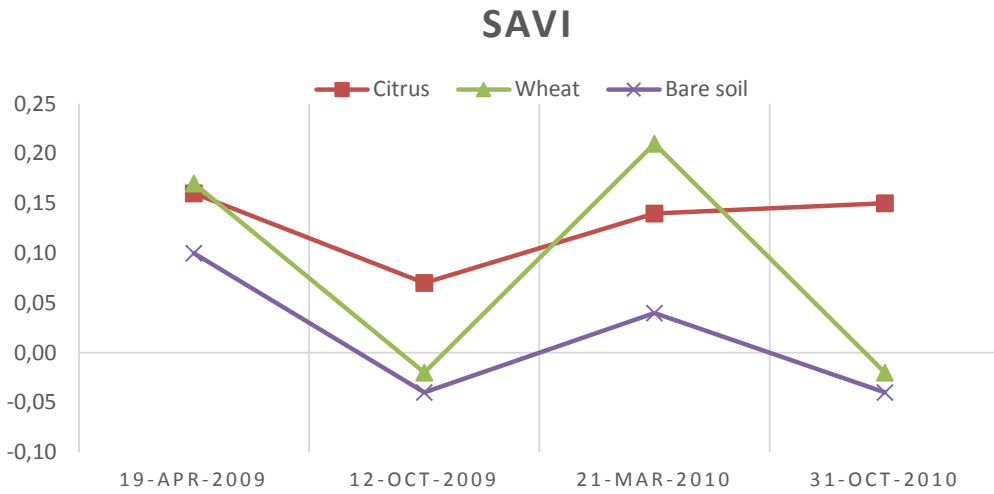
Figure 6.16 : Changes in the average SAVI values in the selected ROI's.

6.5 Correlation Analysis

In this part of the study, the correlation between electrical conductivity of the collected field samples and bands of satellite images is carried out to find the relationship between these variables and assess their efficiency in predicting soil salinity using simple linear regression (SLR) and multiple linear regression (MLR) techniques. Regression modeling techniques are widely used for predicting a variable's spatial distribution [47].

6.5.1 Simple linear regression

The OLS model, as a first method for correlation analysis was applied by using a single band for predicting soil salinity, whereas in multiple linear regression, different bands are used and each band can contribute some degree of correlation. To compute the single band correlation, the digital number of each samples in the Landsat images were extracted for each band and this has been carried out for all data set (19th April, 2009, 12th October, 2009, 21st March, 2010, 31st October, 2010) to develop the relationship with measured electrical conductivity in both vertical and horizontal orientations. The same process was applied to the radiometrically corrected TOA value of sample points in order to evaluate the correlation band with salinity measurements (Table 6.8). The correlation among DN and TOA values with EC value was assessed, using the Excel 2010 software.

Thermal bands of all Landsat images were removed from analysis and Band 7 of Landsat 7 ETM$^+$ is noted as band 6 in all of the following Tables.

Table 6.8 : Correlation of DN and TOA values of satellite bands with EC values (horizontal and vertical).

Date of satellite pass	Date of Field measurements	Time interval	Number of soil samples	Number of used soil samples	DN &TOA	Correlation with band values (Horizontal)					
						B1-H	B2-H	B3-H	B4-H	B5-H	B6-H
19-Apr-09	2-May-09	13 days	153	121	DN	2.69%	0	0.59%	-13.27%	-0.90%	0%
					TOA	1.64%	1.71%	1.98%	-0.02%	1.04%	1.59%
12-Oct-09	4-Oct-09	8 days	688	650	DN	17.34%	9.84%	6.49%	-3%	0.93%	1.18%
					TOA	15.56%	9.82%	6.63%	2.73%	0.83%	1.22%
21-Mar-10	24-Mar-10	3 days	27	22	DN	-13.51%	-12.50%	-3.24%	-1.87%	-21.90%	-7.11%
					TOA	-17.21%	-9.20%	-5.89%	-1.91%	-18.77%	-4.70%
31-Oct-10	4-Oct-10	27 days	269	259	DN	-0.04%	-0.48	-0.97%	-0.48%	-0.70%	-0.69%
					TOA	0	-0.34%	-1.06%	-0.50%	-0.64%	-0.70%
Date of satellite pass	Date of Field measurements	Time interval	Number of soil samples	Number of used soil samples	DN &TOA	Correlation with band values (Vertical)					
						B1-V	B2-V	B3-V	B4-V	B5-V	B6-V
19-Apr-09	2-May-09	13 days	153	121	DN	0.07%	-0.69%	-0.13%	-6.20%	-2.93%	-0.84%
					TOA	1.01%	1.34%	1.01%	-0.02%	0.80%	0.86%
12-Oct-09	4-Oct-09	8 days	688	650	DN	23.02%	13.76%	9.30%	-4.17%	1.17%	1.46%
					TOA	20.73%	13.73%	9.34%-	-3.91%	1.04%	1.42%
21-Mar-10	24-Mar-10	3 days	27	22	DN	-12.94%	-17.56%	-7.62%	-2.76%	-30.89%	-17.43%
					TOA	-16.99%	-12.59%	-10.21%	-2.93%	-27.78%	-13.94%
31-Oct-10	4-Oct-10	27 days	269	259	DN	-0.01%	-0.49%	-1.12%	-0.70%	-0.66%	-0.74%
					TOA	0	-0.54%	-1.33%	-0.74%	-0.58%	-0.70%

The univariate analysis shows that all bands are not statistically significant predictors of salinity, yet bands 1 and 5 of the 21st March, 2010 and bands 1 of the 12th October, 2009 show the high correlation among the individual bands in vertical orientation. The correlation of 21st March, 2010 between DN and TOA values of band 5 (shortwave infrared) with EC shows 30.89% and 27.78% of salinity correlation, respectively. However, in overall, there are not any specific differences between the correlation of EC value with DN and correlation of EC value with TOA in all satellite dates.

Band 5 of Landsat 7 ETM$^+$ with band width of 1.55-1.75 µm in electromagnetic spectrum (short wave infrared), provides a good contrast between different types of vegetation, and also with salinization on soil surface.

Twenty indices including sixteen salinity indices and four vegetation indices were used as a part of the correlation analysis. These indices were chosen with regard to the relevant literature based on their likelihood for exhibiting high correlation with surface soil salinity. Correlation between each indices with EC value in each date were undertaken using linear regression method to investigate the strongest correlation with the sampled soil salinity values (Table 6.9 up to Table 6.12).

Table 6.9 : Correlation of EC value with several salinity indices (horizontal and vertical).

Date of satellite pass	Date of Field measurements	Time interval	Number of soil samples	Number of used soil samples	DN &TOA	Correlation with salinity indices (Horizontal)					
						SI 1-H	SI 2-H	SI 3-H	SI 4-H	SI 5-H	SI 6-H
19-Apr-09	02-ma2009	13 days	153	121	DN	1.29%	0.22%	-15.19%	0.26%	-2.63%	5.83%
					TOA	1.94%	0.20%	0.23%	1.86%	-0.32%	-0.95%
12-Oct-09	4-Oct-09	8 days	688	650	DN	8.07%	8.16%	1.40%	7.97%	-1.14%	3.49%
					TOA	10.36%	-0.39%	0	8.37%	-1.88%	-3.08%
21-Mar-10	24-Mar-10	3 days	27	22	DN	-5.29%	-5.99%	-3.65%	-6.32%	0	0.44%
					TOA	-15.46%	-7.37%	-2.57%	-7.41%	3.95%	0.27%
31-Oct-10	4-Oct-10	27 days	269	259	DN	-0.55%	-0.75%	-0.73%	-0.76%	0	0
					TOA	-0.53%	-0.65%	-0.75%	-0.62%	0	-0.11%
Date of satellite pass	Date of Field measurements	Time interval	Number of soil samples	Number of used soil samples	DN &TOA	Correlation with salinity indices (Vertical)					
						SI 1 -V	SI 2-V	SI 3-V	SI 4-V	SI 5-V	SI 6-V
19-Apr-09	02-ma2009	13 days	153	121	DN	-0.03%	-0.24%	-10.14%	0.30%	-0.18%	4.57%
					TOA	1.02%	0.12%	0.15%	1.16%	0	-0.57%
12-Oct-09	4-Oct-09	8 days	688	650	DN	11.04%	11.54%	2.04%	11.31%	1.47%	4.75%
					TOA	14.24%	-0.64%	0	11.76%	-1.73%	-4.30%
21-Mar-10	24-Mar-10	3 days	27	22	DN	-8.99%	-11.07%	-5.36%	-11.46%	2.11%	0
					TOA	-26.91%	-11.86%	-3.71%	-11.42%	2.14%	0
31-Oct-10	4-Oct-10	27 days	269	259	DN	-0.59%	-0.82%	-0.90%	-0.85%	0.05%	0.12%
					TOA	-0.66%	-0.75%	-1.13%	-0.92%	0	-0.33%

Table 6.10 : Correlation of EC values with several salinity indices (horizontal and vertical).

Date of satellite pass	Date of Field measurements	Time interval	Number of soil samples	Number of used soil samples	DN &TOA	Correlation with salinity indices (Horizontal)					
						SI 7_H	SI 8-H	SI 9-H	SI 10_H	SI 11-H	SI 12-H
19-Apr-09	02-ma2009	13 days	153	121	DN	-2.43%	-7.72%	-5.83%	-0.01%	-2.24%	0.08%
					TOA	-0.64%	0.24%	0	-1.98%	-2.15%	1.83%
12-Oct-09	4-Oct-09	8 days	688	650	DN	-0.97%	-0.22%	0	-0.32%	-0.05%	4.18%
					TOA	-1.28%	-0.27%	0.11%	-0.46%	-0.42%	-2.62%
21-Mar-10	24-Mar-10	3 days	27	22	DN	0	-6.76%	-17.29%	1.67%	1.41%	-4.02%
					TOA	0	-7.05%	-18.34%	5.03%	4.61%	-4.89%
31-Oct-10	4-Oct-10	27 days	269	259	DN	0.01%	-0.08%	-0.14%	2.46%	-0.30%	-1.15%
					TOA	0	0	0.12%	3.54%	3.21%	-0.21%
Date of satellite pass	Date of Field measurements	Time interval	Number of soil samples	Number of used soil samples	DN &TOA	Correlation with salinity indices (Vertical)					
						SI 7-V	SI 8-V	SI 9-V	SI 10-V	SI 11-V	SI 12-V
19-Apr-09	02-ma2009	13 days	153	121	DN	-0.19%	-3.75%	-5.78%	0.15%	-1.10%	-0.77%
					TOA	-0.19%	0	0	-0.48%	-0.64%	1.14%
12-Oct-09	4-Oct-09	8 days	688	650	DN	-1.24%	-0.27%	0	-0.67%	-0.06%	6.30%
					TOA	-1.44%	-0.23%	0.22%	-0.81%	-0.76%	-3.45%
21-Mar-10	24-Mar-10	3 days	27	22	DN	1.65%	-2.83%	-15.87%	5.73%	5.81%	-9.99%
					TOA	2.18%	-3.16%	-24.26%	9.25%	9.12%	-10.07%
31-Oct-10	4-Oct-10	27 days	269	259	DN	0.08%	0	-0.08%	3.09%	-0.39%	-1.34%
					TOA	0.12%	0	0	4.33%	3.96%	-0.30%

Table 6.11 : Correlation of EC value with several salinity indices (horizontal and vertical).

Date of satellite pass	Date of Field measurements	Time interval	Number of soil samples	Number of used soil samples	DN &TOA	Correlation with vegetation indices (Horizontal)			
						SI 13-H	SI 14-H	SI 15-H	SI16-H
19-Apr-09	02-ma2009	13 days	153	121	DN	1.82%	-15.87%	6.69%	-15.68%
					TOA	2.07%	0.33%	2.17%	0
12-Oct-09	4-Oct-09	8 days	688	650	DN	0.33%	-2.74%	6.28	0
					TOA	8.22%	-2.01%	6.33%	-0.72%
21-Mar-10	24-Mar-10	3 days	27	22	DN	-3.54%	-4.86%	0	-2.69%
					TOA	-6.74%	-15.46%	0	-2.26%
31-Oct-10	4-Oct-10	27 days	269	259	DN	-0.59%	-0.84%	0	0.81%
					TOA	-0.42%	-0.80%	0	-0.72%
Date of satellite pass	Date of Field measurements	Time interval	Number of soil samples	Number of used soil samples	DN &TOA	Correlation with vegetation indices (Vertical)			
						SI 13-V	SI 14 -V	SI 15-V	SI 16-V
19-Apr-09	02-ma2009	13 days	153	121	DN	-0.02%	-11.74%	1.69%	-9.16%
					TOA	0.73%	0	1.06%	0
12-Oct-09	4-Oct-09	8 days	688	650	DN	0.58%	-3.74%	8.87	0
					TOA	11.13%	-2.92%	9.02%	-1.04%
21-Mar-10	24-Mar-10	3 days	27	22	DN	-4.04%	-11.48%	0	-4.10%
					TOA	-9.41%	-26.91%	0	-3.36%
31-Oct-10	4-Oct-10	27 days	269	259	DN	-0.66%	-1.22%	0	1.05%
					TOA	-0.49%	-1.15%	0	-0.99%

Table 6.12 : Correlation of EC value with several vegetation indices (horizontal and vertical).

Date of satellite pass	Date of Field measurements	Time interval	Number of soil samples	Number of used soil samples	DN &TOA	Correlation with vegetation indices (Horizontal)			
						NDVI-H	RVI-H	SAVI-H	EVI-H
19-Apr-09	02-ma2009	13 days	153	121	DN	-6.67%	-5.47%	-6.69%	11.72%
					TOA	-2.17%	-0.68%	-1.31%	-1.36%
12-Oct-09	4-Oct-09	8 days	688	650	DN	-5.81%	-5.55%	-6.28%	3.50%
					TOA	-6.33%	-5.44%	-5.84%	-4.99%
21-Mar-10	24-Mar-10	3 days	27	22	DN	0	0.23%	0	11.63%
					TOA	0	1.84%	0.11%	0
31-Oct-10	4-Oct-10	27 days	269	259	DN	-0.01%	0.02%	0	0.70%
					TOA	0	0	0	0
Date of satellite pass	Date of Field measurements	Time interval	Number of soil samples	Number of used soil samples	DN &TOA	Correlation with vegetation indices (Vertical)			
						NDVI-V	RVI -V	SAVI-V	EVI-V
19-Apr-09	02-ma2009	13 days	153	121	DN	-1.62%	-1.27%	-1.70%	4.46%
					TOA	-1.06%	-0.18%	-0.66%	-0.61%
12-Oct-09	4-Oct-09	8 days	688	650	DN	-8.12%	-7.78%	-8.87%	5.41%
					TOA	-9.02%	-7.62%	-8.31%	-7.12%
21-Mar-10	24-Mar-10	3 days	27	22	DN	0	0.43%	0.11%	13.01%
					TOA	0	2.34%	0.46%	0.14%
31-Oct-10	4-Oct-10	27 days	269	259	DN	0	0	0	0.76%
					TOA	0	0	0	0

Similar to correlation of DN and EC values, the correlation of different indices with soil salinity data did not reveal the meaningful results. Specially, the correlation of vegetation indices with DN values was not satisfactory because of the chemical and physical properties of vegetation; therefore, the EC value can also correlate with other yield variables such as chlorophyll content, biomass, and leaf area [48].

While considering the salinity indices, some of them like SI1, SI9, and SI14 on 21st March, 2010 demonstrate higher correlation among all other salinity indices. The output images of applied indices are given in Figure 6.17.

(a)   (b)
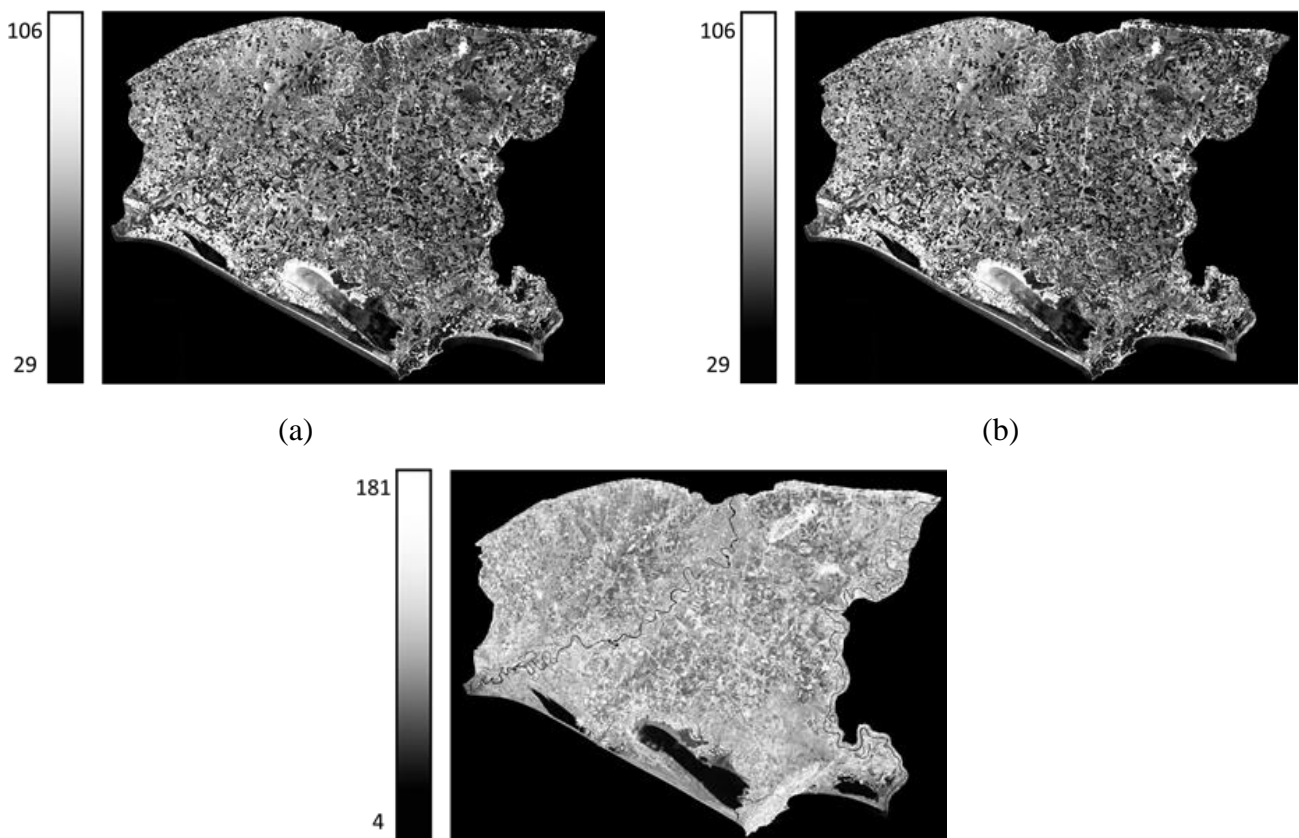
Figure 6.17 : Salinity indices images of Seyhan plate (a) SI 1 on 21st March, 2010, (b) SI 9 on 21st March, 2010 (c) SI 14 on 21st March, 2010

6.5.2 Multiple linear regression with all bands

Since the result of simple linear regression survey was not satisfactory, a second approach, as multiple linear regression (MLR) was applied using Minitab 17 statistical program. MLR allows multivariable analysis and is applied to predict the degree of salinity in multiple variables, using the known measured values.

In this regression method, pixel value of all six bands of Landsat 7 (bands 1-5 and 7) were used as an independent variable, and EC value of soil was introduced to Minitab system as a dependent variable. After completing the regression, an equation is derived for each correlation with known data and satellite bands. This formula can be applied to other imageries to examine salinity of non-measured point by the availability of the close date of satellite imagery to filed measuremnts dates. Thus, it is also possible to predict salinity values without the cost and time of field observations [49].

In multiple regression, two quantitative criteria between measured and predicted values are calculated. R^2 values indicate the strength of the statistical linear relationship between measured and predicted soil salinity values and P-value tests the hypothesis for each term in linear regression. A low p-value (< 0.05) indicates that it is possible to reject the null hypothesis and there is sufficient evidence to conclude that the coefficient does not equal zero and that changes in the predictor are associated with changes in the response variable. In the Minitab software, high p-values (>0.05) are regarded as disqualified points and removed from analysis. After removing some sample points multiple regressions was reapplied, until there was not any disqualified sampled point. The results of each regression are the regression equation and scatterplots of relationship between salinity data and pixel values.

One other problem is that, it is not always very easy to decide which independent variable should include or remove from the regression because using too much variables may lead to poor prediction. Therefore, stepwise regression was used as a solution to overcome this issue. The correlation analysis of all bands with EC value in each date using multiple linear regression are given in the Table 6.13.

Table 6.13 : Multiple linear regression of high correlated bands and indices with EC values (horizontal and vertical).

Date of satellite pas	Date of field measurements	Horizontal and vertical mode	Multiple Regression				Stepwise method			
			H	V	H	V	H	V	H	V
19-Apr-09	2-May-09	Regression	32.70%	21.90%	54.44%	52.93%	33.45%	21.92%	51.51%	66.42%
		Number of samples	121	121	102	82	121	121	74	105
		Number of bands	All bands	All bands	All bands	All bands	B1,B2,B4,B6	B1,B2,B4,B6	B1,B2,B4,B6	B1,B2,B4,B6
12-Oct-09	4-Oct-09	Regression	23.47%	31.49%	28.06%	42.06%	23.57%	31.54%	26.15%	36.44%
		Number of samples	650	650	299	265	650	650	298	290
		Number of bands	All bands	All bands	All bands	All bands	B2,B4,B6	B2,B4,B6	B2,B4,B6	B2,B4,B6
21-Mar-10	24-Mar-10	Regression	46.19%	36.56%	75.86%	78.40%	18%	27.43%	48.90%	65.12%
		Number of samples	22	22	17	18	22	22	21	18
		Number of bands	All bands	All bands	All bands	All bands	B5	B5	B1,B2,B3,B5	B1,B5
31-Oct-10	4-Oct-10	Regression	2.27%	4.13%	23.25%	32.72%	3.57%	5.02%	4.12%	6.22%
		Number of samples	259	259	137	139	259	259	242	238
		Number of bands	All bands	All bands	All bands	All bands	B1,B3	B1,B3	B1,B3	B1,B3

As obvious from the Table 6.13, among all the correlation results, in both multiple regression and stepwise method, the correlation of 21st March, 2010 is higher than the others. The correlation amount of six bands of Landsat images in 21st March, 2010 with EC value in vertical oriantation was 36.56%, however after removing some of the sampled points, the R^2 value increase to 78.40% (Figure 6.18 and Figure 6.19).

Figure 6.18 : Multiple linear regression of 21th March, 2010 with all bands and 22 sampled points.

Regression Equation:

Predicted Soil Salinity = 2.24 - 0.0341 B1 - 0.0093 B2 + 0.0576 B3 + 0.00125 B4 -0.0089 B5 - 0.0410 B6

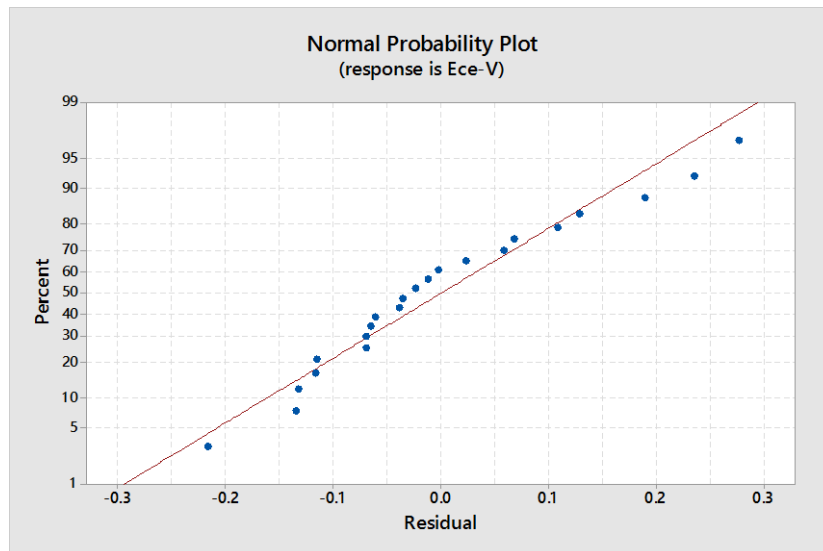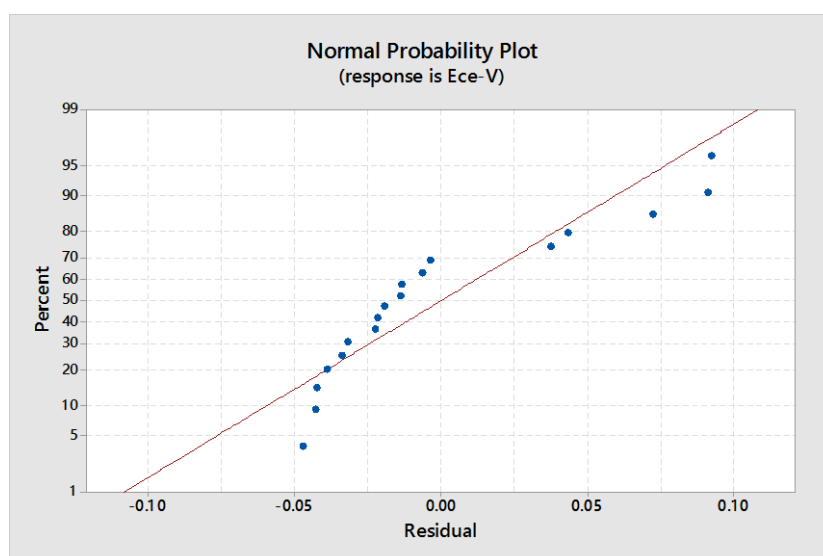**Figure 6.19 :** Multiple linear regression of 21st March, 2010 with all bands and 18 sampled points.

Regression Equation:

Predicted Soil Salinity= -0.378+ 0.0535 B1- 0.0431 B2+ 0.0308 B3+ 0.00715 B4- 0.02946 B5 - 0.0015 B6

6.5.3 Multiple linear regression with highest correlated bands and indices

As a final approach, multiple regression analysis with combination of 1) individual bands having the highest correlation, 2) salinity indices 3) vegetation indices with EC value was conducted (Table 6.14). The purpose of this analysis is to it select only the bands that have high correlation with field-collected data, and eliminate the bands that do not correlate with soil salinity data.

In order to get more precise results with high value of correlation, the following set of bands were selected for each image and these band combinations were introduced to Minitab program as independent variables (Table 6.15).

Table 6.14 : Different set of band combinations.

Satellite date	Satellite band	Salinity index
19-Apr-2009	Band 4	SI 4 and SI 9
12-Oct-2009	Bands 1 and 2	SI 1 and SI 2
21-Mar-2010	Band 2, 5 and 6	SI 4 and SI 9
31-Oct-2010	Band 3	SI 10

Table 6.15 : Multiple linear regression of high correlated bands and indices with EC values (horizontal and vertical).

Date of satellite pas	Date of field measurements	Horizontal and vertical mode	High correlated band+ High correlated index				Stepwise method			
			H	V	H	V	H	V	H	V
19-Apr-09	2-May-09	Regression	13.69%	9.14%	30.67%	24.14%	15.16%	11%	36.96%	45.46%
		Number of samples	121	121	102	92	121	121	99	72
		Number of bands	B4,SI14, SI3,BI	B4,SI14, SI3,BI	B4,SI14, SI3,BI	B4,SI14, SI3,BI	SI14	SI14	SI14	SI14
12-Oct-09	4-Oct-09	Regression	19.91%	25.76%	14.90%	27.89%	25.98%	20.12%	32.45%	26.12%
		Number of samples	650	650	299	302	650	650	290	297
		Number of bands	B1,B2, SI1,SI2	B1,B2, SI1,SI2	B1,B2, SI1,SI2	B1,B2, SI1,SI2	B1,SI2	B1,SI2	B1,SI2	B1,SI2
21-Mar-10	24-Mar-10	Regression	11.78%	40.20%	26.18%	68.78%	18%	27.43%	37.38%	44.02%
		Number of samples	22	22	20	16	22	22	20	18
		Number of bands	B2,B5,B6 SI4,SI9	B2,B5,B6 SI4,SI9	B2,B5,B6 SI4,SI9	B2,B5,B6 SI4,SI9	B5	B5	SI9	B6,SI4,SI9
31-Oct-10	4-Oct-10	Regression	2.75%	3.91%	5.55%	8.75%	2.75%	3.91%	2.84%	3.91%
		Number of samples	259	259	236	240	259	259	241	221

		Number of bands	B3,SI10	B3,SI10	B3,SI10	B3,SI10	B3,SI10	B3,SI10	B3,SI10	B3,SI10

As given in the Table 6.15, for both multiple regression and stepwise method the highest correlation valueis observed in the 21st March, 2010. The correlation was calculated among Band 2, Band 5 and Band 6 together with the SI 4 and SI 9, as an independet variabes with EC value as dependent variable. In this correlation 6 sample points are removed from analysis and the correlation value has raised to 68.78% from 40.20 % in vertical oriantation.

Figure 6.20 shows the the distributaion of residuals in the correlation anlysis of 21st March, 2010.
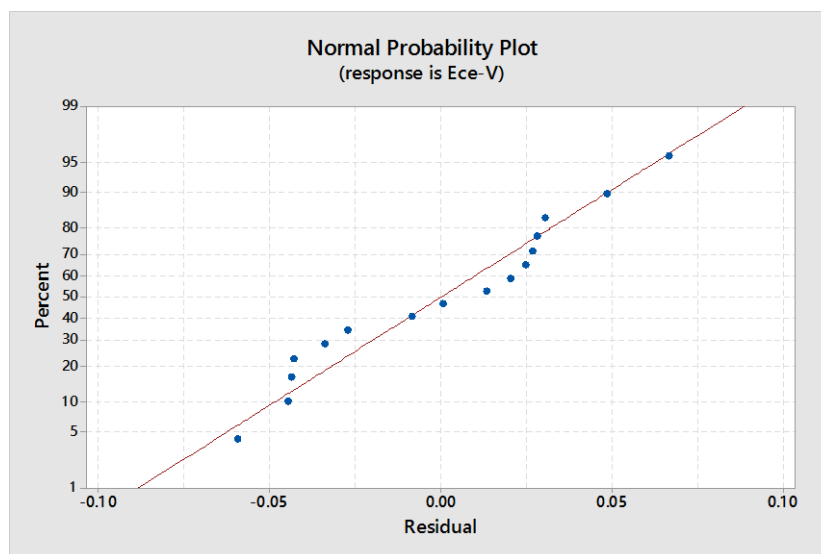

Figure 6.20 : Multiple linear regression of 21st March, 2010 with different combination of bands and indices.

Regression Equation:

Predicted Soil Salinity = 0.955 - 0.0406 B2 + 0.0081 B5 - 0.0370 B6 + 0.0471 SI 4 - 0.0454 SI 9

Once all the developed regression methods were tested, models with a high R^2 values signifying a high correlation between satellite data and field measurements data, were selected as a best regression model in order to create the soil salinity map of the study area. As discussed in this section, the highest correlation value (78.40%) is obtained by the multiple linear regression method in 21st March, 2010.

6.6 Soil Salinity Map Production

Mapping and assessing of the soil salinity require integration of the remote sensing data with the field data. To generate accurate soil salinity maps, it is necessary to obtain high correlation between EC value and band values. To do so, the correlation of EC value and band values in

four dates (19th April, 2009, 12th October, 2009, 21st March, 2010,31st October, 2010) was considered. Among all the methods used, i.e simple linear regression, multiple linear regression and stepwise regression, the best results were obtained from the multiple linear regression. The satellite data dated on (21st March, 2010) which had the highest correlation (78.40%) in comparison with other data sets, was used for soli salinity mapping. The regression equation related to the highest correlation observed, was used for the soil mapping. Then density slicing method was applied in order to classify the different salinity levels. The global standard ranges of density slicing are provided by Landscape Planning Department of the Cukurova University. Ranges are given in the Table 6.16.

Table 6.16 : Global standard salinity ranges.

Levels of salinity	Saturation extract salinity (EC_e, dS/m)
Non salinity	0-2
Low salinity	2-4
Medium salinity	4-8
High salinity	8-16
Extra high salinity	>16

Using the ranges given in the Table 6.16, the soil salinity map that indicates the salinization level in the area is given in Figure 6.21.
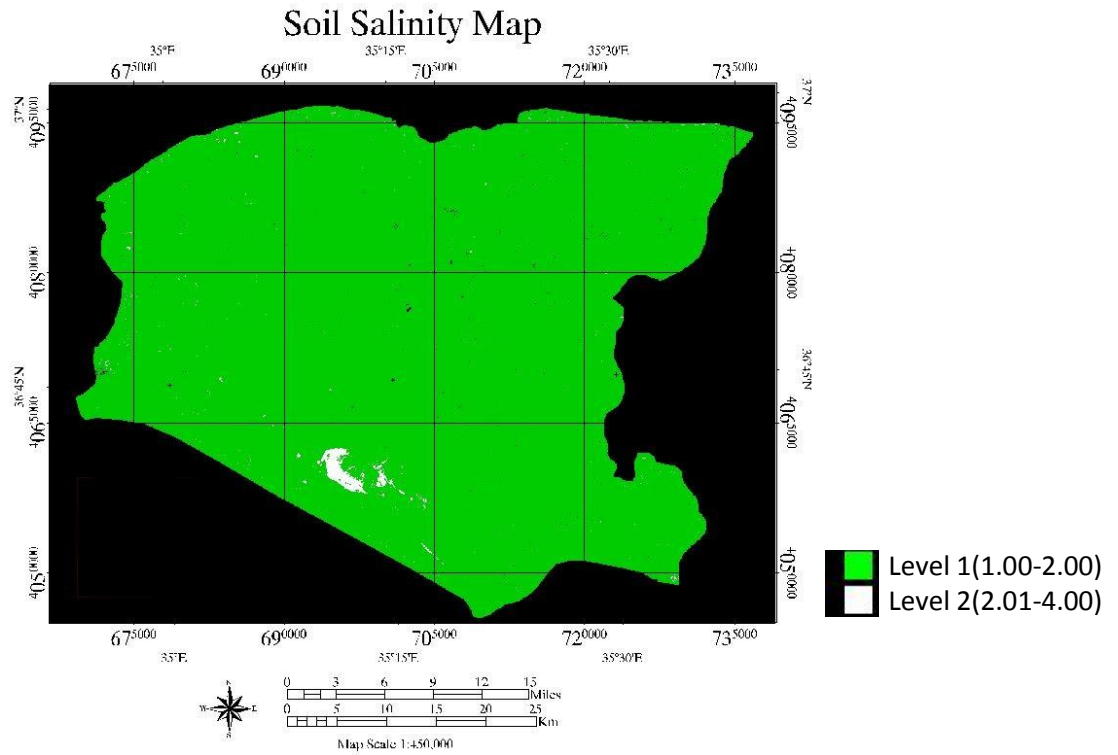
Figure 6.21 : Soil salinity map according to global standard salinity ranges.

From Figure 6.21, it can be seen that the small part of Seyhan plate are being affected by soil salinity. As obvious, the salt is mostly accumulated in the reeds region and in other parts such as farmland, not much impact is seen ,in the 2009 to 2010 periods of time.

In the second approach, the salinity ranges used by previous research study done in the study area is considered for mapping the soil salinity. The soil salinization map produced by DSI is given in the Figure 6.22[50]. The same process is applied again to the highest correlated data (21st March, 2010) by considering the levels shown in Figure 6.22.

Figure 6.23 shows the result map of density slicing process regarding to the soil salinity.
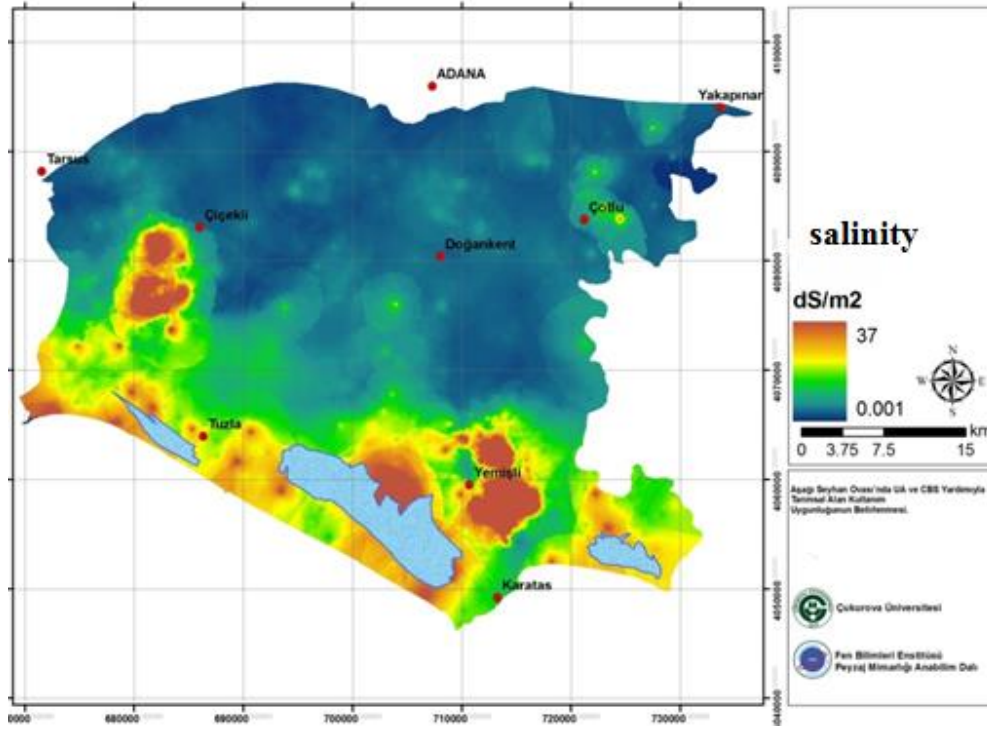
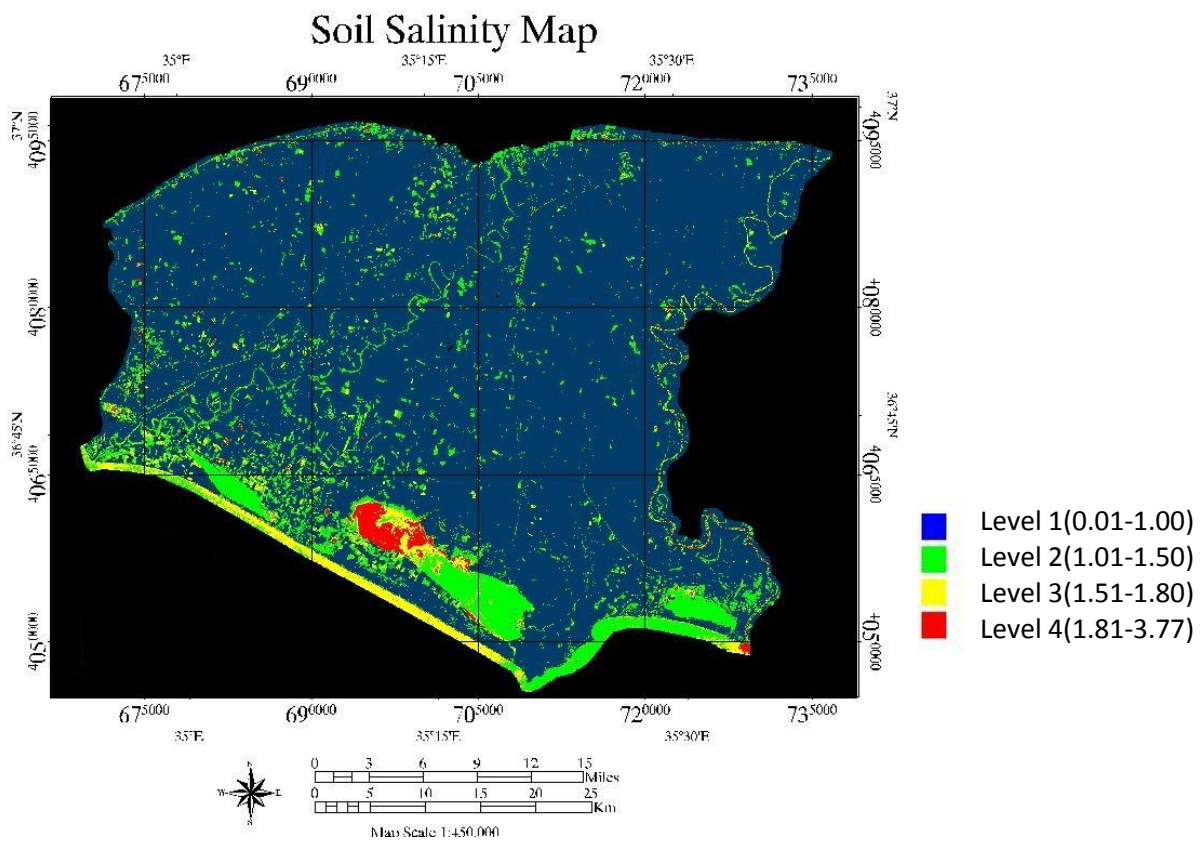**Figure 6.22 :** Soil salinity map produced by DSI.

Figure 6.23 : Soil salinity map according to DSI's ranges.

As illustrated in Figure 6.23, the highest saline soils in the study area again are taking place in the region covering reeds due to the presence of high amount of salt in the lake. It can be seen that the other parts of Seyhan plate are being affected by medium to low soil salinity and the salt is mostly accumulated in the lower part of the study area.

6.7 Analysis of Soil Salinity Levels with the Crop Types

In this part of the study, intersection of the main fields with the soil salinity ranges is calculated to find out the percentage of soil-affected farmlands. According to the sizes, two main fields, namely Wheat and Bare soil fields are taken into consideration. Hence as a first field, the Wheat fields and soil salinity ranges is calculated to find out the percentage of soil-affected Wheat farmlands. The result of this intersection is given in the Figure 6.24. As can be seen from the Figure, in general, most of the Wheat fields are not much influenced by saline soil, however only the Wheat fields covering lower part of the study area are affected by low to medium salinization shown by green and yellow colors in the legend. Areal extent of salinization in the Wheat fields are given in Table 6.17.
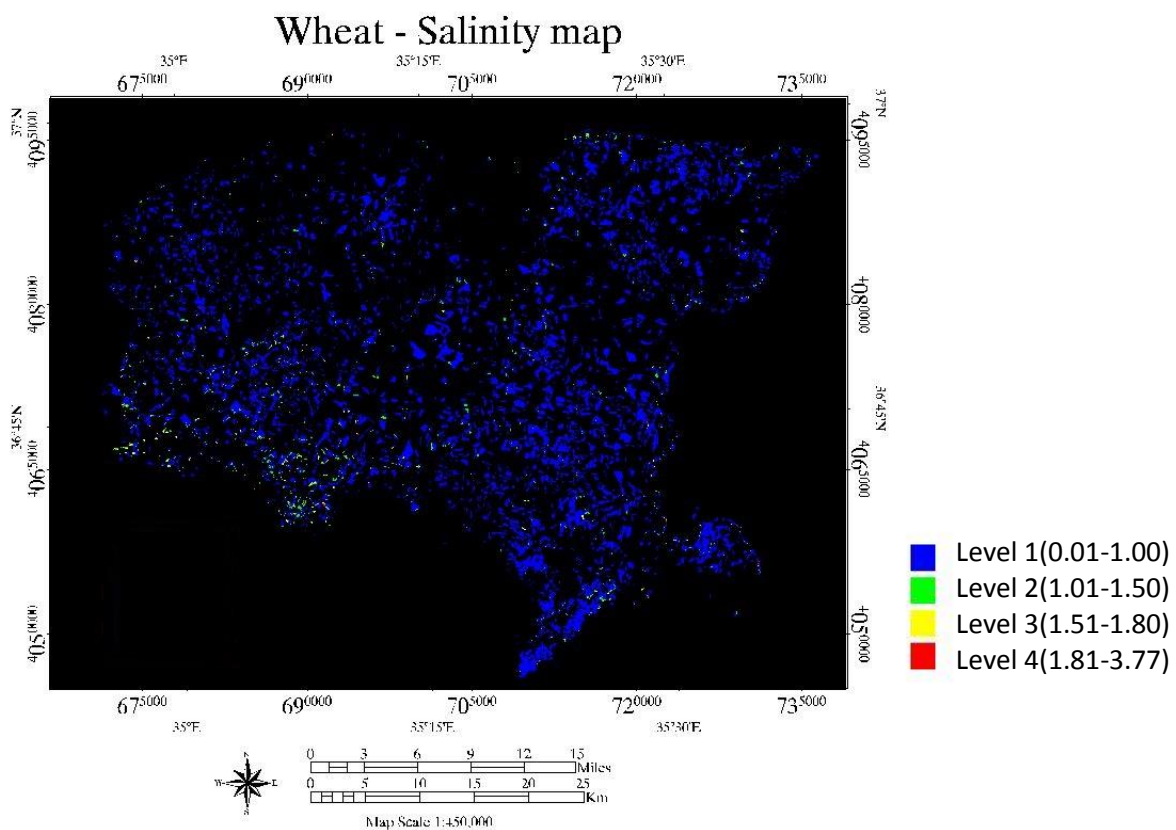

Figure 6.24 : The map of the salinization in the Wheat fields

Table 6.17 : Areal extent of salinization in the Wheat fields

Density slice ranges	Salt- affected Wheat fields (ha)	Percentages (%)
Level 1 (Blue)	26 242 740	95
Level 2 (Green)	1 216 530	4
Level 3 (Yellow)	239 040	0.8
Level 4 (Red)	60 930	0.2

Secondly, the effect of salinization in the Bare soils was also analyzed and the result of salt-affected Bare soils is given in the Figure 6.25. As shown in the Figure below, the Bare soils, which are close by to the reeds region, are more affected (%35) than the other parts. In comparison with the Wheat fields, it can be concluded that the Bare soils are rather more influenced by salinazition than the Wheat fields. The main reason for that is thought as the lack of plantation in the Bare soils, i.e direct interaction with the saline soils.
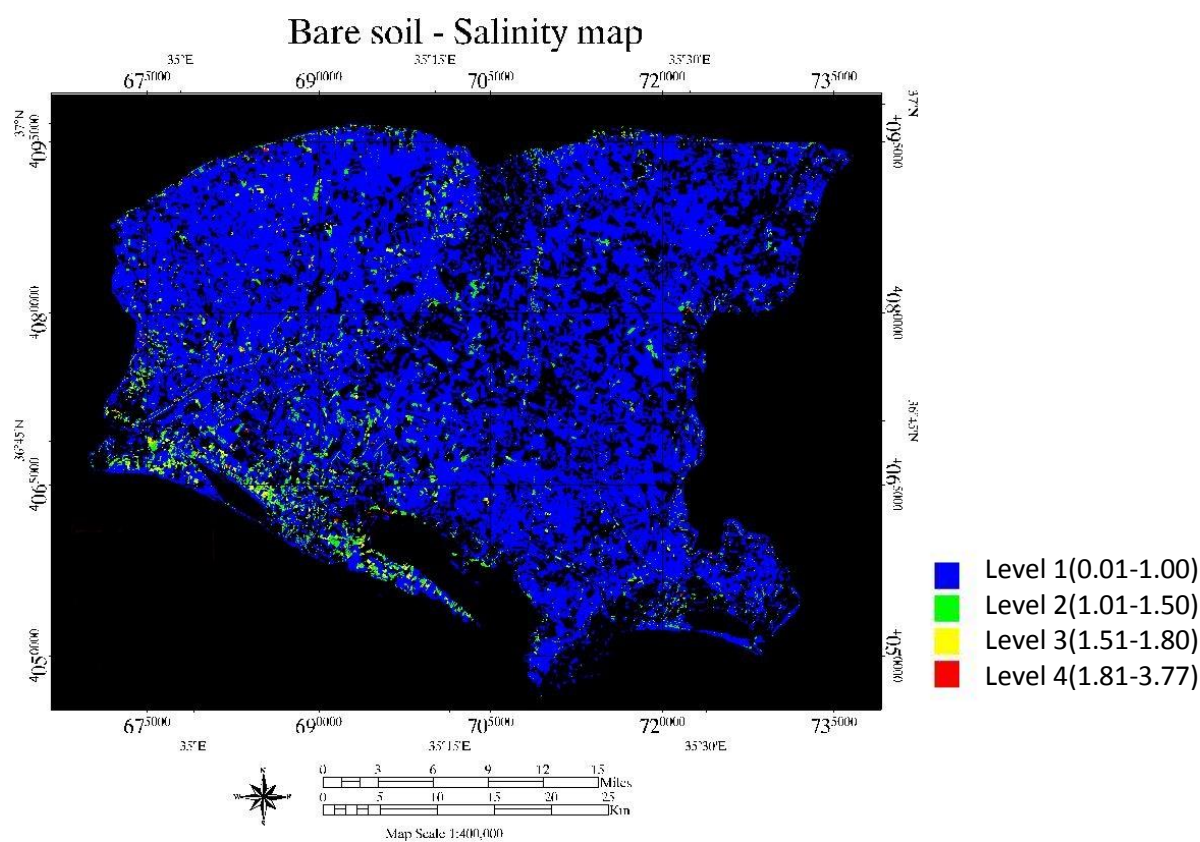
Figure 6.25 : The map of the salinization in the Bare soils.

Areal extent of salinization in the Bare soils are given in Table 6.18.

Table 6.18 : Areal extent of salinization in the Bare soils.

Density slice ranges	Salt- affected Bare soils (ha)	Percentages (%)
Level 1 (Blue)	122 210 1000	56.4
Level 2 (Green)	7 604 5500	35
Level 3 (Yellow)	1 501 1100	7
Level 4 (Red)	344 7900	1.6

7. RESULTS AND CONCLUSIONS

There are extensive areas of salt-affected soils all over the world, caused the loss of large area of productive lands through salinization. From the agricultural point of view, soil salinity is one of the biggest threats for crop productivity and in some countries; soil salinity may even threaten the national economy. To keep track of the changes in salinity levels, monitoring and mapping of soil salinity is required to make a proper and timely decision. One of the most useful approaches for soil salinity detection and mapping is the remote sensing techniques in conjuction with field EC measurements.

Since soil has dynamic and complex nature, soil salinity detection processes are very difficult. Beside the dynamic nature of soil, soil characteristics such as, soil moisture, soil texture, soil organic matter content can affect the soil salinity level. The effective control of soil salinity and waterlogging requires the knowledge of magnitude, extent and distribution of root zone salinity which is not easy to obtain.

In this thesis, four Landsat 7 ETM$^+$ data obtained in four different dates (19th April, 2009, 12th October, 2009, 21st March, 2010, 31st October, 2010) were used to monitor the seasonal and annual changes of soil salinity in the Seyhan plate in Adana.

Overall, twenty spectral indices, including sixteen salinity indices and four vegetation indices were analyzed. In this study, the most powerful indices used in literature were taken into consideration. Normalized Difference Salinity Index (NDSI) and Normalized Difference Vegetation Index (NDVI) are founded as the most useful ones. The correlation analysis between electrical conductivity (EC) of soil and pixel values of individual bands of satellite images and different indices were calculated by using regression techniques. Since the soil salinity is a dynamic phenomenon, it can change rapidly due to the precipitation, soil moisture and evaporation. Therefore, correlation between EC value and pixel value is found low in many studies in the literature. As a first approach, simple linear regression technique is applied and the result of this correlation was found very low (-30.89% to 20.02%). One of the main reasons, regarding to the low correlation of simple linear regression is, the field measurements and

satellite data were not obtained simuntaneously. As a second approach, the multiple linear regression was applied for the correlation analysis. In this method, instead of individual bands, all bands of satellite images were used. Among all results, the correlation of 18 sampled points of 21st March, 2010 with EC value, showed the highest correlation (78.40%). The main reason for that is having three days difference between field measurements date and satellite pass. Main conclusions, which are drawn from this study, are summarized below:

- The more simultaneous satellite data and field measurments are used, the better correlation can be observed.

- Besides the importance of compatability between satellite data and field data, the map projection compatability of both satellite data and field-collected data are also crucial.

- Another issue that should be considered is the radiometric quality of Landsat 7 ETM$^+$. The missed lines sometimes can make it difficult to get the exact value of a pixel or visually affect the image interpretation. Although the scan line error of Landsat 7 ETM$^+$ can be corrected using some of remote sensing softwares, the original values are modified.

- One other problem is the spatial resolution of Landsat 7 satellites (30 meters). The higher resolution makes the sampling easier in the image data. In this study, the sampling of soil salinity measurements could be easier in the case of using higher spatial resolution.

- Besides the spatial resolution, spectral resolution also plays an important role for better interpretation of the satellite imageries. Hyperspectral sensors can be a better solution, since they capture a large amount of narrow bands which refered to as a high spectral; however, multispctral satellites such as Landsat 7 captures the small number of wide bands. High spectral resolution makes it easy to distinguish between features spectrally in the image. Since saline soil in the near infrared (NIR) portion of electromagnetic spectrum has a strong reflectance that enables better detection, the more the NIR band is available, the saline soils would be detected more precisely. As a result, using the hyperspectral satellites in soil salinity detection could be more effective than multispectral satellites.

After the correlation analysis, the satellite data dated on 21st March, 2010 were chosen to map the soil salinity in the area due to having highest correlation. As observed, the highest saline soils in the study area are taking place in the region covering reeds due to the presence of high

amount of salt in the lake. Besides, it can be concluded that the other parts of Seyhan plate are being affected by medium to low soil salinity and the salt is mostly accumulated in the lower part of the study area.

As a final step, the intersection of the main fields with the soil salinity ranges is evaluated by calculating the percentages of soil-affected farmlands. According to the sizes, two main fields, namely Wheat and Bare soils are taken into consideration. According to the percentages obtained, it can be concluded that the Bare soils are rather more influenced by salinazition than the Wheat fields. The main reason for that is thought as the lack of plantation in the Bare soils, i.e direct interaction with the saline soils.

As a conclusion, some issues named above should be considered as recommendations for the future studies to be planned on this topic.

REFERENCES

[1] **Allbed, A., Kumar, L.** (2013). Soil salinity mapping and monitoring in arid and semi-arid regions using remote sensing technology: A review. *Advances in Remote Sensing*;2013.

[2] **Al-Khaier, F.** (2003). Soil salinity detection using satellite remote sensing. *Geo-information Science and Earth Observation, International Institute for Geo-information Science and Earth Observation*;70.

[3] **Garcia, L., Eldeiry, A., Elhaddad, A.** (2005). Estimating soil salinity using remote sensing data. *Proceedings of the 2005 Central Plains Irrigation Conference*. p: 1-10.

[4] **Oštir, K., Veljanovski, T., Podobnikar, T., Stančič, Z.** (2003). Application of satellite remote sensing in natural hazard management: the Mount Mangart landslide case study. *International Journal of Remote Sensing*;24,20. p: 3983-4002.

[5] **Farifteh, J., Farshad, A., George, R.** (2006). Assessing salt-affected soils using remote sensing, solute modelling, and geophysics. *Geoderma*;130,3. p: 191-206.

[6] Web Page: **http://en.wikipedia.org/wiki/Remote_sensing** (Accessed on 15 December 2014)

[7] Web Page: **http://www.shariqa.com/waves%20around%20us.htm** (Accesed on 21 January 2015)

[8] Web Page: **http://en.wikipedia.org/wiki/Electromagnetic_radiation** (Accessed on 27 January 2015)

[9] Web Page: **http://www.gisresources.com/an-insight-to-ndvi_2/**(Accessed on 10 March 2015)

[10] **Streck, N. A., Rundquist, D., Connot, J.** (2003). Spectral signature of selected soils. *Rev Brasil Agrometeorol, Santa Maria*;11,1. p: 184.

[11] Web Page: **https://www.soils.org/publications/sssaj** (Accesssed on 17 March 2015)

[12] Web Page: **http://www.geol-amu.org/notes/m1r-1-8.htm** (Accessed on 4 April 2015)

[13] **Nag, P., Kudrat, M.** (1998). Digital remote sensing: Concept Publishing Company.

[14] **Moreira, L. C. J., dos Santos Teixeira, A., Galvão, L. S.** (2014). Laboratory salinization of Brazilian alluvial soils and the spectral effects of Gypsum. *Remote Sensing*;6,4. p: 2647-63.

[15] **Karlen, D., Mausbach, M., Doran, J., Cline, R., Harris, R., Schuman, G.** (1997). Soil quality: a concept, definition, and framework for evaluation (a guest editorial). *Soil Science Society of America Journal*;61,1. p: 4-10.

[16] **Murphy, C., Macleod, A., Chapman, G., Milford, H., McGaw, A., Edye, J., et al.** (2001). NSW state soil landscape mapping program and derivative products. *Proceedings of the Geospatial Information and Agriculture Symposium, Sydney 2001*.

[17] **Beven, K., Germann, P.** (1982). Macropores and water flow in soils. *Water resources research*;18,5. p: 1311-25.

[18] **Madani, A. A.** (2013). Soil Salinity Detection and Monitoring Using Landsat Data: A Case Study from Siwa Oasis, Egypt.

[19] **Rengasamy, P.** (2002). Transient salinity and subsoil constraints to dryland farming in Australian sodic soils: an overview. *Animal Production Science*;42,3. p: 351-61.

[20] **Noaman, M. N., El-Haddad, E.-S.** (2000). Effects of irrigation water salinity and leaching fraction on the growth of six halophyte species. *The Journal of Agricultural Science*;135,03. p: 279-85.

[21] **Goossens, R., El Badawi, M., Ghabour, T., De Dapper, M.** (1993). A simulation model to monitor the soil salinity in irrigated arable land in Arid areas based upon remote sensing and GIS. *EARSeL Advances in remote sensing*;2,3. p: 165-71.

[22] **Ahmed, I., Andrianasolo, H.** (1997). Comparative assessment of multisensor data for suitability in study of the soil salinity using remote sensing and GIS in the Fordwah irrigation division, Pakistan. *Geoscience and Remote Sensing, 1997 IGARSS'97 Remote Sensing-A Scientific Vision for Sustainable Development, 1997 IEEE International*4. p: 1627-9.

[23] **Elnaggar, A. A., Noller, J. S.** (2009). Application of remote-sensing data and decision-tree analysis to mapping salt-affected soils over large areas. *Remote Sensing*;2,1. p: 151-65.

[24] **Matinfar, H. R., Panah, S. K. A., Zand, F., Khodaei, K.** (2013). Detection of soil salinity changes and mapping land cover types based upon remotely sensed data. *Arabian Journal of Geosciences*;6,3. p: 913-9.

[25] **Platonov, A., Noble, A., Kuziev, R.** Soil Salinity Mapping Using Multi-Temporal Satellite Images in Agricultural Fields of Syrdarya Province of Uzbekistan. Developments in Soil Salinity Assessment and Reclamation: Springer; 2013. p. 87-98.

[26] **Ibrahim, H. M., El Falaky, A. A.** Soil salinity mapping in the Sinai Peninsula of Egypt using geographic information system and remote sensing techniques. Developments in Soil Salinity Assessment and Reclamation: Springer; 2013. p. 113-25.

[27] **Schowengerdt, R. A.** (2006). Remote sensing: models and methods for image processing: Academic press.

[28] **Sheather, S.** (2009). A modern Approach to Regression with R: Springer Science & Business Media.

[29] **Chen, J., Zhu, X., Vogelmann, J. E., Gao, F., Jin, S.** (2011). A simple and effective method for filling gaps in Landsat ETM+ SLC-off images. *Remote Sensing of Environment*;115,4. p: 1053-64.

[30] **Jensen, J. R.** (2009). Remote sensing of the environment: An earth resource perspective 2/e: Pearson Education India.

[31] **Huete, A. R.** (1988). A soil-adjusted vegetation index (SAVI). *Remote sensing of environment*;25,3. p: 295-309.

[32] **Fukuhara, M., Hayashi, S., Yasuda, Y., Asanuma, I., Emori, Y., Iisaka, J.** (1979). Extraction of soil information from vegetated area. *LARS Symposia*. p: 277.

[33] **Khan, N. M., Rastoskuev, V. V., Shalina, E. V., Sato, Y.** (2001). Mapping salt-affected soils using remote sensing indicators-a simple approach with the use of GIS IDRISI. *Paper presented at the 22nd Asian Conference on Remote Sensing*5. p: 9.

[34] **Metternicht, G., Zinck, A.** (2008). Remote sensing of soil salinization: Impact on land management: CRC Press.

[35] **Douaoui, A. E. K., Nicolas, H., Walter, C.** (2006). Detecting salinity hazards within a semiarid context by means of combining soil and remote-sensing data. *Geoderma*;134,1. p: 217-30.

[36] **Bannari, A., Guedon, A., El-Harti, A., Cherkaoui, F., El-Ghmari, A.** (2008). Characterization of Slightly and Moderately Saline and Sodic Soils in Irrigated Agricultural Land using Simulated Data of Advanced Land Imaging (EO-1) Sensor. *Communications in soil science and plant analysis*;39,19-20. p: 2795-811.

[37] **Abbas, A. a. S. K.** (2007). Using remote sensing techniques for appraisal of irrigated soil salinity. *International Congress on Modelling and Simulation" CONFÉRENCE MODELLING AND SIMULATION SOCIETY of Australia and New Zealand Christchurch, New Zealand*. p: 2632-8.

[38] **Lobell, D. B., Asner, G. P.** (2003). Comparison of Earth Observing-1 ALI and Landsat ETM+ for crop identification and yield prediction in Mexico. *Geoscience and Remote Sensing, IEEE Transactions on*;41,6. p: 1277-82.

[39] **González, M. E. P., Rodríguez, M. d. P. G., González-Quiñones, V., Ballesta, R. J.** (2006). Spatial variability of soil quality in the surroundings of a saline lake environment. *Environmental geology*;51,1. p: 143-9.

[40] **Van Niel, T. G.** (1995). Classification of vegetation and analysis of its recent trends at Camp Williams, Utah using remote sensing and geographic information system techniques.

[41] **Jackson, R. D., Huete, A. R.** (1991). Interpreting vegetation indices. *Preventive Veterinary Medicine*;11,3. p: 185-200.

[42] **Huete, A., Jackson, R.** (1987). Suitability of spectral indices for evaluating vegetation characteristics on arid rangelands. *Remote sensing of environment*;23,2. p: 213-IN8.

[43] **Dr. Takanori Nagano** Assessment of long-term changes of shallow water table fluctuation in the irrigated alluvial plain in the East Mediterranean Turkey (In review).

[44] **McCutcheon, M., Farahani, H., Stednick, J., Buchleiter, G., Green, T.** (2006). Effect of soil water on apparent soil electrical conductivity and texture relationships in a dryland field. *Biosystems Engineering*;94,1. p: 19-32.

[45] **Selch, D.** (2012). Comparing salinity models in Whitewater Bay using remote sensing: Florida Atlantic University.

[46] Web Page: **http://landsathandbook.gsfc.nasa.gov/**(Accessed on 12 April 2015)

[47] **Palialexis, A., Georgakarakos, S., Karakassis, I., Lika, K., Valavanis, V.** (2011). Fish distribution predictions from different points of view: comparing associative neural networks, geostatistics and regression models. *Hydrobiologia*;670,1. p: 165-88.

[48] **Song, K., Wang, Z., Blackwell, J., Zhang, B., Li, F., Zhang, Y., et al.** (2011). Water quality monitoring using Landsat Themate Mapper data with empirical algorithms in Chagan Lake, China. *Journal of Applied Remote Sensing*;5,1. p: 053506--16.

[49] **Xie, Z., Zhang, C., Berry, L.** (2013). Geographically weighted modelling of surface salinity in Florida Bay using Landsat TM data. *Remote Sensing Letters*;4,1. p: 75-83.

[50] **ŞATIR, O.** (2013). Aşağı seyhan ovası'nda uzaktan algılama ve coğrafi bilgi sistemleri yardımıyla tarımsal alan kullanım uygunluğunun belirlenmesi. Fen bilimleri enistitüsü, Çukurova universitesi.

CURRICULUM VITAE

Name Surname: Anali AZABDAFTARI

Place and Date of Birth: 16.11.1988

E-Mail: a.azabdaftari@gmail.com

B.Sc.: 2007-2011 Azad University of Tabriz, Information Technology, Computure Department.